

Synthesis and design of planar microstrip bandpass filters with multi-mode resonators

Zhang, Runqi

2013

Zhang, R. (2013). Synthesis and design of planar microstrip bandpass filters with multi-mode resonators. Doctoral thesis, Nanyang Technological University, Singapore.

<https://hdl.handle.net/10356/62569>

<https://doi.org/10.32657/10356/62569>

**Synthesis and Design of
Planar Microstrip Bandpass Filters
with Multi-Mode Resonators**

ZHANG Runqi

School of Electrical & Electronic Engineering

A dissertation submitted to the Nanyang Technological University

in fulfillment of the requirements for the degree of

Doctor of Philosophy

2013

STATEMENT OF ORIGINALITY

I hereby certify that the work embodied in this dissertation is the result of original research and has not been submitted for a higher degree to any other University or Institution.

Date

Runqi Zhang

ACKNOWLEDGEMENTS

Thousands of thanks go to my supervisor, Prof. Lei Zhu, who has professionally and patiently guided my research work for my study in the school and also kindly give me much help and advice with his wise understanding for a meaningful life. It is really a memorable journey to work under his direction for the past three years. These great things like introducing the research mythology of my topic, working with me to solve difficulties and enlightening me with his past experience are always kept in my mind.

Also, great appreciate Prof. Lu Yilong, who has helped me a lot for my final stage of Ph.D. studying.

Besides, there is an obligation to appreciate other professors in our lab. During their courses, I grasp the most fundamental concepts and rules, which turn out to be extremely helpful to my next research work. Their diverse research backgrounds broaden my understanding of the electromagnetic field.

Next, I feel much grateful towards my friends, lab mates and technicians in the Communication Research Lab, who have companied me to go through a very happy time. The laughter with you adds a vivid color to my hard time and the discussion with you clears my minds to find the solutions.

Finally, I would like to express my sincere thanks to Nanyang Technology University for providing me this precious opportunity and the financial support to carry on my Ph. D. study.

ABSTRACT

Planar microwave bandpass filters (BPFs) are an essential component in many communication systems. Traditional BPF design focuses on the application of frequency-invariant K -/ J -inverters inserted between the two resonant modes or served as the external coupling to feed the resonators. This design method is most suitable for narrow bandwidth BPFs, but for wideband cases it is difficult for a direct application. To solve this problem, a synthesis method based on a modified general Chebyshev function and the Richard's transformation has been proposed to characterize the frequency response over the whole frequency range for the wideband BPF designs. As for the corresponding circuit structure, short-circuited stepped-impedance multi-mode resonators (MMRs) serve as the foundation to the designs in this dissertation. By parallel-connecting or folding the MMRs, a class of dual-wideband BPFs has been developed. Based on the above discussion, this dissertation presents the wideband BPF designs in two aspects, the proposed filter synthesis procedure and a new class of circuit structures to realize the target filtering responses.

As the foundation of this research work, short-circuited MMRs have been researched in the first place for a single-wideband BPF design. n sections of cascaded commensurate lines are used to group the resonances, and short-ended stubs are shunt on its two sides to inductively feed the MMR. For the filter design, a Chebyshev filtering function is used to characterize the frequency response of the circuit. By equating the filtering function to the transfer function of the circuit, the design parameters are obtained.

The first set of dual-wideband BPFs is formed by parallel-connecting two dissimilar single-wideband BPFs, both formed by stepped-impedance MMRs. The two transmitting paths of 180° phase difference are used to generate up to two pairs of transmission zeroes (TZs) with symmetry to the dual-wide passbands. By appropriately choosing the characteristic impedances of the two paralleled MMRs, one pair of TZs is located in real frequencies contributing to the attenuation between the two passbands, whereas the second pair of TZs is located in imaginary

frequencies adjusting the group delay within the passbands. The short-circuited stubs, in shunt connection on the two sides of the MMR, act as the inductive loading element to feed the MMR and to flatten the passband. In the meanwhile, they introduce TZs at multiple of π to suppress the DC-component.

Following a similar design principle, the second set of dual-wideband BPF has been proposed as an improved design in terms of realizing a more compact size, the greater flexibility in terms of reflection zeros in the passband and an extra degree of freedom in choosing characteristic impedances. The generic structure of the proposed filters is formed by folding a MMR along its symmetrical plane and by coupling a pair of short-circuited stubs on the two ends of the MMR. Thus, two signal transmitting paths, one from the folded MMR and another from the loaded stubs, are used to generate additional TZs between the two passbands. By increasing sections of the loaded MMR, the reflection zeros in the passband is enlarged. Under fully-coupled structure, the merit of compact size and extra design freedom is obtained.

For these two sets of dual-wideband BPFs mentioned above, the even-/odd-mode analysis method has been used to derive the transfer function to characterize their frequency responses. Given the properties of the proposed filters, the commonly used generalized Chebyshev filtering function as well as its transferred dual-band function is not appropriately used herein. Instead, a generalized Chebyshev filtering function, originally developed for a single-wideband BPF design, is readily applied. By directly formulating a filtering function with mirror to the origin, it has dual passbands respectively located at positive and negative frequency ranges. To accurately account for the wideband response, a TZ is assigned at the origin. Next, the Richard's transformation is applied to transfer the normalized frequency response to its dual-band counterpart. With this proposed synthesis procedure, the targeted filtering function is characterized by a ratio of two polynomials. By equating these two aforementioned functions, which are the ideal filtering function from the specifications and the transfer function from the circuits, all the circuit design parameters are obtained.

Finally, the proposed single-/dual-wideband bandpass filters have been synthesized and designed for practical implementation. The experimental results of the fabricated filter circuits have strongly verified these new filter structures and their corresponding synthesis method proposed.

TABLE OF CONTENTS

ACKNOWLEDGEMENTS.....	II
ABSTRACT.....	III
TABLE OF CONTENTS.....	VI
LIST OF FIGURES	IX
LIST OF TABLES.....	XII
CHAPTER 1 INTRODUCTION.....	1
1.1 MOTIVATION	2
1.1.1 Basics of RF/Microwave Bandpass Filters.....	2
1.1.2 Limitations of Traditional Synthesis Methods for Wideband BPF Design.....	5
1.1.3 The Proposed Wideband Bandpass Filters and the Synthesis Method..	7
1.2 OBJECTIVES	9
1.3 MAJOR CONTRIBUTIONS OF THE DISSERTATION	11
1.4 ORGANIZATION OF THE DISSERTATION.....	12
CHAPTER 2 LITERATURE REVIEW.....	14
2.1 INTRODUCTION	14
2.2 FILTERING FUNCTIONS	15
2.2.1 Chebyshev Filtering Function	15
2.2.2 General Chebyshev Filtering Function	18
2.2.3 Modified General Chebyshev Filtering Function	22
2.3 FREQUENCY TRANSFORMATION.....	25
2.3.1 Typical Lowpass to Bandpass Transformation	25
2.3.2 Richard's Transformation	26
2.3.3 Single-Band to Dual-/Multi-Band Design	27
2.4 SINGLE-WIDEBAND BANDPASS FILTER DESIGN.....	28
2.4.1 Wideband Filters Using MMRs	28
2.4.2 Wideband Filters Using Optimum Distributed Structures	29
2.5 DUAL-NARROW/WIDEBAND BANDPASS FILTER DESIGN.....	30
2.6 COMPUTER AIDED DESIGN OF PLANAR FILTERS	32
2.6.1 Basic Concept and Definitions for Optimization.....	32
2.6.2 Optimization for Microwave BPF Design.....	33

2.7	CAPACITIVE COMPENSATION FOR COUPLED LINES	34
2.8	CONCLUSIONS	36
CHAPTER 3 SYNTHESIS AND DESIGN OF A WIDEBAND BANDPASS FILTER WITH INDUCTIVELY FED SHORT-CIRCUITED MULTI-MODE RESONATOR...37		
3.1	INTRODUCTION	37
3.2	SYNTHESIS AND DESIGN OF CHEBYSHEV-RESPONSE WIDEBAND FILTER	38
3.2.1	Working Mechanism of the Proposed Circuit.....	38
3.2.2	Circuit Analysis and Synthesis Procedure.....	40
3.2.3	Experimental Results and Discussions.....	44
3.3	DESIGN OF THE WIDEBAND FILTER WITH TZS	48
3.3.1	Working Mechanism and Circuit Analysis	48
3.3.2	Experimental Results and Discussions.....	56
3.4	SUMMARY	58
CHAPTER 4 SYNTHESIS AND DESIGN OF WIDEBAND DUAL-BAND BANDPASS FILTERS WITH CONTROLLABLE IN-BAND RIPPLE FACTOR AND DUAL-BAND ISOLATION59		
4.1	INTRODUCTION	59
4.2	SYNTHESIS PROCEDURE OF THE DUAL-BAND BPF	59
4.2.1	Circuit Analysis of the Proposed Dual-Band Filters	60
4.2.2	Generalized Chebyshev Filtering Function	64
4.2.3	Frequency Transformation to Dual-Band BPF	65
4.2.4	Circuit Parameter Calculation	67
4.2.5	Synthesis Procedure	68
4.3	SYNTHESIS AND DESIGN OF DUAL-BAND BPFs	69
4.3.1	Prototype I with One Pair of Controllable TZs.....	69
4.3.2	Prototype II with Two Pair of Controllable TZs.....	73
4.3.3	Prototype III with Controllable In-Band Ripple	75
4.3.4	Circuit Transformation for Appropriate Characteristic Impedances ...	78
4.4	EXPERIMENTAL RESULTS AND DISCUSSIONS	79
4.4.1	Filter Prototype I	80
4.4.2	Filter Prototype II.....	81
4.4.3	Filter Prototype III	82
4.5	SUMMARY	85
CHAPTER 5 SYNTHESIS AND DESIGN OF A CLASS OF DUAL-WIDEBAND BANDPASS FILTERS WITH INTERNALLY-COUPLED MICROSTRIP LINES.....86		

5.1	INTRODUCTION	86
5.2	DESIGN AND SYNTHESIS PROCEDURE	87
5.2.1	Circuit Analysis of the Proposed Dual-Band Filters	87
5.2.2	Dual-Band Filtering Function.....	90
5.2.3	Synthesis of the Proposed Dual-Band BPFs	91
5.3	SYNTHESIS AND DESIGN OF DUAL-BAND BPFs	93
5.3.1	1 st -Order Dual-Band BPF Design	94
5.3.2	2 nd -Order Dual-Band BPF Design	96
5.3.3	3 rd -Order Dual-Band BPF Design.....	99
5.4	EXPERIMENTAL RESULTS AND DISCUSSIONS	101
5.4.1	2 nd -Order Dual-Band BPF Design	101
5.4.2	3 rd -Order Dual-Band BPF Design.....	103
5.4.3	4 th -Order Dual-Band BPF Design.....	104
5.5	SUMMARY	107
CHAPTER 6	CONCLUSIONS AND RECOMMENDATIONS.....	108
6.1	CONCLUSIONS	108
6.2	RECOMMENDATIONS FOR FUTURE WORK	110
REFERENCES	112
AUTHOR'S PUBLICATIONS.....		120

LIST OF FIGURES

Figure 1-1. Commonly used design specifications for the BPFs.....	2
Figure 1-2. Comparison of the frequency responses with the two types of inverters, the quarter-wavelength transmission line and the ideal inverter ($Z_0= 50 \Omega$, $L_1= 2 \text{ nH}$, $C_1= 2 \text{ pF}$, $Z_r= 100 \Omega$ and $J= 0.01$).	5
Figure 1-3. The stepped-impedance MMRs of four sections. (a) Open-circuited MMR. (b) Short-circuited MMR (Every section is denoted as the transmission line with the electrical length θ)	7
Figure 1-4. The general synthesis procedure used in this dissertation.....	7
Figure 2-1. The 4 th - and 5 th -order Chebyshev function as a function of Ω	16
Figure 2-2. Typical 5 th -order Chebyshev frequency response with $\varepsilon= 0.1$	16
Figure 2-3. $\Omega_1(\Omega)$ as a function of Ω with TZ located at $\Omega_{TZ1}= 1.2$	19
Figure 2-4. The real and imaginary part of $\cosh^{-1}(\Omega)$ as a function of Ω	19
Figure 2-5. Typical 5 th -order general Chebyshev frequency response (the design specifications: $\varepsilon= 0.1$ and $\Omega_{TZ(1,2)}= \pm 2$).	21
Figure 2-6. The functions of $T_2(\omega)/\omega$ and f_1 as a function of ω with the passband defined as $B= [1, 2]$ and the TZ located at $z_1= 2.2$	22
Figure 2-7. Typical 3 rd -order modified general Chebyshev frequency response with the passband defined as $B= [1, 2]$, the TZ located at $z_1= 2.5$ and $z_2= 0.5$ and $\varepsilon= 0.1$	22
Figure 2-8. Frequency responses under the transformation of $\Omega= \tan\theta$ and $\Omega= 1/\tan\theta$ (the prototype Chebyshev function as $\cos(5\cosh^{-1}(\theta))$ and $\varepsilon= 0.1$).	27
Figure 2-9. Flow chart of a typical optimization process [64].	32
Figure 2-10. Equivalent circuits of even- and odd-modes. (a) Even-mode circuit. (b) Odd- mode circuit. (c) Derived odd-mode circuit with modified phase velocity.	34
Figure 3-1. Schematics of a class of inductively fed MMRs formed by cascading n sections of transmission lines. (a) $n= 1$. (b) $n= 2$. (c) $n= 3$. (d) $n= 4$	39
Figure 3-2. (a) The short-end stub is transferred to the inductor via Richard's transformation. (b) The MMR is inductively fed by inductors.	39
Figure 3-3. The synthesis procedure as discussed in this chapter for the single wideband BPFs.	41
Figure 3-4. Characteristic impedance variations under the different cutoff frequencies (θ_c) and the ripple factors (ε) for the circuits of. (a) $n= 1$. (b) $n= 2$. (c) $n= 3$. (d) $n= 4$ in Figure 3-1 (the input and output port impedances are defined as $Z_0= 1 \Omega$).	42
Figure 3-5. Frequency responses and group delays of theoretical, EM simulated and measured results, with a photograph of the fabricated filter in the inset figure. ...	46

Figure 3-6. (a) Basic schematic of the proposed UWB filter. (b) Bisection circuit under even source excitation. (c) Bisection circuit under odd source excitation.	49
Figure 3-7. Frequency responses under the different shunt stubs with the inset figures denoting the characteristic impedances. (a) Short-circuited stubs. (b) Two-section open-circuited stubs. (c) Composite short- and open-circuited stubs.	50
Figure 3-8. (a) LC circuit under even-mode excitation. (b) LC circuit under odd-mode excitation. (c) Equivalent circuit of the proposed filter	52
Figure 3-9. Locations of reflection zeroes and TZs of the proposed BPF. (characteristic impedances: $Z_{oc1}=100\ \Omega$, $Z_{oc2}=100\ \Omega$, $Z_{sc}=30\ \Omega$, $Z_1=300\ \Omega$ and $Z_2=90\ \Omega$).....	54
Figure 3-10. Filtering response and group delay comparison between the wideband filter with the short-circuited stubs and the one with the composite short- and open-circuited stubs which are under the same <i>FBW</i> (the characteristic impedances of the former one is $Z_1=137\ \Omega$, $Z_2=749\ \Omega$, $Z_s=29\ \Omega$ and the characteristic impedances of the latter one is $Z_{oc1}=100\ \Omega$, $Z_{oc2}=100\ \Omega$, $Z_{sc}=30\ \Omega$, $Z_1=300\ \Omega$ and $Z_2=90\ \Omega$).	55
Figure 3-11. (a) Basic circuit schematic of the BPF. (b) Transfer the short-circuited stubs into the MMR by the Kuroda transformation. (c) Absorb the transformer into the transmission line.....	56
Figure 3-12. (a) Photography of the proposed wideband filter. (b) Frequency responses and group delays derived from analysis, EM simulation and measurement.	58
Figure 4-1. (a) Filter 1 formed by uniform MMR with the short-circuited stubs. (b) Filter 2 formed by the stepped-impedance MMR with the short-circuited stubs. (c) Dual-band BPF by parallel connecting filter 1 and filter 2.	60
Figure 4-2. The phase and magnitude of Y_{21} of filter 1 and filter 2 and the frequency responses of the dual-band BPF to illustrate the generation of the TZs between the two passbands. (a) Responses under the real frequency sweep. (b) Responses under the imaginary frequency sweep ($Z_1=81.6\ \Omega$, $Z_2=200.8\ \Omega$, $Z_3=69.4\ \Omega$ and $Z_s=83.8\ \Omega$).....	62
Figure 4-3. Frequency transformation of the filtering function from the Ω -plane to the θ -plane.....	64
Figure 4-4. Synthesis procedure for the dual-band BPFs discussed in this chapter.....	68
Figure 4-5. (a) Even-mode network of the prototype I. (b) Odd-mode network of the prototype I.	69
Figure 4-6. Frequency responses of the prototype I under different values of t_{22} (other design specifications: $\theta_1=112.5^\circ$ and $\theta_2=144^\circ$).....	71
Figure 4-7. (a) Even-mode network of the prototype II. (b) Odd-mode network of the	

prototype II.....	73
Figure 4-8. Frequency responses of the prototype II under different values of t_{z1} (other design specifications: $t_{z2}= 30$, $\theta_1= 112.5^\circ$ and $\theta_2= 144^\circ$).....	74
Figure 4-9. (a) Even-mode network of the prototype III. (b) Odd-mode network of the prototype III.	75
Figure 4-10. Frequency responses of the prototype III under different values of ε (other design specifications: $t_{z1}= -1.5$, $t_{z2}= 50$, $\theta_1= 119.25^\circ$ and $\theta_2= 135^\circ$).....	77
Figure 4-11. Frequency responses of the prototype III under different values of t_{z1} (other design specifications: $\varepsilon= 0.2$, $t_{z2}= 50$, $\theta_1= 117^\circ$ and $\theta_2= 135^\circ$).....	77
Figure 4-12. (a) Applying Kuroda transformation to the prototype I. (b) Z_2 absorbing the two inverters into Z_2'	78
Figure 4-13. Characteristic impedances of the prototype I under varied locations of TZs (θ_{z2}) and 1 st -passband FBW ($FBW_{band\ 1}$) with a fixed dual-band frequency ratio of 0.4 (the frequency ratio is defined as the ratio of the center frequency of the first over second passband).....	79
Figure 4-14. Frequency responses and group delays of the theoretical, EM simulated and the measured results of the prototype I.....	81
Figure 4-15. Frequency responses and group delays of the theoretical, EM simulated and the measured results of the prototype II.	82
Figure 4-16. Frequency responses and group delays of the theoretical, EM simulated and the measured results of the prototype III.....	84
Figure 4-17. (a) Circuit schematic of prototype III with the electrical length of the open- and short-stub labelled as θ_{oc} and θ_{sc} . (b) Simulated results of prototype III under different set of θ_{oc} and θ_{sc}	84
Figure 5-1. General schematic of the proposed dual-wideband BPF with the internally-coupled microstrip lines.	88
Figure 5-2. Synthesis procedure for the proposed dual-band BPFs.	92
Figure 5-3. (a) Transmission-line characterization of the parallel-coupled short-circuited stubs and its even-/odd-bisection circuits. (b) The stepped-impedance stub and its even-/odd-bisection circuits. (c) Locations of the reflection zeroes under different Z_{s1e} ($Z_{s2e}= 30\ \Omega$).....	94
Figure 5-4. (a) Comparison between the theoretical and the circuit responses of a 2 nd -order filter with $\varepsilon= 0.1$, $\theta_{tz2}= 76.5^\circ$, $\theta_1= 123.75^\circ$ and $\theta_2= 139.5^\circ$. (b) Phase responses. (c) Characteristic impedances versus Z_{1e} and Z_1 for achieving the responses in Figure 5-4(a)-(b).....	96
Figure 5-5. (a) Theoretical and circuit responses of a 3 rd -order filter with $\varepsilon= 0.1$, $\theta_1= 117^\circ$	

and $\theta_2 = 144^\circ$. (b) Characteristic impedances versus different locations of TZs (θ_{TZ2}).....	99
Figure 5-6. (a) Photograph of the fabricated 2 nd -order dual-band filter with dimensions labelled. (b) Comparison between the theoretical, EM simulated and measured results of the dual-band filter.....	102
Figure 5-7. (a) Photograph of the fabricated 3 rd -order dual-band filter with dimensions labelled. (b) Comparison between the theoretical, EM simulated and measured results of the dual-band filter.....	103
Figure 5-8. (a) Photograph of the fabricated dual-band filter of cascaded structure with dimensions labelled. (b) Comparison between the theoretical, EM simulated and measured results of the dual-band filter.....	106
Figure 6-1. Circuit schematic of cascading i filter blocks.....	110

LIST OF TABLES

Table 3.1 Comparison with the reported ultra-wideband BPFs	47
Table 4.1 Structures of the Proposed Dual-Band BPF Prototypes.....	61
Table 4.2 Design Parameters of Prototype I under Different t_{z2}	71
Table 4.3 Design Parameters of Prototype I under Different t_{z1}	74
Table 4.4 Design Parameters of Prototype III under Different ε	77
Table 4.5 Design Parameters of Prototype III under Different t_{z1}	78
Table 5.1 Structures of the Proposed Dual-Band BPF Prototypes.....	90

CHAPTER 1

INTRODUCTION

RF/Microwave bandpass filters (BPFs) are widely used in many modern communication systems to effectively suppress the spurious and harmonic frequencies [1–5]. Most existing BPFs design methods are explored and applied for the narrow bandwidth cases, where the mutual coupling coefficient, external coupling, quality factor of a resonator, mode coupling scheme etc. are the most important issues to be considered [1]. However, these design methods could not be readily transferred to a wideband case for some limitation factors. To solve this problem, a concept of multi-mode resonators (MMRs) has recently been proposed by grouping the resonances to form the wide passband [6-8].

This dissertation presents some new circuit structures of single-/dual-wideband BPFs based on the concept of MMRs as well as their corresponding synthesis method to exactly determine the design parameters for a set of required design specifications. The presented circuit structures have the merits of compact size, high isolation between the two passbands and the extra degree of freedom in choosing appropriate characteristic impedances.

In this chapter, the motivations for the wideband BPFs have been briefly introduced with a focus on the comparison between the narrowband BPF design and the wideband ones, the discussion on the proposed circuit structures and the traditional circuit topologies. Next, the objectives of this dissertation have been discussed. Finally, the major work and contributions have been summarized the next two sub-sections.

1.1 Motivation

The proposed wideband structures are used for single-/dual-band cases. To exactly determine the design parameters, an exactly synthesis method has been proposed to cover the whole interested frequency range. Therefore, these two aspects, circuit schematic and the synthesis procedure, form the primary orientations for the motivation of this research work. In the following paragraphs, first the basic theory about the RF/microwave BPF has been introduced. Next, the limitation of the existing circuit schematics and the design method for single-/dual-wideband BPFs has been presented. Following that, the motivation of this dissertation has been introduced.

1.1.1 Basics of RF/Microwave Bandpass Filters

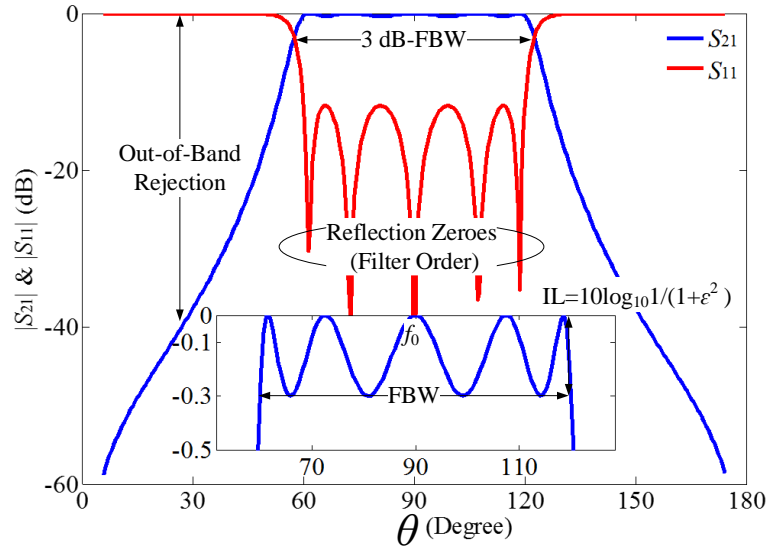


Figure 1-1. Commonly used design specifications for the BPFs.

For any practical RF/microwave BPFs, the target design specifications are considered in the first place. They include center frequency (f_0), fractional bandwidth (FBW), insertion loss (IL) or ripple factor (ϵ) within the passband, desired

out-of-band rejection and so on. The synthesis procedure is to find the appropriate circuit scheme as well as its corresponding design parameters to meet all these design requirements. For the convenient discussion in the latter part of this dissertation, a brief introduction/definition to these design requirements is listed in Figure 1-1. It is noted that for all the designs in this dissertation, they are related to the quarter-wavelength transmission lines with respect to the center frequency of a single passband or the middle frequency of the two passbands, which is the arithmetic mean of the two center frequencies. Therefore, Figure 1-1 is plotted with respect to the θ -plane for a general discussion.

Reflection zeroes: places permit absolute transmission of energy ($|S_{11}|=0$).

Transmission zeroes: places permit no transmission of energy ($|S_{21}|=0$).

Ripple factor: the difference between the maximum and minimum attenuation within the passband.

Fractional bandwidth: the two edge frequencies defined by the ripple factor over the middle value of these two frequency points.

Insertion loss: the ratio of the power transmitted to load before and after insertion of the filter.

Out-of-band attenuation: the attenuation equal to or larger than a specified figure at the desired frequency.

Frequency ratio (for dual-band BPF): the ratio of the center frequency of the first over second passband.

Once the design specifications are given, a mathematical filtering function, F_n , is used to model the required BPF response, such as the magnitude of S_{21} (for a theoretical discussion the losses including metallic loss, dielectric loss and radiation

loss for filters have not been considered). These two are related by the following equation as

$$|S_{21}|^2 = \frac{1}{1 + |\varepsilon F_n|^2} \quad (1.1)$$

where ε donates as the in-band ripple factor.

Therefore, the process of a filter design starts with the design specifications, and then transfers from an ideal mathematical filtering function to the practical circuit in the end. If the frequency response of a certain circuit is managed to match with the ones of the expected filtering function, the synthesis procedure is finished. To characterize a circuit response, a transfer function, F_{cir} , is extracted by [2]

$$F_{cir} = \frac{S_{11}}{S_{21}} \quad (1.2)$$

Once the transfer function has been obtained, the transfer function is set to be equal to the filtering function to end the synthesis procedure as

$$|F_{cir}| = \varepsilon |F_n| \quad (1.3)$$

To speed up the filter design procedure, some typical filtering functions as well as their circuit schemes have been tabulated or programmed to immediately get the initial circuit design parameters [1–5]. The well-known ladder type filter made up of J -/ K -inverter and shunt/series LC components are tabulated to obtain the Chebyshev or Butterworth filtering responses [4]. An advanced general-Chebyshev filtering response, with the re-allocated TZ, could be programmed to get the mutual-/self-coupling coefficients and the external quality factor [1].

1.1.2 Limitations of Traditional Synthesis Methods for Wideband BPF Design

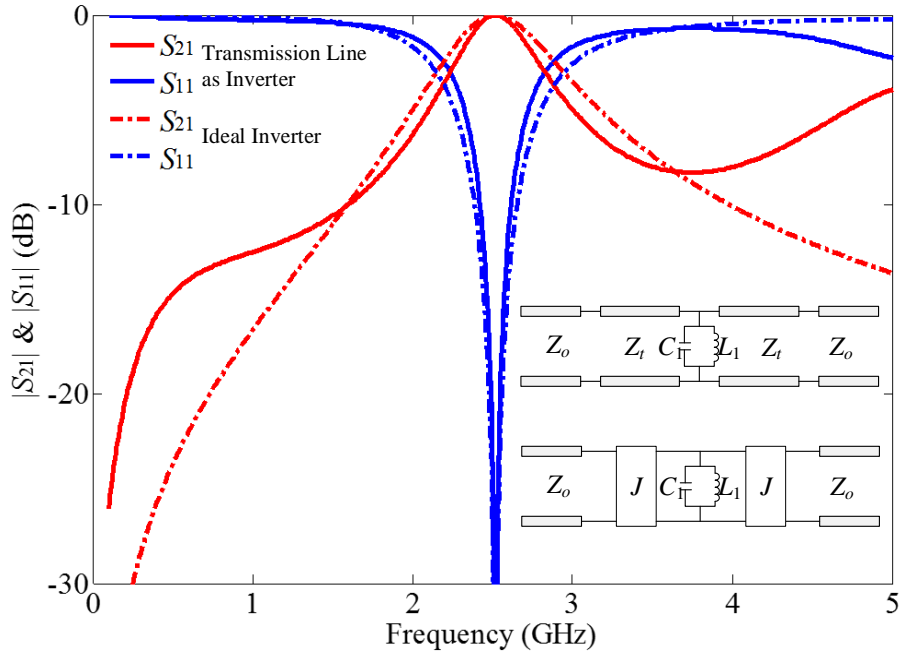


Figure 1-2. Comparison of the frequency responses with the two types of inverters, the quarter-wavelength transmission line and the ideal inverter ($Z_0 = 50 \Omega$, $L_1 = 2 \text{ nH}$, $C_1 = 2 \text{ pF}$, $Z_t = 100 \Omega$ and $J = 0.01$).

Single-/dual-wideband BPF designs are different from its narrowband counterparts, there are two main limiting factors facing their synthesis procedure:

- (a) Frequency variant inverters to be considered within a relatively wide frequency range;
- (b) Circuit schematic to permit the required mutual/external coupling coefficients.

For the narrowband case, the variation of the inverter within the interested frequency band is negligible. For the convenience of the mathematical and circuit's modeling, these inverters are treated as the ideal ones with respect to the center

frequency of the band. As the bandwidth expands, the interested frequency range is widened accordingly. The issue of the frequency variation of the inverters has to be considered. Figure 1-2 illustrates the comparison between the ideal inverter and the frequency variant one, i.e., the quarter wavelength transmission line. Although some discussions on frequency-dependent coupling have been reported [9], [10], most of which are still in the range of narrow band range.

The $ABCD$ parameters of these two kinds of inverters are [2]

$$\begin{bmatrix} A & B \\ C & D \end{bmatrix}_{J\text{-inverter}} = \begin{bmatrix} 0 & \pm \frac{1}{jJ} \\ \pm jJ & 0 \end{bmatrix} \quad (1.4)$$

$$\begin{bmatrix} A & B \\ C & D \end{bmatrix}_{\text{Quater-wavelength Line}} = \begin{bmatrix} \cos \theta & jZ_t \sin \theta \\ \frac{j \sin \theta}{Z_t} & \cos \theta \end{bmatrix} \quad (1.5)$$

where θ is the electrical length of the transmission line and Z_t the characteristic impedance of the transmission line.

Therefore, only at the center frequency of the interested passband ($\theta = 90^\circ$), the $ABCD$ parameters can be made equal to each other.

Another critical issue facing the design of the wideband BPF is about choosing an appropriate circuit prototype. First of all, the stronger the coupling, the wider the separation of the two resonances, which is normally required to design a wideband BPF, as demonstrated in section 8.4 of [2].

Next, there is little effective method to analyze the reflection zeroes within the passband if it is not in the traditional transmission line or cavity model, which directly results to the failure of mathematical analyzing the frequency responses of the circuits. Thus, traditional forms for narrow band BPF designs face many difficulties for wideband ones.

1.1.3 The Proposed Wideband Bandpass Filters and the Synthesis Method

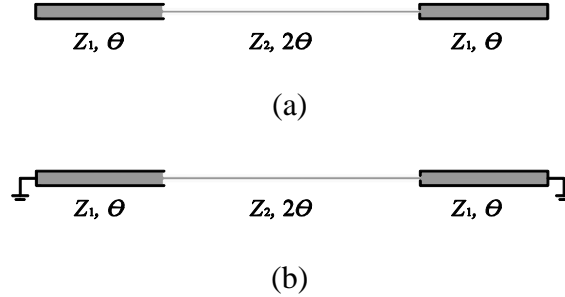


Figure 1-3. The stepped-impedance MMRs of four sections. (a) Open-circuited MMR. (b) Short-circuited MMR (Every section is denoted as the transmission line with the electrical length θ).

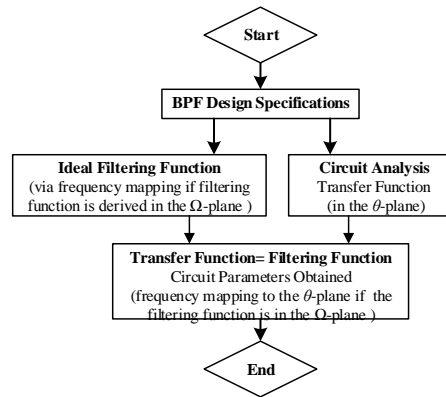


Figure 1-4. The general synthesis procedure used in this dissertation.

The motivation of this dissertation falls into two parts according to the above argument. The first one is about the synthesis method used to cover the whole frequency range of the wideband BPF, including selecting the filtering function, bridging among design specifications, transfer functions and filtering functions. The second part is about choosing an appropriate circuit prototype. It has to include the following two characteristics:

(a) being capable to be analyzed or derived by mathematical solutions to deduce the transfer function;

(b) matching with the chosen filtering function in order to get a set of non-linear equations to obtain the design parameters in the end.

To meet these requirements, the stepped-impedance MMR are selected as the foundation to realize the single-/dual-wideband BPFs, as shown in Figure 1-3. A systematic analyzing method to calculate or determine the resonances and their ratios have been reported in [11]. From the discussion in [3], open-circuited stepped-impedance MMR has been successfully used to design a single-band ultra-wideband (UWB) BPF. After that, a synthesis method for this class of filters has been proposed and used for several UWB filter designs [12]-[13]. As its counterpart, the short-circuited stepped-impedance MMR has also been used to achieve similar filtering responses, which would be discussed later.

For a better understanding of the target of this dissertation, the definitions of the “synthesis” and “design” are listed as below.

“Synthesis” in this dissertation refers to get the circuit schematic parameters according to the design specifications.

“Design” refers to the process of implementing the practical microstrip circuit according to the circuit schematic parameters.

“Synthesis and design” refers to the whole filter implementation process with a synthesis procedure to determine the circuit parameters and a practical realization with the microstrip lines.

The synthesis procedure of obtaining the circuit parameters is summarized as (it is also as seen in Figure 1-4.)

(a), starting with the targeted design specifications (f_0 , FBW , ε etc.);

(b), deriving the required filtering function (F_n) according to the edge frequency (if the filtering function is derived in the Ω -plane the frequency mapping is required to transform the edge frequency) and the transfer function in the θ -plane (F_{cir});

(c), equating the filtering function to the transfer function (if the filtering function is not in the θ -plane, a frequency mapping is required to transform from the Ω -plane to the θ -plane) and after that solving a set of non-linear equations to obtain the circuit design parameters.

After the synthesis procedure is completed, the filter design is realized by using the microstrip line structure for the practical circuit design. It is noted that the selection criteria for the design specifications of the experimental filter circuit follows the rules mentioned below. First, the chosen specifications are based on the consideration of the easiness of the fabrication. For example, some circuit is using coupled lines, thus a too wide bandwidth or too tightened ripple factor would result to extremely narrow slot or trace width. Then, within the valid fabrication range, the “common” numbers or coefficients, such as 2.0 and 3.2, are used to verify the proposed design principle. Finally, the specification is aesthetically adjusted to distribute the TZs more evenly.

1.2 Objectives

The above paragraphs have shown the difficulties facing the current filter design for the single-/dual-wideband BPF. In response to these problems, this dissertation aims to propose an effective synthesis method to be capable to target at the desired design specifications, and in the meantime, a class of single-/dual-wideband circuits is proposed to practically realize the design using this synthesis method. The objectives of this dissertation start with formulating the ideal filtering function, analyzing the chosen filter circuit, obtaining the design parameters and designing/fabricating, and through which, it is hoped that the reader could easily design a wideband BPF for one’s application. To be more specific, the objectives include the following parts:

- a. A comprehensive literature review of the RF/microwave BPF design is conducted in the first place as the foundation to the research work. The purpose of this step includes introducing the state-of-art filter design and synthesis procedure, understanding the working mechanism of the existing filter structures and identifying their limitations towards a wider bandwidth design.
- b. Then, as an effective circuit structure, the stepped-impedance MMR has been investigated to design a single-wideband BPF. This objective focuses on the discussion of the MMR, the excitation approach and the practical realization. Especially, the resonator and the feed lines are examined to find their property in contribution to the in-band reflection zeroes and out-of-band TZs. With the knowledge of this primary filter structure, it is expected that an advanced filter structure is explored.
- c. As the recent development of the dual-band communication systems, there is a need of the dual-band BPFs, which mainly forms the research background of this dissertation. To be suitable for practical applications, the circuit schematic is designed to be adjustable in-band ripple factor (ϵ), flexible in choosing the number of the reflection zeros and the bandwidth, controllable locations of TZs in determining the out-of-band rejection etc..
- d. For the objectives mentioned above, corresponding synthesis methods are proposed. The first step is to select an appropriate filtering function, which fully relies on the working mechanism of the circuit and its transfer function. Then, the frequency transformation among the design specifications, the chosen filtering function and the transfer function from circuits are used to link each other to form the whole design chart.
- e. Once the circuit schematic and the corresponding synthesis procedure have been proposed, microstrip single-/dual-wideband BPFs based on

commensurate lines are designed and fabricated as examples to verify the reported filter structure.

1.3 Major Contributions of the Dissertation

This dissertation introduces a class of single-/dual-wideband BPFs based on the concept of stepped-impedance MMRs. Major contributions of this dissertation are summarized in the following:

1. A class of wideband BPFs with short-circuited MMRs is proposed. The MMRs are formed by n sections of cascaded transmission lines, which are all set to be one quarter wavelength long with respect to the center frequency of the passband. Short-ended stubs are then added at the two ends of the MMR as inductive loading elements. With this method, design curves of different orders and ripple factors are provided to aid the design of a class of wideband BPFs.
2. A class of wideband dual-band BPFs with both controllable in-band ripple factor and the isolation between the dual-passband has been investigated as the second part. Two MMRs with the short-circuited stubs are in parallel connected to form the basic structure of the proposed dual-band BPFs. Up to two pairs of TZs could be created with reference to the dual-wideband. By choosing the characteristic impedances of the two paralleled MMRs, one pair of TZs could be moved from the imaginary to the real frequencies, whereas the second pair of TZs could be adjusted by folding one of the MMRs to form coupled lines. For these two prototypes, short-circuited stubs are utilized to feed the two paralleled MMRs, but not adequate to obtain a determined ripple factor. To provide an additional degree of freedom for controlling the in-band ripple factor, a combination of the short- and open-circuited stubs is used.
3. A class of wideband dual-band BPFs with internally-coupled microstrip lines has been proposed and exactly synthesized in this dissertation. The generic structure of the proposed filters is formed by folding a MMR along its symmetrical plane and coupling a pair of short-circuited stubs on the two ends

of the MMR. Thus, two signal transmitting paths, one from the folded MMR and another from the coupled stubs, are used to generate additional TZs between the two passbands. By increasing sections of the coupled MMR, the order of the filter is enlarged with a potential to introduce more TZs.

4. A general synthesis procedure is developed for the BPFs discussed in this dissertation. It is mainly divided into three steps, (a) a generalized Chebyshev filtering function is formulated to meet the design specifications; (b) a circuit prototype is analyzed to derive its transfer function; (c) all the circuit design parameters are obtained by equating these two aforementioned functions.

1.4 Organization of the Dissertation

The dissertation is divided into six chapters. The first chapter introduces the motivation behind this research work, with a focus on the limitations of the current BPF designs. Based on the argument of motivations, the objectives of this dissertation are targeted to design a class of single-/dual-wideband BPFs as well as their synthesis methods. Following that, there is a brief introduction to the proposed design principle.

Chapter 2 focuses on the literature review of some well-known filter design methods/techniques and planar filter structures. First, a commonly used filtering function is introduced. Following that, frequency transformation techniques have been discussed to transfer the filtering function to the required frequency plane. Next, some circuit or filter structures have been discussed to realize the wideband BPF design.

Chapter 3 presents a class of single-wideband BPFs using the short-circuited MMR and short-circuited stubs in shunt connection with the two sides of the MMR. By changing the characteristic impedances of the MMR which is in the form of cascading four sections of the transmission lines, the first three reflection zeroes are quasi-equally located within the passband. By parallel connecting the short-circuited

stubs at the two ends of the MMR, additional two reflection zeroes are found in the passband. A Chebyshev filtering function is used to characterize the frequency responses of the filter.

Chapter 4 proposes a class of dual-wideband BPFs formed by parallel connecting the two aforementioned wideband BPFs, which are discussed in chapter 3. With this transversal structure, TZs are generated between the two passbands so as to improve the rejection there. The proposed circuit structures have the capabilities to control the ripple factor within the two passbands and to locate two pairs of TZs at imaginary and real frequencies. Also, the proposed synthesis method for dual-wideband BPFs is discussed in detail within this chapter, including transferring the specifications to the filtering function, matching the filtering function with the transfer function to obtain the design parameters.

Chapter 5 formulates another class of dual-wideband BPFs with improved features. The general structure of this class of filters is formed by internally coupled MMR and the folded short-circuited stubs. Therefore, there are two signal transmitting paths, one from the coupled MMR and another from the folded stubs. With these two paths, TZs are generated in the middle of the two passbands. Compared with the proposed design in chapter 3, the internal-coupled dual-band filters serve as an improved case. They have the capability in choosing the number of reflection zeros in each passband, thereby obtaining an extra degree of freedom and promising a compact circuit size when fully internal-coupled structure is used. With the same synthesis method, this class of circuits is designed to meet specific specifications of a wide frequency range.

Chapter 6 summarizes the dissertation by concluding the general synthesis procedure and the similar design concept among the proposed wideband circuits. With the proposed circuit design principle, more advanced wideband BPFs could be synthesized and designed to meet the required specifications. As the ending part, some future works are described.

CHAPTER 2

LITERATURE REVIEW

2.1 Introduction

RF/Microwave bandpass filters (BPFs) have been extensively studied and developed for a long time to meet various requirements in many modern communication systems [2-5]. A number of papers and textbooks in filter design have summarized different classes of design method and their applicable circuit topologies or layouts [14–20]. For the literature review in this section, it mainly discusses from these two aspects, the wideband BPF design/synthesis method and the circuit structures for wideband BPF design.

To meet various design targets, several kinds of filtering functions have been explored to achieve equal ripples within the passbands of the interest, but there are different methods of locating the TZs. The most commonly used one would be Chebyshev filtering function with all the TZs locating at the infinity [1]. The general Chebyshev one re-locates the TZs from the infinity to the edges of the passband to improve the rejection or to modify the group delay [21], [22]. Some other modified general Chebyshev filtering functions with its special features have been introduced in the second part of this chapter [23].

The next part introduces some widely used circuit schematics to design the single-/dual-wideband BPFs. One of the direct methods for the single-wideband BPF design is to inter-connect short-circuited stubs and the commensurate line [2], and another is to use the concept of MMR such that the resonances are grouped to form the desired passband [6]. Following the similar design techniques, the design of the dual-wideband BPF has also been briefly introduced.

In the last part, the computer-aided-design (CAD) techniques for the microwave circuit design and the compensation methods for the coupled lines have been briefly introduced.

2.2 Filtering Functions

Almost all of the frequency responses of the filter could be characterized by the filtering functions formed by the ratio of two polynomials. Depending on the locations of the TZs and their usage, there are a few classes, namely, Chebyshev, general Chebyshev, the modified one etc.. In this section, the derivation of the Chebyshev function is briefly introduced. After that, a recursive method to expand this filtering function into a ratio of two polynomials is discussed. Based on the aforementioned function and its mathematical manipulation skills, the general Chebyshev filtering function is readily followed with a similar formulating strategy and recursive expanding method. Finally, a more advanced filtering function is presented with the capability to model a wideband BPF frequency response.

2.2.1 Chebyshev Filtering Function

From the relationship between the filtering function and the transmission coefficient as listed in (1.1), the transfer function varies as a function of the filtering function F_n as

$$|S_{21}|^2 = \begin{cases} 1, & F_n = 0 \\ \frac{1}{1 + \varepsilon^2}, & F_n = 1 \\ 0, & F_n = \infty \end{cases} \quad (2.1)$$

Within the normalized passband $(-1, 1)$, the filtering function varies between $(-1, 1)$, making the square of the transmission coefficient changing between $(1/(1+\varepsilon^2), 1)$. Outside of the passband, the filtering function increasingly goes to the infinity,

leading to the growth of the out-of-band rejection. Examples of 4th- and 5th-order Chebyshev functions are plotted in Figure 2-1.

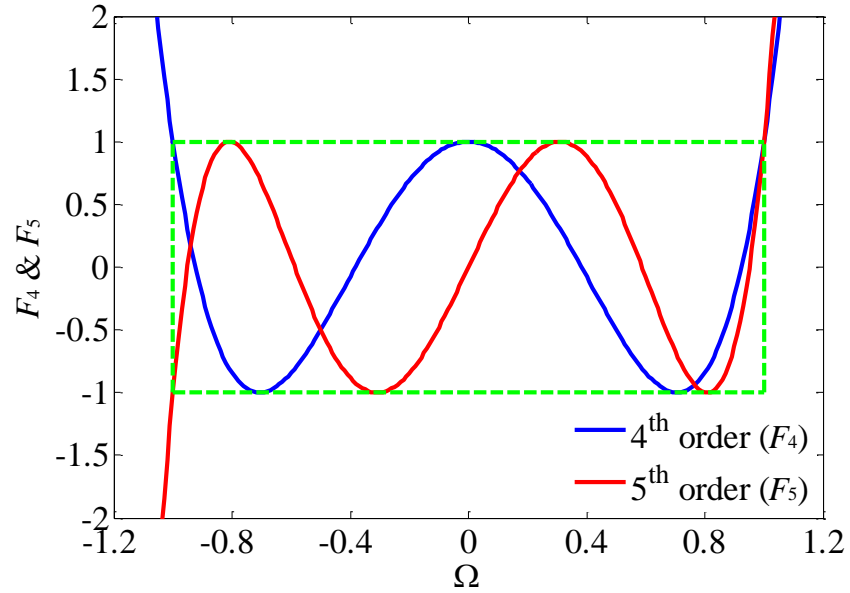


Figure 2-1. The 4th- and 5th-order Chebyshev function as a function of Ω .

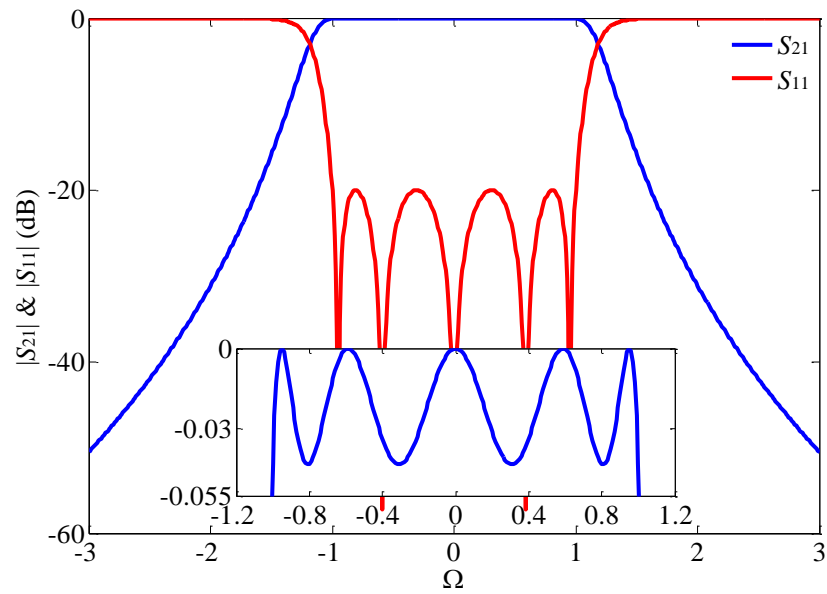


Figure 2-2. Typical 5th-order Chebyshev frequency response with $\epsilon = 0.1$.

The n^{th} -order Chebyshev function F_n has the following properties: [17]

(a) F_n is even (odd) polynomial if n is even (odd);

(b) F_n locates all the zeroes within the range $-1 < \Omega < 1$;

(c) F_n varies between $-1 < F_n < 1$ within the range $-1 < \Omega < 1$;

(d) for the two boundary points ($\Omega = \pm 1$), $F_n(1) = 1$ and $F_n(-1) = \pm 1$, which can be rewritten as $|F_n(\pm 1)| = 1$.

Thus, the function F_n is defined in the form of (which satisfies all the properties mentioned above from (a)-(d))

$$\frac{dF_n}{d\Omega} = C_m \frac{\sqrt{1-F_n^2}}{\sqrt{1-\Omega^2}} \rightarrow \frac{dF_n}{\sqrt{1-F_n^2}} = C_m \frac{d\Omega}{\sqrt{1-\Omega^2}} \quad (2.2)$$

where C_m is defined as a constant.

Integrating both sides gives

$$\begin{cases} \cos^{-1}(F_n) = C_m \cos^{-1}(\Omega) \\ F_n = \cos(C_m \cos^{-1}(\Omega)) \end{cases} \quad (2.3)$$

For F_n having n zeroes within $-1 < \Omega < 1$, C_m is readily chosen as n . Therefore, the n^{th} -order Chebyshev function is written as

$$F_n = \cos(n \cos^{-1}(\Omega)) \quad (2.4)$$

Using the property of trigonometric functions, the Chebyshev function of $(n+1)^{\text{th}}$ - and $(n-1)^{\text{th}}$ -order are expanded in the form of

$$\begin{aligned}
F_{n+1}(\Omega) &= \cos((n+1)\cos^{-1}(\Omega)) \\
&= \cos(n\cos^{-1}(\Omega))\cos(\cos^{-1}(\Omega)) - \sin(n\cos^{-1}(\Omega))\sin(\cos^{-1}(\Omega))
\end{aligned} \tag{2.5}$$

$$\begin{aligned}
F_{n-1}(\Omega) &= \cos((n-1)\cos^{-1}(\Omega)) = \cos(n\cos^{-1}(\Omega) - \cos^{-1}(\Omega)) \\
&= \cos(n\cos^{-1}(\Omega))\cos(\cos^{-1}(\Omega)) + \sin(n\cos^{-1}(\Omega))\sin(\cos^{-1}(\Omega))
\end{aligned} \tag{2.6}$$

By canceling the common component, $\sin(n\cos^{-1}(\Omega))\sin(\cos^{-1}(\Omega))$, a recursive formula is obtained as

$$\begin{cases} F_{n+1}(\Omega) = 2\Omega F_n(\Omega) - F_{n-1}(\Omega) \\ F_0(\Omega) = \cos(0\cos^{-1}(\Omega)) = 1 \\ F_1(\Omega) = \cos(1\cos^{-1}(\Omega)) = \Omega \end{cases} \tag{2.7}$$

A typical 5th-order Chebyshev filtering is illustrated in Figure 2-2. As Ω approaches to the infinity, the out-of-band rejection increases continuously.

2.2.2 General Chebyshev Filtering Function

The Chebyshev filtering function has been widely used for the BPF design. However, since all its TZs are at infinity, to increase the out-of-band rejection, there is no way but to add the order of the filter. The general Chebyshev filtering function is reported as an alternative one to re-locate the TZs near the edges of the passband, as shown in Figure 2-3. Ω_{TZi} represents the i^{th} TZ ($i= 1, 2, \dots$). $\Omega_i(\Omega)$ is defined as a function of Ω as [1]

$$\Omega_i(\Omega) = \frac{1 - \Omega\Omega_{TZi}}{\Omega - \Omega_{TZi}} \tag{2.8}$$

Therefore, $\Omega_i(\Omega)$ satisfies the following characteristics:

(a), approaching infinity at Ω_{TZi} ;

(b), having no influence on the normalized bandwidth, $|\Omega_i(\pm 1)| = 1$.

Thus the general Chebyshev function is in the form of

$$C_n(\Omega) = \cosh \left(\cosh^{-1} \left(\sum_{i=1}^n \frac{1 - \Omega \Omega_{TZi}}{\Omega - \Omega_{TZi}} \right) \right) = \cosh \left(\cosh^{-1} \left(\sum_{i=1}^n \Omega_i(\Omega) \right) \right) \quad (2.9)$$

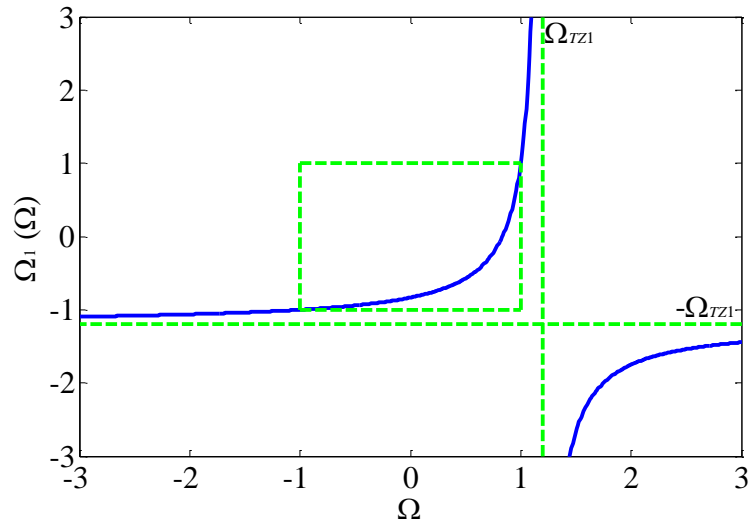


Figure 2-3. $\Omega_1(\Omega)$ as a function of Ω with TZ located at $\Omega_{TZ1} = 1.2$.

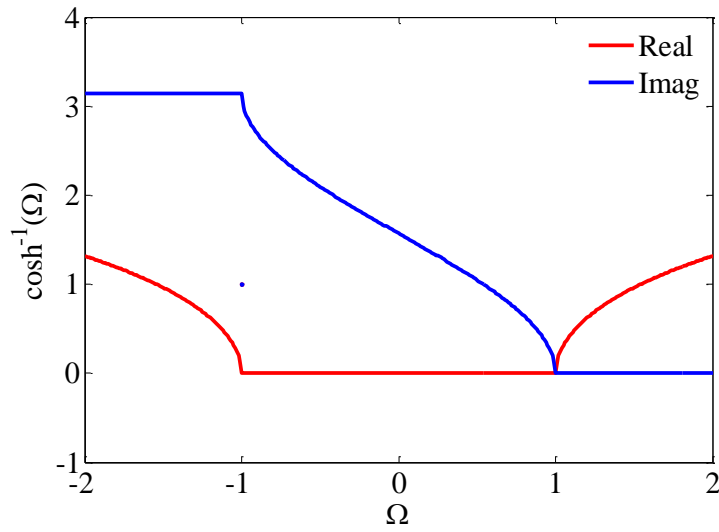


Figure 2-4. The real and imaginary part of $\cosh^{-1}(\Omega)$ as a function of Ω .

An example of $\Omega_i(\Omega)$ with $i=1$ ($\Omega_1(\Omega)$) is plotted in Figure 2-3.

A further investigation into the property of the function \cosh and \cosh^{-1} reveals that the combination of these two functions creates an equal ripple factor within the band of $[-1, 1]$ and an increasing attenuation beyond that band, as shown in Figure 2-4. When sweeping between $[-1, 1]$, the real part of $\cosh^{-1}(\Omega)$ ($= 0$) has no influence towards the result, and the imaginary part of $\cosh^{-1}(\Omega)$ varies between $[0, \pi]$, leading to the ripple-curve within the passband. Beyond the range of $[-1, 1]$, the real part increases monotonously, contributing to the attenuation of the rejection band.

Similar to the Chebyshev function, a recursive formula is derived here to expand the general Chebyshev function $C_n(\Omega)$ as a ratio between the two polynomials, the denominator $D_n(\Omega)$ and numerator $P_n(\Omega)$. They are in the form of

$$C_n(\Omega) = \frac{P_n(\Omega)}{D_n(\Omega)} = \frac{P_n(\Omega)}{\prod_{i=1}^n (1 - \frac{\Omega}{\Omega_{TZi}})} \quad (2.10)$$

where $D_n(\Omega)$ collects all the TZs. Further, using the property of the triangular function, $C_{n+1}(\Omega)$ and $C_{n-1}(\Omega)$ are expanded as

$$\begin{aligned} \frac{P_{n+1}(\Omega)}{D_{n+1}(\Omega)} &= \cosh\left(\sum_{i=1}^n \cosh^{-1}(\Omega_i) + \cosh^{-1}(\Omega_{n+1})\right) \\ &= \Omega_{n+1} \frac{P_n(\Omega)}{D_n(\Omega)} + \sinh\left(\sum_{i=1}^n \cosh^{-1}(\Omega_i)\right) \sinh(\cosh^{-1}(\Omega_{n+1})) \end{aligned} \quad (2.11)$$

$$\begin{aligned} \frac{P_{n-1}(\Omega)}{D_{n-1}(\Omega)} &= \cosh\left(\sum_{i=1}^n \cosh^{-1}(\Omega_i) - \cosh^{-1}(\Omega_n)\right) \\ &= \Omega_n \frac{P_n(\Omega)}{D_n(\Omega)} + \sinh\left(\sum_{i=1}^n \cosh^{-1}(\Omega_i)\right) \sinh(\cosh^{-1}(\Omega_n)) \end{aligned} \quad (2.12)$$

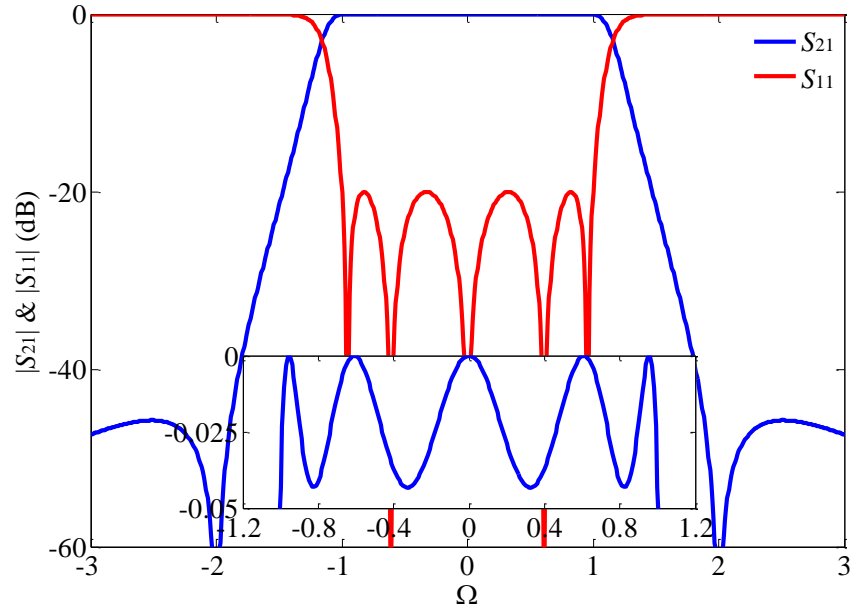


Figure 2-5. Typical 5th-order general Chebyshev frequency response (the design specifications: $\epsilon = 0.1$ and $\Omega_{TZ(1,2)} = \pm 2$).

By canceling the common component, $\sinh(\sum_{i=1}^n \cosh^{-1}(\Omega_i))$, the numerator

$P_{n+1}(\Omega)$ is calculated by its previous counterparts by [16]

$$P_{n+1}(\Omega) = \begin{cases} \left(\left(\Omega - \frac{1}{\Omega_{TZn}} \right) \sqrt{\frac{(1 - \frac{1}{\Omega_{TZ(n+1)}^2})}{(1 - \frac{1}{\Omega_{TZn}^2})}} + \left(\Omega - \frac{1}{\Omega_{TZ(n+1)}} \right) \right) P_n(\Omega) \\ - \left(1 - \frac{\Omega}{\Omega_{TZn}} \right)^2 \sqrt{\frac{(1 - \frac{1}{\Omega_{TZ(n+1)}^2})}{(1 - \frac{1}{\Omega_{TZn}^2})}} P_{n-1}(\Omega) \end{cases}$$

$$P_0(\Omega) = 1$$

$$P_1(\Omega) = \Omega - \frac{1}{\Omega_{TZ1}}$$
(2.13)

A typical 5th-order general Chebyshev filtering response is illustrated in Figure 2-5. A pair of TZs (one at $\Omega= 2$ and the other at $\Omega= -2$) is located at the real frequencies in the passband, thus improving the attenuation near the edge of the passband.

2.2.3 Modified General Chebyshev Filtering Function

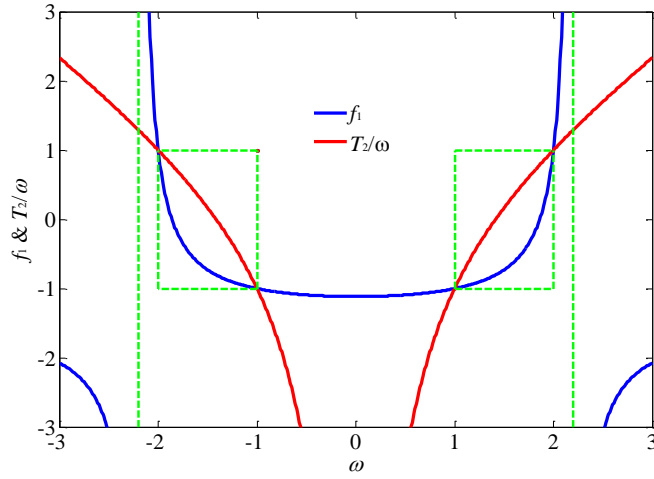


Figure 2-6. The functions of $T_2(\omega)/\omega$ and f_1 as a function of ω with the passband defined as $B= [1, 2]$ and the TZ located at $z_1= 2.2$.

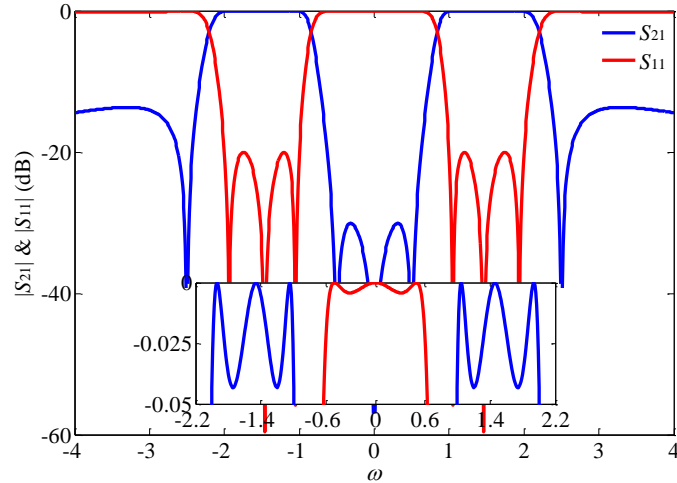


Figure 2-7. Typical 3rd-order modified general Chebyshev frequency response with the passband defined as $B= [1, 2]$, the TZ located at $z_1= 2.5$ and $z_2= 0.5$ and $\epsilon= 0.1$.

In this section, a modified general Chebyshev filtering function has been discussed. It is noted that this filtering function is firstly proposed for a single-wideband BPF design, which asks for no frequency transformation. Therefore, it is discussed directly in the ω frequency plane. It has some unique characteristics which are listed below [23].

(a) Having a passband at $B = [\omega_1, \omega_2]$;

(b) Being symmetrical with respect to the origin with another band at $-B$;

(c) Assigning a TZ at the origin and the rest at the arbitrary place of the finite frequencies z_k ($k = 1, 2, \dots, n-1$, where n is the number of reflection zeros).

The definition of the modified Chebyshev function is

$$F_n(\omega) = \cosh(\cosh^{-1}(\frac{T_2(\omega)}{|\omega|}) + \sum_{k=1}^{n-1} \cosh^{-1}(f_k(\omega))) \quad (2.14)$$

where $T_2(\omega)$ contributes to the TZ at the origin and $f_k(\omega)$ the TZs at the arbitrary places of the finite frequencies. These two functions are defined as

$$T_1(\omega) = \frac{1}{\omega_2^2 - \omega_1^2} (2\omega^2 - (\omega_1^2 + \omega_2^2)) \quad (2.15)$$

$$f_k(\omega) = \frac{T_1(\omega) - \frac{1}{T_1(z_k)}}{1 - \frac{T_1(\omega)}{T_1(z_k)}} \quad (2.16)$$

$$T_2(\omega) = \frac{1}{\omega_2 - \omega_1} (\omega^2 - \omega_2\omega_1) \quad (2.17)$$

A sample of $T_2(\omega)/\omega$ and f_1 versus ω is plotted in Figure 2-6.

The function $F_n(\omega)$ is rational, i.e.,

$$F_n(\omega) = \frac{r_n(\omega)}{h_n(\omega)} = \frac{r_n(\omega)}{\omega \prod_{k=1}^{n-1} \left(1 - \frac{T_1(\omega)}{T_1(z_k)}\right)} \quad (2.18)$$

where the denominator of $F_n(\omega)$ collects all the TZs, $\{0, -z_{n-1}, \dots, -z_1, z_1, \dots, z_{n-1}\}$. To compute $r_n(\omega)$, the following recursion relations are used

$$\begin{cases} r_0(\omega) = \cosh(0) = 1 \\ f_1(\omega) = \cosh(\cosh^{-1}(\frac{T_2(\omega)}{\omega})) = \frac{T_2(\omega)}{\omega} \Rightarrow r_1(\omega) = T_2(\omega) \\ r_2(\omega) = -\gamma_1(\omega^2 - r_1(\omega)^2) + r_1(\omega)(T_1(\omega) - s_1) \\ r_k(\omega) = -\gamma_{k-1}r_{k-2}(\omega)(1 - s_{k-2}T_1(\omega))^2 \\ \quad + r_{k-1}(\omega)(T_1(\omega) - s_{k-1} + \gamma_{k-1}(T_1(\omega) - s_{k-2})), \quad k > 2. \end{cases} \quad (2.19)$$

where

$$\begin{aligned} s_k &= \frac{1}{T_1(z_k)} \\ \gamma_1 &= \frac{2}{\omega_1 + \omega_2} \sqrt{1 - s_1^2} \\ \gamma_k &= \sqrt{\frac{1 - s_k^2}{1 - s_{k-1}^2}}, \quad k > 1. \end{aligned} \quad (2.20)$$

For each passband, a 3rd-order modified general Chebyshev frequency response is illustrated in Figure 2-7. A symmetrical response with respect to the origin is obtained and a TZ is located in the center. Some other methods to get the required filtering function have also been reported in [24].

2.3 Frequency Transformation

The aforementioned filtering functions are formulated in the normalized frequency or applicable to a single-band design. Thus, a frequency transformation is required to move the filtering function to obtain the target center frequency and the bandwidth or to transfer a single-band response to a dual-/multi-band one.

In the following paragraphs, a brief review of the commonly used frequency transformations for a bandpass filter design is introduced. Then, the Richard's transformation is discussed for the convenience of distributed circuit design. Finally, there is an introduction on some newly reported techniques to transfer the single-band to dual-/multi-band design.

2.3.1 Typical Lowpass to Bandpass Transformation

One of the most commonly used frequency transformation from lowpass to bandpass is defined as [1]

$$\Omega = \frac{1}{FBW} \left(\frac{j\omega}{\omega_0} + \frac{\omega_0}{j\omega} \right) \quad (2.21)$$

where ω_0 represents the center frequency of the passband and FBW the fractional bandwidth.

Therefore, an inductor/capacitor (L/C) extracted in the normalized frequency is transformed to a series/parallel connected LC component, respectively, which brings the lowpass to a bandpass response.

2.3.2 Richard's Transformation

The typical lowpass to bandpass transformation could be conveniently modeled by the transformation of LC circuits. To apply the distributed transmission line in the BPF design, Richard's transformation is used as [25]

$$\Omega = \tan \theta \quad (2.22)$$

where $\theta = \theta_0 \omega / \omega_0$, with θ_0 as the electrical length at a reference frequency ω_0 .

It is also noted that using the Richard's transformation leads to the periodic characteristics due to the introduction of the $\tan \theta$ function. The direct result of the Richard's transformation is to equate the input impedances of both the LC component and the distributed transmission line, although they are located in the different planes (the θ -plane and the Ω -plane). Thus, the inductor is transformed as the short-circuited stub, and the capacitor as the open-circuited stub by (2.22). There is another class of distributed element, the unit element, which has no corresponding LC equivalent. Its $ABCD$ matrix is in the form of ($t_r = j \tan \theta$)

$$\begin{bmatrix} A & B \\ C & D \end{bmatrix} = \frac{1}{\sqrt{1-t_r^2}} \begin{bmatrix} 1 & Z_u t_r \\ t_r / Z_u & 1 \end{bmatrix} \quad (2.23)$$

After the Richard's transformation, the corresponding $ABCD$ matrix becomes

$$\begin{bmatrix} A & B \\ C & D \end{bmatrix} = \begin{bmatrix} \cos \theta & jZ_u \sin \theta \\ j \sin \theta / Z_u & \cos \theta \end{bmatrix} \quad (2.24)$$

which is a two-port transmission line with the characteristic impedance of Z_u .

There is another transformation ($\Omega = 1/\tan \theta$), which transfers the inductor as the open-circuited stub and the capacitor as the short-circuited stub. The difference

between the two transformations is mainly at the location of the center frequency. Figure 2-8 illustrates two transformed frequency responses via the function of $\tan\theta$ and $1/\tan\theta$ to form the lowpass and bandpass filtering response, respectively.

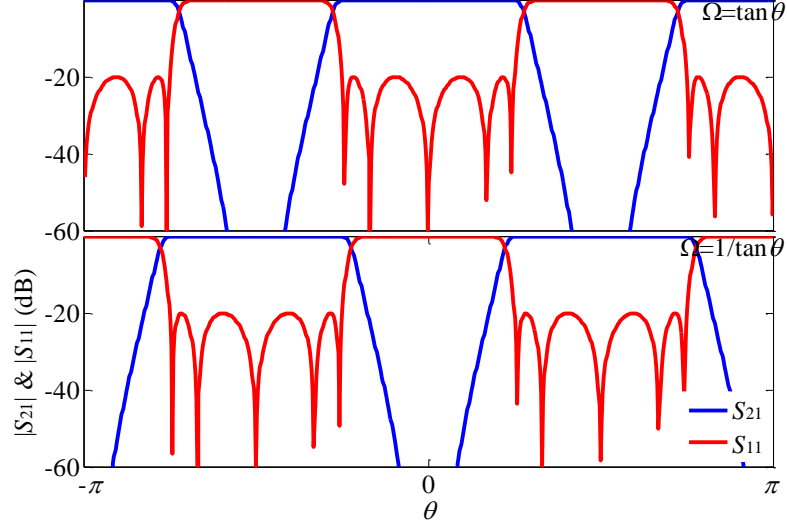


Figure 2-8. Frequency responses under the transformation of $\Omega = \tan\theta$ and $\Omega = 1/\tan\theta$ (the prototype Chebyshev function as $\cos(5\cosh^{-1}(\theta))$ and $\epsilon = 0.1$).

2.3.3 Single-Band to Dual-/Multi-Band Design

Recently, some mapping/frequency transformation techniques have been proposed to design more advanced BPFs [26–30]. One example is using the following mapping equation to transfer a single resonator to a multi-band block [26]

$$\bar{\omega} = \omega - \sum_{j=1}^{n-1} \frac{ks_j^2}{\omega + bs_j} \quad (2.25)$$

where n is the number of passbands that is to transfer, bs_j is the frequency invariant susceptance and ks_j is the admittance inverter.

After the mapping, a single resonance within the normalized passband is transferred to the n resonances with one for each passbands. Then, a design

algorithm is applied to accurately determine the values of b_j and k_j in order to have the desired center frequency of the specified passbands, the bandwidth and the determined locations of TZs.

2.4 Single-Wideband Bandpass Filter Design

A number of design techniques and synthesis methods on the wide or ultra-wideband BPFs with the FBW about 110% have been extensively studied for UWB systems [31]. The concept of the MMR has been proposed for the exploration of a class of UWB filters. The resonant modes of the MMR are quasi-equally placed within the passband and the frequency-dependent external loading structures are utilized to feed the MMR [6]. An alternative method to design the UWB filter is based on the optimum distributed structure, which is originally derived for a highpass filter design [32].

2.4.1 Wideband Filters Using MMRs

One of the most effectively and widely used techniques for the wideband BPF design is the MMR-oriented methodology [3]. By using the first and the next few higher-order resonances, the bandwidth is roughly determined. Further, by appropriately introducing external loading structure of the MMR, the passband with flat frequency response is formed. Different forms or geometries of MMRs have been reported based on this design method [33–36]. However, most of these MMRs lack an analytical approach to determine the location of the reflection zeroes and are mainly designed on a cut-and-try process. To solve this problem, the stepped-impedance MMRs are explored with a set of determinant equations to predict its frequency response [12], [37–41]. By using parallel coupled lines or short-circuited stubs, the multi-resonances of the MMR are excited.

The synthesis method follows the general steps, as documented in [1-5]. First, the response is derived in the form of a transfer function. After that, a filtering

function is selected as the target to fulfill the design specifications, and finally, the circuit design parameters are set to apply the transfer function to the filtering function.

Other techniques have also been reported based on the above mentioned MMR and its design procedure. With this technique, the constructed filters can realize the steep rejection slope, wide rejection bandwidth, compact circuit size and the capability in introducing a notch band as required [42], [43].

2.4.2 Wideband Filters Using Optimum Distributed Structures

An alternative method to design a wideband bandpass filter is by cascading the commensurate line with the short-circuited stubs shunt on its two sides [2], [32], [44]. The design principle of the circuit scheme is different from that of the MMR, though there seems to have some similarities in the circuit layout. The commensurate line serves as an admittance inverter, and the short-circuited stub is viewed as a parallel connected LC resonator. Thus, the number of the reflection zeros in the passband is obtained as $(2n-1)$ with n as the number of short-circuited stubs. A detailed design flow chart and the related formulas have been documented in [2], and a table for the specific ripple factor is used for a quick determination of the design parameters.

2.5 Dual-Narrow/Wideband Bandpass Filter Design

There are many techniques and design methods proposed to design dual-band BPFs. One of the direct design methods for the dual-band BPFs is to parallel connect two single-band BPFs [45], [46]. In [45], two monolithic narrowband BPFs with different center frequencies are parallel connected by dual-band impedance matching networks. Thus, each single-band BPF is responsible for filtering one passband. Using a similar technique, a dual-band BPF for ultra-wideband (UWB) systems has been developed in [46]. However, this method requires a complex design process and relatively large circuit size, since two BPFs as well as the related matching network are involved.

Another class of dual-band BPFs is formed by inserting a bandstop filtering response into a wide passband to divide it into two passbands [47], [48]. In [47], a bandstop filter (BSF) is cascaded after a wideband BPF, and in [48], the BSF is integrated into the BPF filter. Both designs have successfully realized the dual-band designs and have the capability to adjust the bandwidths of each passband and the rejection band. However, it still needs tuning and optimizing effort after the combination of the BPF and the BSF, even if the detailed synthesis and design procedures are available for the two basic filter components.

To simplify the dual-band bandpass filter design process, some frequency transformation techniques have been proposed [49], [26]. A method by successive frequency transformations from a lowpass to a bandpass, and then to a dual-band bandpass frequency response has been proposed in [49]. After the transformation, the dual-band BPF is realized with only the J -inverters and series LC resonators. In [26], a mapping method based on transferring a single-band resonator to a multiple-band network has been used to formulate the filtering function and the corresponding filtering structure. However, for the existing designs based on the frequency transformations, they are limited to the narrowband dual-band BPF design.

On the other hand, a great amount of the research work focuses on applying the fundamental- and its higher-order resonances to form the various dual-band BPFs, as discussed in [50–55]. Stepped-impedance resonators (SIRs) capacitively coupled by parallel coupled lines and inductively fed by short-circuited stubs have been proposed in [50] and [51], respectively. To reduce the overall size of the circuit, single ring/patch resonators have also been used to form a dual-mode dual-band BPFs [52], [53]. Other techniques include using the even-/odd- modes of a dual-mode resonator to form different signal transmitting paths for each passband, as discussed in [54], [55]. The general design procedure for these classes of filters follows by assigning the 1st- and 2nd-order resonances of the resonator to the center frequencies of each band, deriving the dual-band J -/ K -inverters and applying the BPF prototype to design each passband. However, due to the approximate conditions used, they are only applicable to narrow band design.

A concept of signal interference has been used for a BSF design [56-60]. By parallel connecting two transmission lines of 180° phase difference, TZs are introduced to form a stopband [56], [57]. Based on this technique, dual-band BPFs are realized in [58-60] with the additional stubs to further define the two passbands. In [61], a transversal structure formed by the upper and lower sections of the coupled lines is used to introduce TZs between the two passbands. However, most of the designs lack a systematic design procedure to fulfill specific design specifications. As for more practical cases, the synthesis method for the dual-band BPFs with the asymmetry frequency response has been discussed in [62], and realized by stepped-impedance lines to individually adjust the bandwidth of the two passbands in [63].

2.6 Computer Aided Design of Planar Filters

A typical circuit design based on the optimization methods starts with the predefined specifications. Then, a modeling technique or the analysis method is applied to evaluate the circuit performance. After that, this circuit response is compared with the given specifications. If it meets the requirement, the design process ends, otherwise, the design parameters are altered until specifications are satisfied. A basic flow chart for the computer-aided-design (CAD) of a circuit is shown in Figure 2-9.

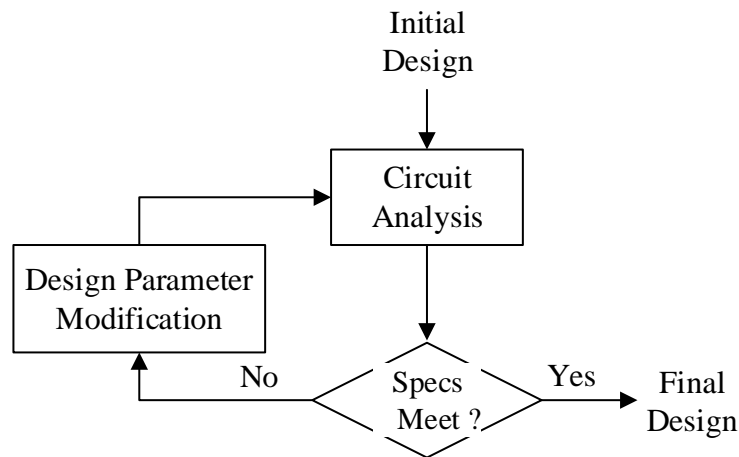


Figure 2-9. Flow chart of a typical optimization process [64].

2.6.1 Basic Concept and Definitions for Optimization

Following the discussion in the previous paragraph, there are two kinds of methods to modify the design parameters. One is the gradient method using the derivatives of the functions/numeric results to approach the optimum values and another one is the direct search method to search for the optimum ones in a systematic way [64]. In the following paragraph, some general considerations about the optimization process are discussed.

The general purpose of an optimization procedure is to minimize the gap between the response obtained from a circuit and the ideal response generated from the design specifications. The function to describe this difference is defined as the objection function. Occasionally, to speed up the optimization process, a concept of weighted error is introduced as

$$e(\phi, \psi) = w(\psi)[F(\phi, \psi) - S(\psi)] \quad (2.26)$$

where $S(\psi)$ is the ideal response as a function of frequency or time ψ , $F(\phi, \psi)$ the response from the circuit analysis of a certain design parameter ϕ , $w(\psi)$ the weighting function to determine the priority of a chosen variable ψ , and the weighted function is defined by $e(\phi, \psi)$. There are many techniques and methods documented in the literature [65–68] to find the minimum value of $e(\phi, \psi)$.

2.6.2 Optimization for Microwave BPF Design

Optimization process has also been extensively used in the design of microwave filters, as documented in [69–72]. One example is to use the optimization method to get the ideal filtering function to meet the required design target [70]. The coupling matrix to represent a frequency response meeting the specifications is synthesized by a gradient based optimization method, in which analytical expression of the gradient for cost function is derived. Another example is to use the optimization process to determine the circuit design parameters [71]. Once the ideal filtering function is obtained, the circuit response is forced to match with the ideal one. Thus, a set of non-linear equations is obtained. By solving these equations with the optimization method, the circuit design parameters are obtained in the end. Other example is like using the optimization process to determine the quality factor [72].

2.7 Capacitive Compensation for Coupled Lines

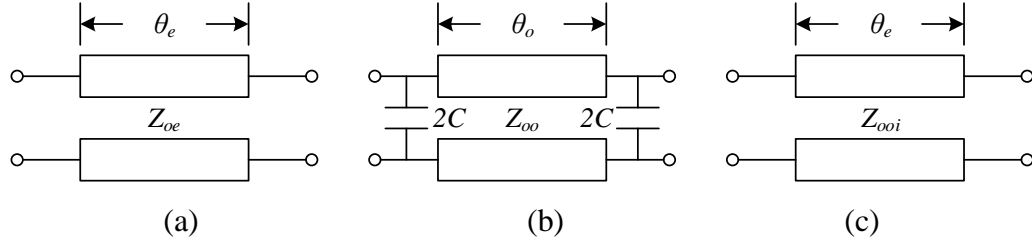


Figure 2-10. Equivalent circuits of even- and odd-modes. (a) Even-mode circuit. (b) Odd-mode circuit. (c) Derived odd-mode circuit with modified phase velocity.

A compensation method for coupled lines has been discussed for the success of the practical design/layout of the circuit structure. To simplify the discussion and to permit the application of the filtering function, the phase velocities of the even- and odd-modes are set to be equal to each other. As for the practical property of the coupled lines, this is not the real case. To compensate for this effect, many techniques have been proposed [73–76].

Herein, a method by loading capacitive coupling on the two sides of the coupled line has been used [73]. Three main steps are used to derive the equal phase velocities between the even- and odd-modes at the center frequency of the coupled line, as illustrated in Figure 2-10. First, an even-/odd-mode analysis method is applied to the coupled line to obtain the two-port network in Figure 2-10 (a) and (b). Next, a modified equivalent circuit is obtained by neglecting the loaded capacitive coupling and equating the phase velocity as that of the even-mode circuit. To permit the above mentioned modifications, the odd-mode characteristic impedance is changed from Z_{oo} to Z_{ooi} . The $ABCD$ matrix of the three equivalent circuits is listed as

$$\begin{bmatrix} A & B \\ C & D \end{bmatrix}_e = \begin{bmatrix} \cos \theta_e & jZ_{oe} \sin \theta_e \\ jY_{oe} \sin \theta_e & \cos \theta_e \end{bmatrix} \quad (2.27)$$

$$\begin{bmatrix} A & B \\ C & D \end{bmatrix}_o = \begin{bmatrix} \cos \theta_o - 2\omega CZ_{oo} \sin \theta_o & jZ_{oo} \sin \theta_o \\ j\left(4\omega C \cos \theta_o + (Y_{oo} - Z_{oo}(2\omega C)^2) \sin \theta_o\right) & \cos \theta_o - 2\omega CZ_{oo} \sin \theta_o \end{bmatrix} \quad (2.28)$$

$$\begin{bmatrix} A & B \\ C & D \end{bmatrix}_{oi} = \begin{bmatrix} \cos \theta_e & jZ_{ooi} \sin \theta_e \\ jY_{ooi} \sin \theta_e & \cos \theta_e \end{bmatrix} \quad (2.29)$$

To equate the equivalent circuit in Figure 2-10 (b) and (c), their corresponding entries in the $ABCD$ matrix are set to be equal as

$$\begin{cases} \cos \theta_e = \cos \theta_o - 2\omega CZ_{oo} \sin \theta_o \\ jZ_{oo} \sin \theta_o = jZ_{ooi} \sin \theta_e \end{cases} \quad (2.30)$$

At the center frequency of the coupled line, the electrical length of the even-mode circuit is 90° , and the one of the odd-mode is calculated related to its counterpart as

$$\begin{cases} \theta_e = \frac{\pi}{2} \\ \theta_o = \frac{2\pi}{\lambda_{go}} l = \frac{\pi}{2} \sqrt{\frac{\epsilon_{effo}}{\epsilon_{effe}}} \end{cases} \quad (2.31)$$

Substituting the calculated phase velocities into equation (2.30), the required capacitor and the practical odd-mode characteristic impedance are obtained by

$$C = \frac{\cos \theta_o}{2\omega CZ_{ooi}} = \frac{\cos \left(\frac{\pi}{2} \sqrt{\frac{\epsilon_{effo}}{\epsilon_{effe}}} \right)}{2\omega CZ_{ooi}} \quad (2.32)$$

$$Z_{oo} = \frac{Z_{ooi}}{\sqrt{1 - \left(\cos \left(\frac{\pi}{2} \sqrt{\frac{\epsilon_{effo}}{\epsilon_{effe}}} \right) \right)^2}} \quad (2.33)$$

2.8 Conclusions

In this chapter, several classes of filtering function have been introduced to meet different design specifications. To connect these normalized functions with the practical circuit responses, the frequency transformation has been applied. The purpose of this transformation is to scale the normalized frequency to the required center frequency and bandwidth as well as to deduce the advanced filtering functions. Next, some commonly used wideband BPF structures have been covered. In the end, a brief introduction on the technique of optimization for the microwave BPF design is introduced.

CHAPTER 3

SYNTHESIS AND DESIGN OF A WIDEBAND BANDPASS FILTER WITH INDUCTIVELY FED SHORT-CIRCUITED MULTI-MODE RESONATOR

3.1 Introduction

In this chapter, two single-wideband BPFs based on the concept of the MMRs have been discussed. The concept of the stepped-impedance MMR has been proposed for a long time with its unique characteristics for the UWB filter design [6]. Most of the wideband BPF designs based on MMRs are in the structure of open-circuited resonator which depends on the degree of coupling provided by parallel coupled lines. For the short-circuited MMR, most designs are based on the coplanar-waveguide (CPW) for its simplicity in providing short-ended circuits. For the designs in this chapter, some new design structures are realized in microstrip structure.

The first wideband BPF design is by inductively loading the MMRs with two identical short-ended stubs, and a Chebyshev frequency response is achieved. Moreover, a general procedure is presented for the design of these filters with the desired frequency responses and the corresponding circuit transfer function.

To improve the filtering response, a new wideband BPF with the composite short- and open-circuited stubs has been proposed. With the use of these two kinds of stubs, a filtering response with steep rejection slope is obtained because of two pairs of TZs excited.

3.2 Synthesis and Design of Chebyshev-Response Wideband Filter

In this chapter a class of wideband BPFs with short-circuited MMRs is proposed and designed. In the meanwhile, to determine its design parameters, a general synthesis approach is also explored. The proposed MMRs are formed by n sections of cascaded transmission lines. For every section, it is set to be one quarter wavelength long with respect to the center frequency of the passband. As the number of the section increases, the filter order increases accordingly. The short-ended stubs at the two ends of the MMR are inductive loading elements to feed the MMR. For the filter synthesis, a transfer function is derived to characterize the circuit responses, and it is enforced to apply to the equal-ripple in-band responses. As such, the characteristic impedance for each section is determined. With this synthesis method, the design curves of different orders and ripple factors are provided to aid the design of a class of wideband BPFs. As an example, a fifth-order ultra-wideband filter is designed, fabricated and measured in the end, which has strongly verified the design principle.

3.2.1 Working Mechanism of the Proposed Circuit

Figure 3-1 shows the schematic of n ($n= 1, 2, 3$ and 4) sections of the cascaded transmission lines loaded by the short-ended stubs on the two sides, where the cascaded lines are viewed as the short-circuited resonators. In the following, the discussion is based on the number of n . For $n= 1$ as seen in Figure 3-1(a), the two short-ended stubs contribute to the two resonances in the passband, and it is the unit element for design of a class of the wideband BPFs, as discussed and tabulated in [2] and [20]. For $n= 2$ as seen in Figure 3-1(b), the resonator is referred to as a half wavelength short-circuited resonator and it works together with the two stubs on the two sides to produce the total three resonances. When n is further increased to 3 and 4 as shown in Figure 3-1(c) and (d), more resonances are introduced in the passband, behaving as 4th and 5th order filtering responses. Thus, the short-circuited resonators

of n sections is similar to the stepped-impedance shaped MMR for wide or ultra-wideband BPF design, as discussed in [6] and [39], which introduces $n-1$ resonances within the passband.

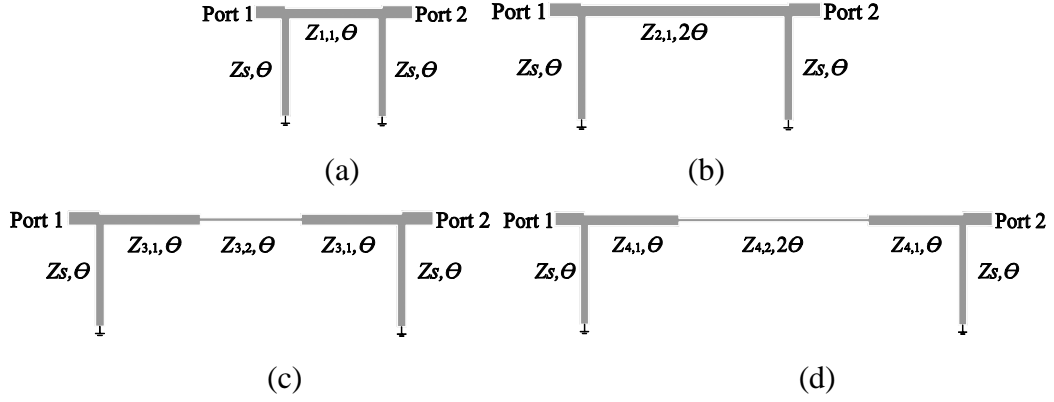


Figure 3-1. Schematics of a class of inductively fed MMRs formed by cascading n sections of transmission lines. (a) $n=1$. (b) $n=2$. (c) $n=3$. (d) $n=4$.

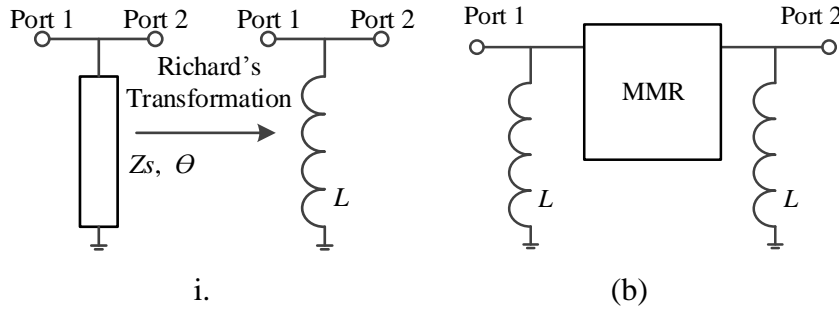


Figure 3-2. (a) The short-end stub is transferred to the inductor via Richard's transformation. (b) The MMR is inductively fed by inductors.

Different from the design in [6] where the parallel coupled lines are used to feed the MMR. The short-end stubs are regarded as inductive loading elements to feed the MMR, as seen in Figure 3-2. A simple explanation of this phenomenon is by applying the Richard's transformation which transfers the bandpass filtering response to the lowpass one. In the meanwhile, the short-end stubs are transferred as the inductors serving as an inductive loading nature. That is, the short-circuited resonators in the form of the cascaded transmission lines have the magnetic fields (or simply referring as the currents) reaching the maximum at the two shorted ends. To feed this resonator, the input and output ports are directly connected to the two

short-circuited ends to provide an inductive loading. To adjust this inductive loading, the short-ends stubs are used on the two sides of the MMR. During this process, the actual grounding on the two sides of the MMR is removed.

3.2.2 Circuit Analysis and Synthesis Procedure

Next, a general synthesis approach to design the filter topologies in Figure 3-1 is discussed. The analysis of these circuit network is to start first. The insertion loss function ($P_{L,cir}$) of these networks can be expressed as a generic form [77]

$$P_{L,cir} = 1 + |F_{cir}|^2 = 1 + H_{n+1}(\cos^2 \theta) / \sin^2 \theta \quad (3.1a)$$

where H_{n+1} is the $(n+1)$ -th order polynomial with the n denoted as the number of cascaded sections, and F_{cir} is the transfer function and can be calculated as [2]

$$\begin{aligned} S_{11} &= \frac{A + B/Z_0 - CZ_0 - D}{A + B/Z_0 + CZ_0 + D} \\ S_{21} &= \frac{2}{A + B/Z_0 + CZ_0 + D} \\ F_{cir} &= \frac{S_{11}}{S_{21}} = \frac{A + B/Z_0 - CZ_0 - D}{2} \\ &= \frac{B_0 - C_0}{2} (z_0 = 1) \end{aligned} \quad (3.1b)$$

where A , B , C and D are entries of the $ABCD$ matrix of the whole circuit network. For a simple discussion, the input/output port impedance Z_0 is normalized as $z_0 = 1 \Omega$ and the notations for the characteristic impedances are in the lowercase. The A_0 , B_0 , C_0 and D_0 are used for the normalized lossless and symmetrical circuits, and the relation $A_0 = D_0$ is applied.

Before discussion the ideal filtering function, the cutoff frequency θ_c and the first kind Chebyshev polynomial $T_n(x)$ of degree n are discussed. θ_c is defined as the

equal ripple frequency point in the θ -plane. Thus, it has the relation to the commonly used cutoff frequency ω_c in the ω -plane as $\theta_c = \pi\omega_c/(2\omega_o)$, where ω_o is the center frequency of the passband. Since the filtering responses are symmetrical with respect to the center frequency, θ_c can be either lower or upper edge frequency. $T_n(x)$ is obtained as $T_n(x) = \cos(n\theta)$, where $x = \cos\theta$. By applying the basic triangular function property, it can be expanded.

For the equal-ripple frequency response, the $(n+1)$ -th order insertion loss function ($P_{L,n+1}$) is in the form of [78]

$$P_{L,n+1} = 1 + \varepsilon^2 |F_{n+1}|^2 = 1 + \varepsilon^2 \left(\frac{\left(\left(1 + \sqrt{1 - x_c^2} \right) T_{n+1} \left(\frac{x}{x_c} \right) - \left(1 - \sqrt{1 - x_c^2} \right) T_{n-1} \left(\frac{x}{x_c} \right) \right)}{2\sqrt{1 - x^2}} \right)^2 \quad (3.2)$$

where ε is the equal-ripple factor, F_n the filtering function, $x = \cos\theta$, $x_c = \cos\theta_c$ with θ_c as the cutoff frequency and $T_n(x)$ the first kind Chebyshev polynomial of degree n .

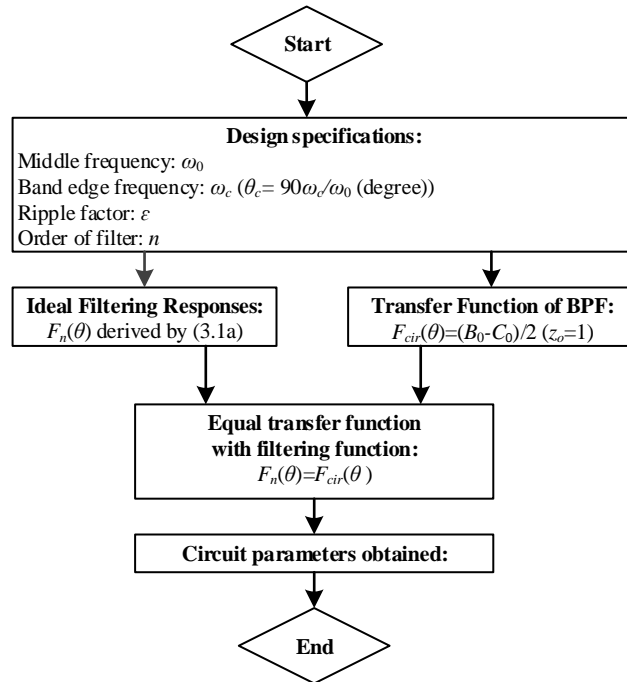


Figure 3-3. The synthesis procedure as discussed in this chapter for the single wideband BPFs.

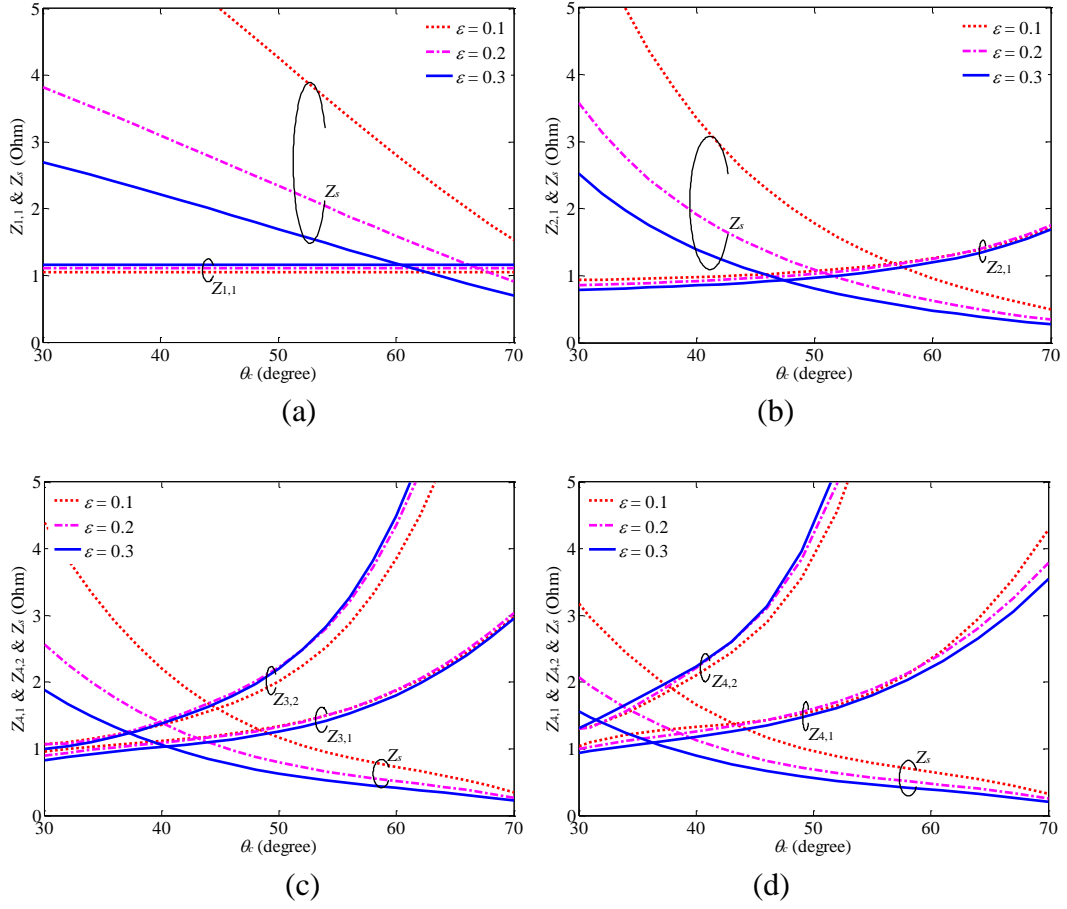


Figure 3-4. Characteristic impedance variations under the different cutoff frequencies (θ_c) and the ripple factors (ε) for the circuits of. (a) $n=1$. (b) $n=2$. (c) $n=3$. (d) $n=4$ in Figure 3-1 (the input and output port impedances are defined as $z_0=1$ Ω).

To implement the synthesis procedure, the two insertion loss functions in (3.1) and (3.2) are set to be equal to each other, that is

$$|F_{cir}| = \varepsilon |F_{n+1}| \quad (3.3)$$

In this way, all the corresponding coefficients for the same factors of these two polynomials become the same, thus all the characteristic impedances in Figure 3-4(a)-(d) are determined given the specified ripple factor (ε) and cutoff frequency (θ_c). Figure 3-3 summaries this synthesis procedure for the proposed wideband BPF.

The design specifications are given in the first place as the center frequency and the edge frequency to determine the *FBW* of the filter and the order of the filter is related the number of the cascaded sections as $(n+1)$. Next, the filtering function and the transfer function are derived respectively. By equating these two functions, the design parameters are obtained by solving a set of non-linear equations.

It is noted that solving the involved non-linear equation requires the input of the initial values, which is closely related to the working mechanism of the filter as mentioned before. The short-circuited MMR in the form of the cascaded transmission lines is to distribute its resonances in the passband. The short-circuited stubs are to feed the MMR. Firstly the physical length of the commensurate lines is determined by the center frequency of the passband. Then, analysis of the stepped-impedance MMR determines the initial values of its characteristic impedances to approximately locate its resonances in the passband. Finally, the short-ended stubs are set as $1\ \Omega$ as an initial value to feed the MMR.

Using this synthesis procedure, a number of design curves are obtained to fasten this process. Figure 3-4 shows the variation of characteristic impedances versus the cutoff frequencies and the ripple factors for the four filter topologies as shown in Figure 3-1. Comparison among the Figure 3-4(a)-(d), the discussion is divided into two parts as the MMR and the short-circuited stubs.

Increasing n adds the order of the filter, and it also alleviates the strict characteristic impedance requirement for a wider passband. Varying the stepped-impedance ratio of the short-circuited MMR is to quasi-equally distribute the desired resonances within the passband, as discussed in [6] and [39]. Therefore, for a certain filter topology, especially for $n > 2$, increasing the cutoff frequency (θ_c) decreases the characteristic impedance ratio of the MMR. This also explains that the variation of the ripple factor hardly affects their characteristic impedances.

A larger ripple factor requires a smaller degree of loading. Thus the characteristic impedance of the short-ended stub ($z_{s,s}$) is lowered to lessen the energy fed into the MMR.

To verify the above discussion, take $n=4$ (Figure 3-4(d)) for example. As increasing the cutoff frequency, $z_{4,1}$ increases slower than $z_{4,2}$. As the ripple factor varies from 0.1 to 0.3, compared to z_s there is little change of $z_{4,1}$ and $z_{4,2}$. This is because z_s is as the inductive loading structure and $z_{4,1}$ and $z_{4,2}$ are used to adjust the resonances of the MMR.

In summary, the proposed synthesis procedure is mainly divided into three steps. First equation (3.1b) is used to derive the transfer function of the chosen BPF in the form of (3.1a). Then, an appropriate filtering function is chosen. Finally equating these two function together, the design parameters of the proposed BPF are obtained.

3.2.3 Experimental Results and Discussions

Based on the synthesis procedure, a 5th-order ultra-wideband BPF ranging from 1.55 to 5.3 GHz ($\varepsilon=0.2$) is designed using the filter schematic in Figure 3-1(d). The cutoff frequency in θ -plane is calculated as $\theta_c=90^\circ\omega_c/\omega_o=40^\circ$. The substrate used has a dielectric constant of 10.8, loss tangent of 0.0023, thickness of 50 mils, and copper thickness of 0.017 mm.

First, the transfer function F_{cir} is derived by $(B_0-C_0)/2$ according to the $ABCD$ matrix of the circuit network in Figure 3-1(d) as (the input/output port impedance is set to $z_0=1\ \Omega$ as discussed)

$$\begin{aligned}
ABCD = & \begin{bmatrix} 1 & 0 \\ \frac{1}{jz_s \tan \theta} & 1 \end{bmatrix} \begin{bmatrix} \cos \theta & jz_{4,1} \sin \theta \\ \frac{j \sin \theta}{z_{4,1}} & \cos \theta \end{bmatrix} \begin{bmatrix} \cos \theta & jz_{4,2} \sin \theta \\ \frac{j \sin \theta}{z_{4,2}} & \cos \theta \end{bmatrix} \times \\
& \begin{bmatrix} \cos \theta & jz_{4,2} \sin \theta \\ \frac{j \sin \theta}{z_{4,2}} & \cos \theta \end{bmatrix} \begin{bmatrix} \cos \theta & jz_{4,1} \sin \theta \\ \frac{j \sin \theta}{z_{4,1}} & \cos \theta \end{bmatrix} \begin{bmatrix} 1 & 0 \\ \frac{1}{jz_s \tan \theta} & 1 \end{bmatrix} \quad (3.4) \\
F_{cir} = & (k_5 \cos^5 \theta + k_3 \cos^3 \theta + k_1 \cos \theta) / \sin \theta
\end{aligned}$$

where

$$k_5 = \frac{-j}{z_{4,1}^2 z_{4,2} z_s^2} \begin{pmatrix} z_{4,1}^4 z_s^2 + z_{4,1}^2 z_{4,2}^2 z_s^2 + 2z_{4,1}^3 z_{4,2} z_s^2 - z_{4,1}^2 z_s^2 \\ -2z_{4,1} z_{4,2} z_s^2 - z_{4,1}^4 - 2z_{4,1}^3 z_{4,2} - z_{4,1}^2 z_{4,2}^2 \\ -z_{4,2}^2 z_s^2 - 2z_{4,1}^3 z_s - 4z_{4,1}^2 z_{4,2} z_s - 2z_{4,1} z_{4,2}^2 z_s \end{pmatrix} \quad (3.5)$$

$$k_3 = \frac{-j}{z_{4,1}^2 z_{4,2} z_s^2} \begin{pmatrix} -2z_{4,1}^4 z_s^2 - 3z_{4,1}^3 z_{4,2} z_s^2 - z_{4,1}^2 z_{4,2}^2 z_s^2 \\ + z_{4,1}^4 + z_{4,1}^2 z_s^2 + 3z_{4,1} z_{4,2} z_s^2 + 4z_{4,1}^2 z_{4,2} z_s \\ + 2z_{4,1}^3 z_s + z_{4,1}^3 z_{4,2} + 2z_{4,1} z_{4,2}^2 z_s + 2z_{4,2}^2 z_s^2 \end{pmatrix} \quad (3.6)$$

$$k_1 = \frac{-j}{z_{4,1}^2 z_{4,2} z_s^2} \begin{pmatrix} z_{4,1}^4 z_s^2 + z_{4,1}^3 z_{4,2} z_s^2 - z_{4,1} z_{4,2} z_s^2 \\ -z_{4,2}^2 z_s^2 - z_{4,1}^2 z_{4,2} z_s \end{pmatrix} \quad (3.7)$$

Then, according to (3.2), the equal-ripple response function is obtained and expressed in the form of

$$F_{n+1} = (u_5 x^5 + u_3 x^3 + u_1 x) / \sqrt{1-x^2} \quad (3.8)$$

$$u_5 = 8(1 + \sqrt{1-x_c^2}) / x_c^5 \quad (3.9)$$

$$u_3 = -(12 + 8\sqrt{1-x_c^2}) / x_c^3 \quad (3.10)$$

$$u_1 = (4 + \sqrt{1-x_c^2}) / x_c \quad (3.11)$$

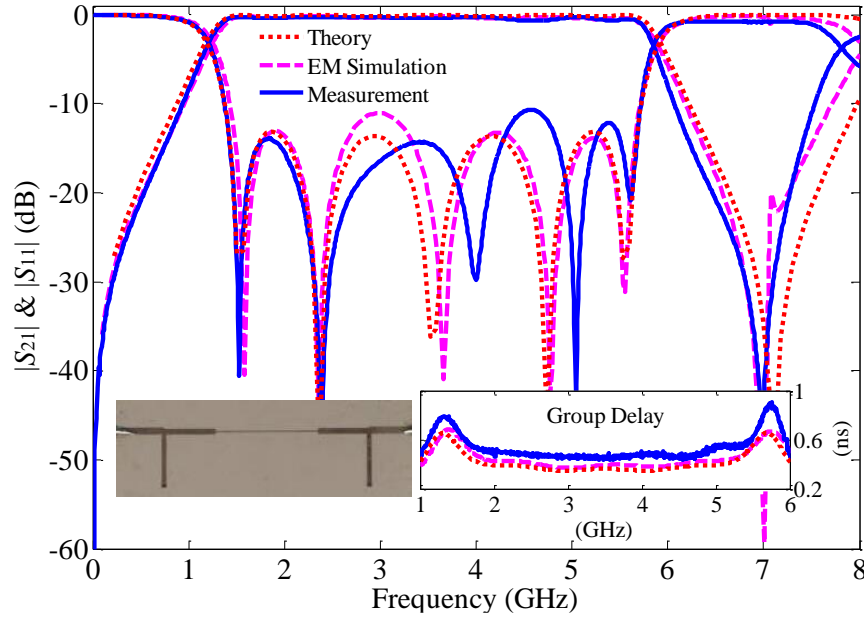


Figure 3-5. Frequency responses and group delays of theoretical, EM simulated and measured results, with a photograph of the fabricated filter in the inset figure.

The process ends by equating the respective coefficients of $|k_5| = |\epsilon u_5|$, $|k_3| = |\epsilon u_3|$ and $|k_1| = |\epsilon u_1|$. To solve this non-linear equation, the initial values are provided as $z_{4,1} = 2.00$, $z_{4,2} = 2.00$ and $z_s = 2.00 \Omega$, a gradient based method (such as the “fsolve” or “lsqnonlin” as integrated in the commercial software MATLAB) is used herein. The characteristic impedances are obtained as $z_{4,1} = 1.22$, $z_{4,2} = 2.22$ and $z_s = 1.08 \Omega$ (referring to the input/output port impedance $z_0 = 1 \Omega$). The evaluated error ($(|k_5| - |\epsilon u_5|) + (|k_3| - |\epsilon u_3|) + (|k_1| - |\epsilon u_1|)$), using $z_{4,1} = 1.22$, $z_{4,2} = 2.22$ and $z_s = 1.08 \Omega$, is around 0.04.

In summary, some key design outcomes are listed as below.

(a), Design specifications are set as $\epsilon = 0.22$, and $\theta_c = 40^\circ$, which are directly obtained from the required bandwidth and insertion loss.

(b), $x_c = \cos \theta_c = 0.766$, F_{n+1} is defined by (3.8) through the design coefficients of (3.9)-(3.11), where n is the number of MMR sections ($n = 4$), $u_5 = 49.836$, $u_3 = -38.141$ and $u_1 = 6.061$.

(c), Through the non-linear equation solving, the design parameters are obtained as $z_{4,1}=1.22$, $z_{4,2}=2.20$ and $z_s=1.07 \Omega$ (the input/output port impedance $z_0=1 \Omega$).

After the synthesis procedure is completed, a filter on the microstrip line is implemented. Figure 3-5 shows the photograph of the fabricated filter and the comparison among the results from the transmission line model, the full-wave simulation and the measurement. The dimensions of the filter are (width/length in mm/mm) 0.69/8.27 for $z_{4,1}$, 0.10/8.80 for $Z_{4,2}$ and 0.95/8.16 for z_s . Both the simulated and measured results are in a good agreement with the predicted ones. The measured results show a center frequency of 3.7 GHz, the 3-dB fractional bandwidth of 130%, the minimum insertion loss less than 0.5 dB and the group delay variation of 0.4 to 0.7 ns within the passband. Table 3.1 shows the comparison the in insertion loss and the overall size between our proposed and those reported ultra-wideband BPFs. From the table, it can be seen that the proposed ultra-wideband BPF has some attractive advantages, i.e., the good insertion and return losses, the simple geometry with only two short-ended stubs and a general synthesis procedure to determine all the filter parameters.

Table 3.1 Comparison with the reported ultra-wideband BPFs

Ref.	f_o (GHz)	N_{rf}	IL (dB)	RL (dB)	Roll-off slope lower & upper side (dB/GHz)	Size ($\lambda_o \times \lambda_o$)
[6]	6.85	5	0.6	10.0	13 & 9	0.36×0.03
[32]	6.85	9	1.1	8.5	50 & 34	0.57×0.32
[79]	3.40	5	0.9	10.0	14 & 50	0.38×0.30
[39]	6.85	5	1.1	10.0	13 & 20	0.22×0.03
[80]	6.85	7	1.4	11.1	54 & 14	0.51×0.37
[81]	6.85	5	0.6	14.0	81 & 81	0.14×0.41
This work	3.40	5	0.5	10.0	25 & 26	0.37×0.1

IL & RL: insertion & return loss; f_o : center frequency of the passband;

N_{rf} : the number of the reflection zeros in the passband;

roll-off slope: defined between 3 and 30 dB rejection frequency points;

λ_o : free-space wavelength at center frequency of the passband;

the bandwidth of the filters are around 110%.

3.3 Design of the Wideband Filter with TZs

In this section, a new wideband BPF with the composite short- and open-circuited stubs is proposed to achieve sharpened rejection slope near the two edges of the passband. When only short-circuited stubs are used at the both sides of a stepped-impedance MMR, the TZs are located at the multiple integer of π . Instead, if the two-section open-circuited stubs are used, the paired TZs can be shifted into the stopband. By using the composite short- and open-circuited stubs, these two pairs of TZs are kept almost unmoved while the passband is almost unaffected. For the circuit analysis, the even-/odd-mode analysis method is applied to derive the transfer function. Then, the locations of the reflection zeroes and the TZs are precisely obtained. With a closer examination of the introduced reflection zeros, it is found that there are two pairs of reflection zeroes in the complex frequency plane besides the ones in the real frequency plane of the passband. Different from the traditionally used techniques such as introducing input/output port coupling, the proposed composite short- and open-circuited stubs serve as an alternative method to generate new pair of TZs.

3.3.1 Working Mechanism and Circuit Analysis

To illustrate the characteristics of the wideband filter with composite short- and open-circuited stubs (as shown in Figure 3-6), the design process is divided into three parts with reference to Figure 3-7(a), (b) and (c). First, a pair of short-circuited stubs is shunt connected at the two sides of the stepped-impedance MMR, as seen in Figure 3-7(a). According to the work in the previous section, a 5th-order Chebyshev filtering response is synthesized with the TZs located at the frequencies when the electrical length of those short-circuited stubs is $\pi/2$, which is the twice of the center frequency of the passband. In Figure 3-7(b), a pair of two-section open-circuited stubs produces a pair of TZs in the rejection band, as reported in [82] and [83]. This filter has a steep slope near the cutoff frequencies, but it cannot block the DC component. To solve this problem, composite short- and open-circuited stubs are used simultaneously, as depicted in Figure 3-7(c). Thus, two pairs of TZs at the

specified frequencies can be generated by these two kinds of stubs while keeping the bandwidth of the passband to be almost unchanged.

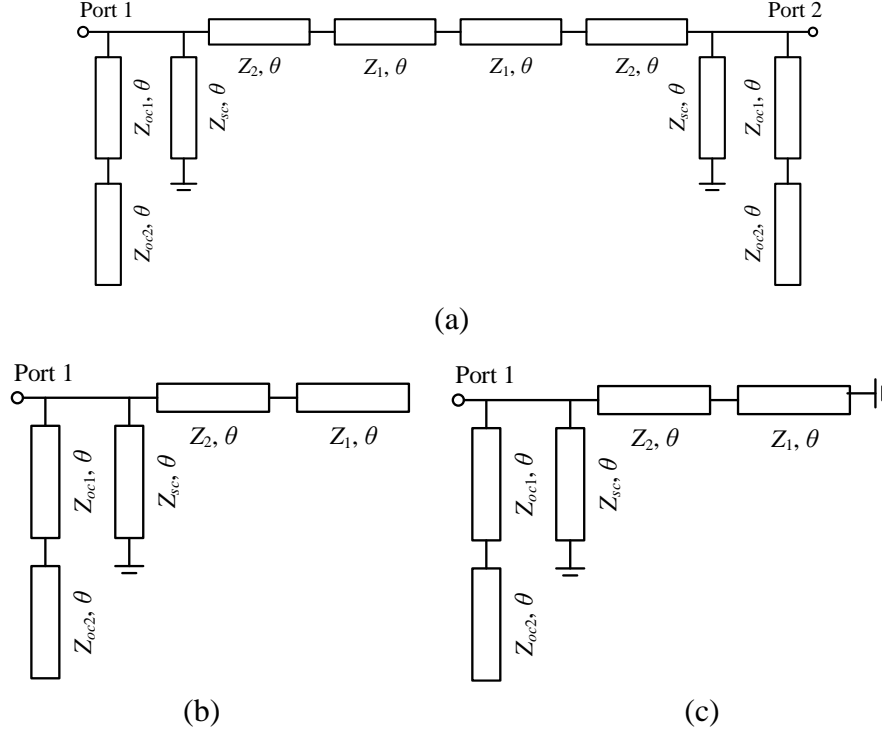


Figure 3-6. (a) Basic schematic of the proposed UWB filter. (b) Bisection circuit under even source excitation. (c) Bisection circuit under odd source excitation.

To analyze this filter, the even-/odd-mode method is used (the even and odd sources are provided at the input and output ports of the proposed filter), and the input admittances of their two bisection circuits are derived as

$$Y_{ine} = \frac{k_4 + k_5 t^2 + k_6 t^4}{k_1 t + k_2 t^3 + k_3 t^5}, \quad Y_{ino} = \frac{k_9 + k_{10} t^2 + k_{11} t^4}{k_7 t + k_8 t^3} \quad (3.12)$$

where $t = \tan \theta$ and k_1 - k_{11} are the coefficients of the polynomials, and they are defined as a function of the characteristic impedances of the transmission lines as

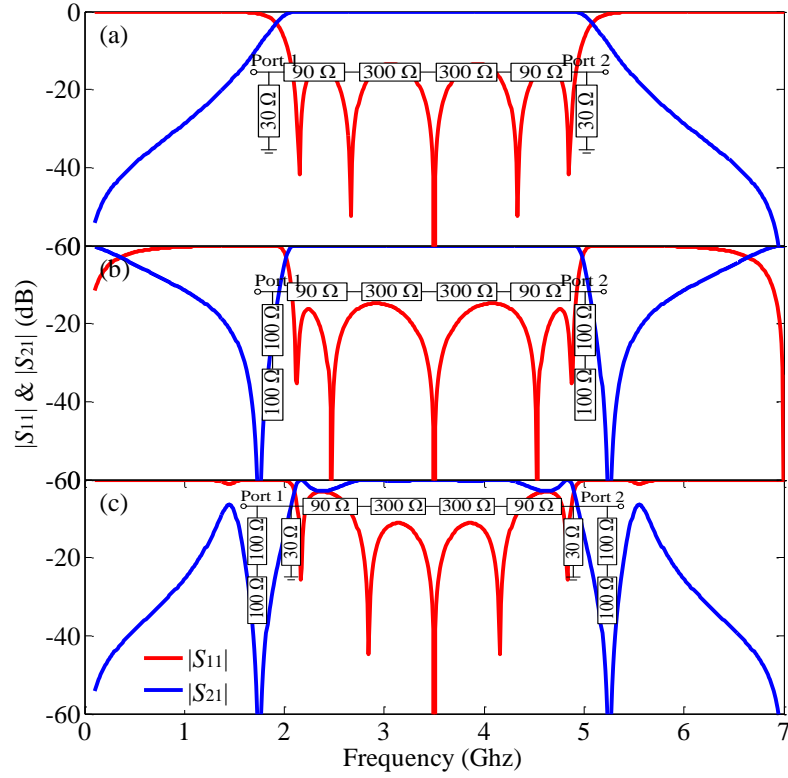


Figure 3-7. Frequency responses under the different shunt stubs with the inset figures denoting the characteristic impedances. (a) Short-circuited stubs. (b) Two-section open-circuited stubs. (c) Composite short- and open-circuited stubs.

$$\begin{cases}
 k_1 = jZ_1Z_{oc2}Z_2Z_{sc}Z_{oc1} \\
 k_2 = -jZ_2Z_{sc}Z_{oc1}(Z_2Z_{oc2} + Z_1Z_{oc1}) \\
 k_3 = jZ_2Z_{sc}Z_{oc1}Z_2Z_{oc1} \\
 k_4 = Z_1Z_{oc2}Z_2Z_{oc1} \\
 k_5 = -Z_{sc}Z_{oc1}Z_{oc2}(Z_2 + Z_1) - Z_1Z_2Z_{sc}(Z_{oc1} + Z_{oc2}) - Z_2Z_{oc2}Z_2Z_{oc1} \\
 \quad - Z_1Z_{oc1}Z_2Z_{oc1} \\
 k_6 = Z_{sc}Z_{oc1}Z_{oc1}(Z_2 + Z_1) + Z_2Z_{oc1}Z_2Z_{oc1} + Z_2Z_2Z_{sc}(Z_{oc1} + Z_{oc2}) \\
 k_7 = -Z_2(Z_1 + Z_2)Z_{sc}Z_{oc1}Z_{oc2} \\
 k_8 = Z_2(Z_1 + Z_2)Z_{sc}Z_{oc1}Z_{oc1} \\
 k_9 = jZ_{sc}Z_{oc1}Z_2Z_{oc2} + jZ_2Z_{oc1}(Z_1 + Z_2)Z_{oc2} \\
 k_{10} = -jZ_{sc}Z_{oc1}Z_1Z_{oc2} - jZ_2Z_{oc1}(Z_1 + Z_2)Z_{oc1} \\
 \quad - jZ_{sc}Z_{oc1}Z_2Z_{oc1} - jZ_2Z_{sc}(Z_1 + Z_2)(Z_{oc1} + Z_{oc2}) \\
 k_{11} = jZ_{sc}Z_{oc1}Z_1Z_{oc1}
 \end{cases} \quad (3.13)$$

where the design parameters Z_1 , Z_2 , Z_{sc} , Z_{oc1} and Z_{oc2} are the characteristic impedances of the transmission lines as illustrated in Figure 3-5.

Next, the transfer function is derived and represented by the ratio of the reflection and transmission coefficient as

$$\begin{aligned} S_{11} &= \frac{Y_0^2 - Y_{ine} Y_{ino}}{(Y_o + Y_{ine})(Y_o + Y_{ino})} \\ S_{21} &= \frac{Y_0(Y_{ino} - Y_{ine})}{(Y_o + Y_{ine})(Y_o + Y_{ino})} \end{aligned} \quad (3.14)$$

$$F_{cir} = \frac{S_{11}}{S_{21}} = \frac{Y_0^2 - Y_{ine} Y_{ino}}{Y_0(Y_{ino} - Y_{ine})} = \frac{\begin{aligned} &-k_9 k_4 \\ &+ (k_1 k_7 Y_0^2 - k_9 k_5 - k_4 k_{10}) t^2 \\ &(k_2 k_7 Y_0^2 + k_1 k_8 Y_0^2 - k_9 k_6 - k_5 k_{10} - k_{11} k_4) t^4 \\ &(k_3 k_7 Y_0^2 + k_2 k_8 Y_0^2 - k_6 k_{10} - k_{11} k_5) t^6 \\ &+ (k_3 k_8 Y_0^2 - k_{11} k_6) t^8 \end{aligned}}{\begin{aligned} &(k_9 k_1 - k_4 k_7) t \\ &+ (k_{10} k_1 + k_9 k_2 - k_4 k_8 - k_7 k_5) t^3 \\ &Y_0 (k_{11} k_1 + k_{10} k_2 + k_9 k_3 - k_8 k_5 - k_7 k_6) t^5 \\ &+ (k_{11} k_2 + k_{10} k_3 - k_8 k_6) t^7 \\ &+ (k_{11} k_3) t^9 \end{aligned}} \quad (3.15)$$

The polynomial in the numerator and the denominator of the transfer function has the degrees of 9 and 8, respectively. Thus, the zeros of the numerator contains the information of 4 pairs of TZs plus an additional one located at $t=0$. Meanwhile, the 8th-degree polynomial leads to 4 pairs of reflection zeroes. Since the numerator has 1 degree higher than the denominator, there is one reflection zero at $t=\infty$.

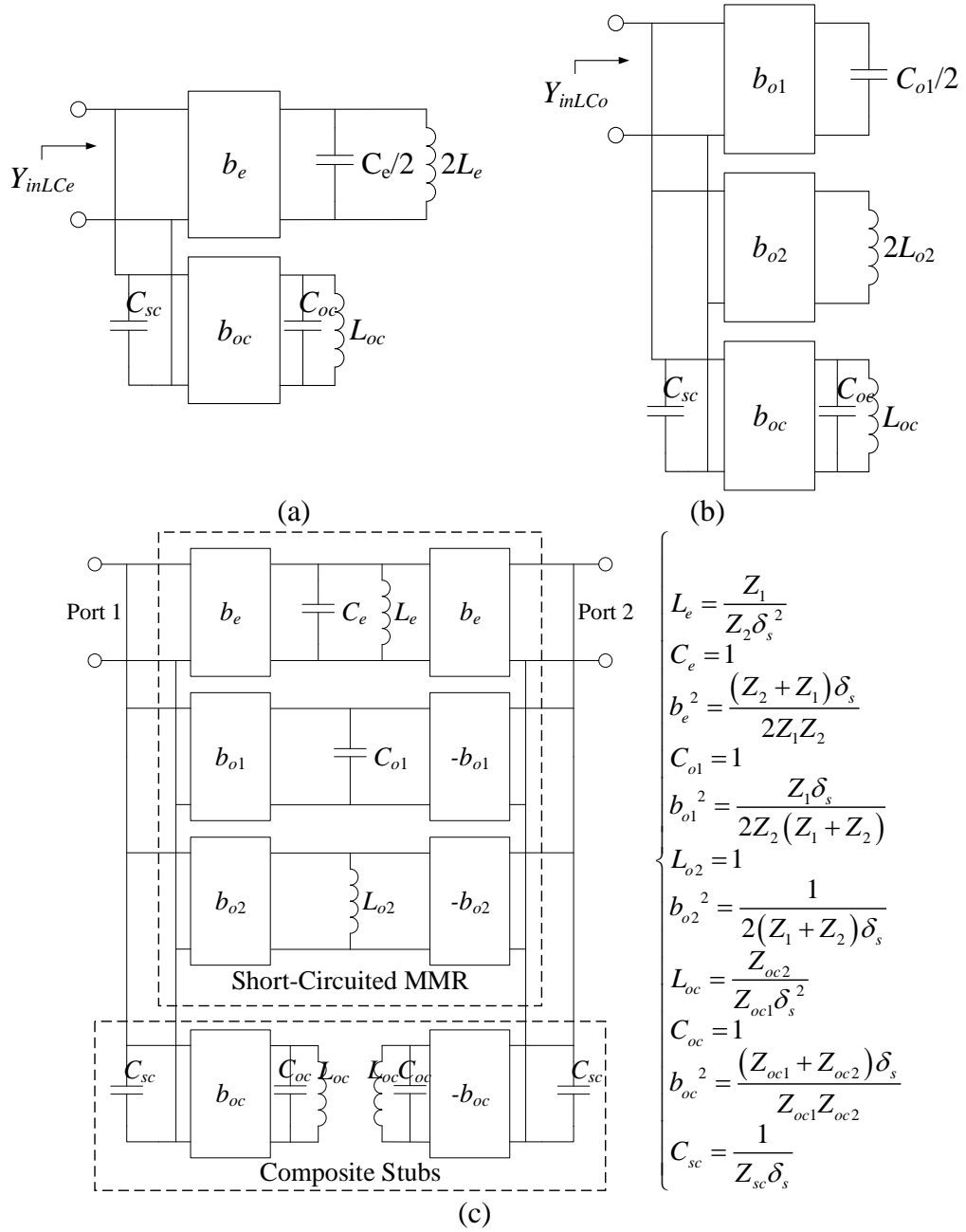


Figure 3-8. (a) LC circuit under even-mode excitation. (b) LC circuit under odd-mode excitation. (c) Equivalent circuit of the proposed filter

The even-/odd-mode analysis is also used to help derive the LC equivalent circuit, which has a direct illustration of the MMR and the composite stubs. To start this process, the Richard's transformation is used to transfer the θ -plane to the Ω -plane by the transformation of

$$\Omega = -\frac{\delta_s}{t} \rightarrow t = -\frac{\delta_s}{\Omega} (t = \tan \theta) \quad (3.16)$$

where δ_s represents a coefficient to scale the cutoff frequency in the normalized Ω -plane.

After the transformation, the input admittances (Y_{ine} and Y_{ino}) are found to be in the same format of the ones of the LC circuits (Y_{inLCe} and Y_{inLCo}), as shown in Figure 3-8(a) and (b), and they are calculated as

$$Y_{inLCe} = \frac{j2L_e b_e^2 \Omega}{1 - C_e L_e \Omega^2} + \frac{j\Omega L_{oc} b_{oc}^2}{1 - \Omega^2 C_{oc} L_{oc}} + j\Omega C_{sc} \quad (3.17a)$$

$$Y_{inLCo} = \frac{2b_{o1}^2}{j\Omega C_{o1}} + j2\Omega L_{o2} b_{o2}^2 + \frac{j\Omega L_{oc} b_{oc}^2}{1 - \Omega^2 C_{oc} L_{oc}} + j\Omega C_{sc} \quad (3.17b)$$

where L_e , L_{oc} and L_{o2} are the shunt inductors, C_e , C_{oc} , C_{sc} and C_{o1} the shunt capacitors, and b_e , b_{oc} , b_{o1} and b_{o2} are the admittance inverters.

By equating the input admittances from the bisection and LC circuits ($Y_{in(e,o)}$ and $Y_{inLC(e,o)}$), the parametric variables are solved as listed in the inset of Figure 3-8(c). Once these variables in the two LC circuits are solved, the equivalent circuit of the filter is obtained by combining them together, as shown in Figure 3-8(c).

For the derived equivalent circuit, it is further divided into two parts. The stepped-impedance MMR is represented as a quasi-transversal structure, introducing three reflection zeros within the passbands. The short-circuited stubs are formed as shunt capacitors, leading to the additional two reflection zeros and one pair of TZs at the infinity. For the open-circuited stubs, it is denoted as a shunt-loaded resonator. At its resonant frequency, the admittance transformer shortens the signal to ground, exciting another pair of TZs. Apart from the resonant frequency, the shunt-loaded resonator also introduces reflection zeros at complex frequency but outside of the passbands.

To illustrate the distribution of these reflection zeroes/TZs, a design example is given as plotted in Figure 3-9. The TZ at $t = 0$ introduces a distribution at multiple integer of π . The TZs at real axis of t contribute to the out-of-band attenuation, and the ones at real/imaginary axis affect the group delay of the filter. Furthermore, 4 reflection zeroes at real axis of t plus one at $t = \infty$ stand for the 5 resonances within the passband. In the meantime, there are 4 reflection zeroes resonating at complex plane of t . Since t is related to the frequency ω by $t = \tan\theta = \tan(\pi\omega/(2\omega_o))$, where ω_o is the center frequency of the passband, the reflection zeros/TZs on the complex t -plane is transformed to the complex frequencies and the ones on the real t -plane to the real frequencies. Based on the above discussion, the function of the two-section open-circuited stubs in the proposed filter is to introduce a pair of TZs in the real frequency plane as well as four reflection zeroes in the complex plane. Fortunately, the latter will not give meaningful influence on the out-of-band response due to the resonances on the complex frequencies and the TZs generated. Therefore, different from the commonly used techniques to include all the reflection zeroes within the passband, the proposed composite stubs distribute reflection zeroes outside of the passband and resonate in complex frequencies.

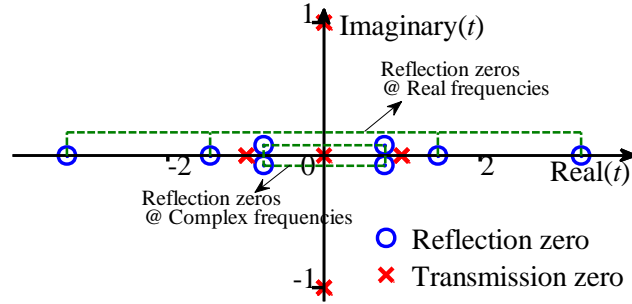


Figure 3-9. Locations of reflection zeroes and TZs of the proposed BPF.
(characteristic impedances: $Z_{oc1} = 100 \Omega$, $Z_{oc2} = 100 \Omega$, $Z_{sc} = 30 \Omega$, $Z_1 = 300 \Omega$ and $Z_2 = 90 \Omega$).

Finally, a comparison between the two filter structures proposed in this chapter is seen in figure 3-10. For the wideband BPF with the composite short- and open-circuited stubs, it introduces a pair of TZs near the edges of the passband, which improves the out-of-band rejection around these places. However, away from the TZs the rejection of the filter is worse than that of the one with only short-circuited stubs. To further improve the out-of-band rejection, a technique of introducing input/output port coupling can be used. For the aspect of the group delay, since the use of the composite short- and open-circuited stubs, the extra pairs of TZs are introduced in the real and imaginary frequency planes. Thus the distribution of the group delay is not as flat as that of the filter with only short-circuited stubs.

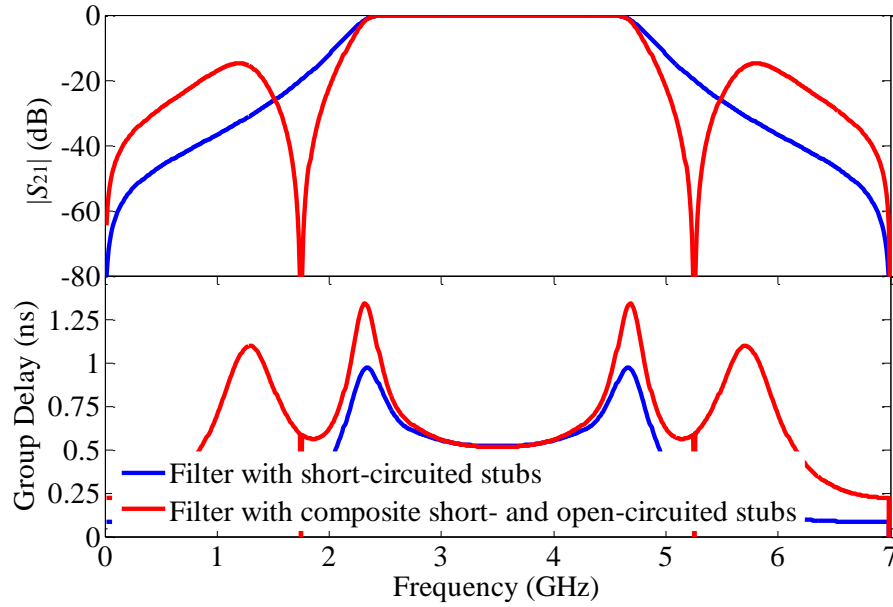


Figure 3-10. Filtering response and group delay comparison between the wideband filter with the short-circuited stubs and the one with the composite short- and open-circuited stubs which are under the same FBW (the characteristic impedances of the former one is $Z_1 = 137 \, \Omega$, $Z_2 = 749 \, \Omega$, $Z_s = 29 \, \Omega$ and the characteristic impedances of the latter one is $Z_{oc1} = 100 \, \Omega$, $Z_{oc2} = 100 \, \Omega$, $Z_{sc} = 30 \, \Omega$, $Z_1 = 300 \, \Omega$ and $Z_2 = 90 \, \Omega$).

3.3.2 Experimental Results and Discussions

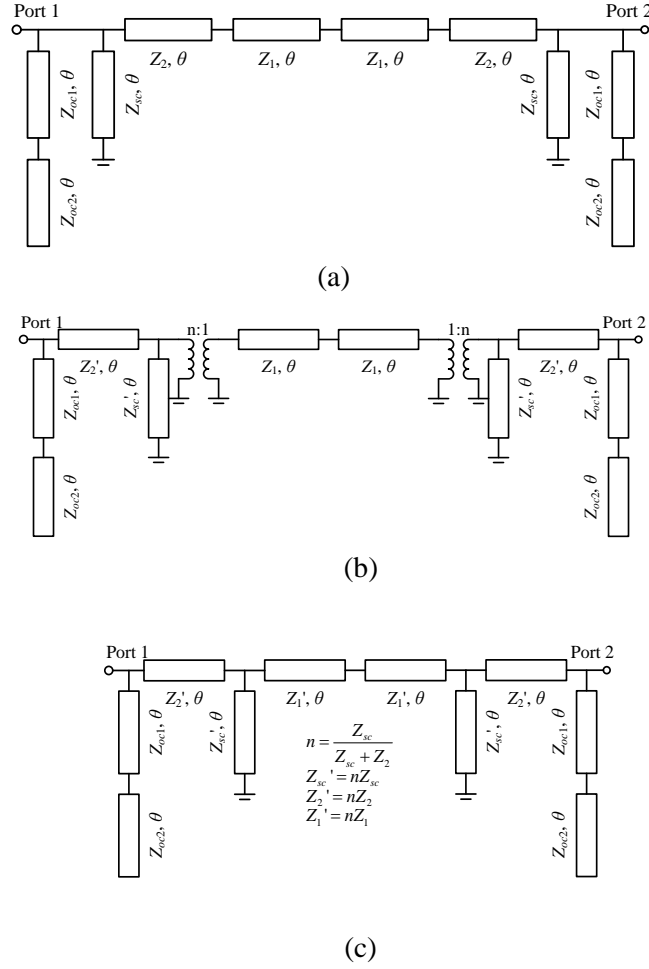


Figure 3-11. (a) Basic circuit schematic of the BPF. (b) Transfer the short-circuited stubs into the MMR by the Kuroda transformation. (c) Absorb the transformer into the transmission line.

Based on the discussion above, a fifth-order wideband BPF is designed on a substrate, i.e., Roger's RT/Duroid 6010, with dielectric constant of 10.8, loss tangent of 0.0023, thickness of 50 mils and copper thickness of 0.017 mm.

As studied in the work of the previous design, the required characteristic impedance in the middle of the MMR is too high to be realized in practice. Therefore, the Kuroda transformation is applied to transfer the short-circuited stubs into the middle section of the MMR, and the inverter left is absorbed by the middle

transmission line section. Figure 3-11(a) shows the basic schematic of the proposed BPF. When applying the Kuroda transformation, the short-circuited stubs are moved into the MMR and a transformer is created on the both sides of Z_1 , as seen in Figure 3-11(b). Finally, the transformer is absorbed by the transmission line with an impedance adjustment as seen in Figure 3-11(c). Since the value of n (as indicated in Figure 3-11(c)) is always smaller than unity, the characteristic impedances of the short-circuited stubs and lines in the MMR can be lowered simultaneously, as illustrated in Figure 3-11(a)-(c).

In this design, the center frequency is set as 3.50 GHz, the in-band ripple factor as 0.07, lower-/upper-band edge frequency as 2.50/4.50 GHz ($FBW=57.14\%$) and a pair of TZs as 1.75 and 5.25 GHz. The characteristic impedances are determined as $Z_{oc1}=103\ \Omega$, $Z_{oc2}=103\ \Omega$, $Z_{sc}=30\ \Omega$, $Z_1'=105\ \Omega$ and $Z_2'=51\ \Omega$. Its dimensions are obtained as (width/length in mm) 0.11/8.5 for Z_{oc1} , 0.11/21.8 for Z_{oc2} , 2.8/7.5 for Z_{sc} , 0.1/8.6 for Z_1 and 1.1/7.9 for Z_2 . Figure 3-12 shows the photograph of the fabricated BPF and the results from the transmission line model, full-wave simulation and measurement. Measured results exhibit a center frequency of 3.55 GHz, 3-dB fractional bandwidth of 68.0 %, insertion loss less than 1.3 dB, group delay variation of 0.4 to 0.7 ns, and out-of-band rejection larger than 15.0 dB. The discrepancy between the measured and the circuit responses is mainly caused by the fabrication tolerance and various parasitic effects. There are two major parasitic effects having great influence towards the final results. One is the cross junction effect, which can be modeled by pi-shaped capacitor network. Another effect is from the via-holes, which can be modeled by inductors [2]. Once these effects are taken into account and further circuit optimization is conducted, better filtering responses can be obtained.

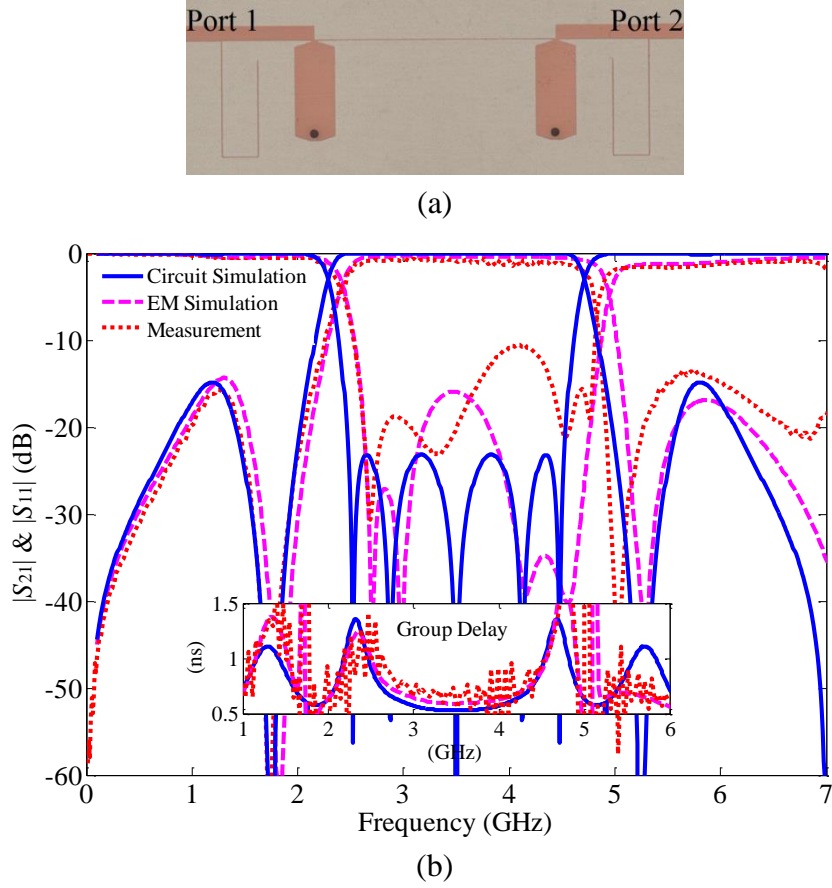


Figure 3-12. (a) Photography of the proposed wideband filter. (b) Frequency responses and group delays derived from analysis, EM simulation and measurement.

3.4 Summary

In this chapter, a class of wideband BPFs has been proposed based on the concept of stepped-impedance MMRs. The basic structure of this class of wideband filter is formed by cascading several sections of commensurate lines with different characteristic impedances. Short-circuited stubs are shunt on the two sides of the MMR to provide an appropriate loading to the resonator. To further improve the out-of-band rejection, a composite of open- and short-circuited stubs is used instead to introduce an additional pair of TZs.

CHAPTER 4

SYNTHESIS AND DESIGN OF WIDEBAND DUAL-BAND BANDPASS FILTERS WITH CONTROLLABLE IN-BAND RIPPLE FACTOR AND DUAL-BAND ISOLATION

4.1 Introduction

In this chapter, a class of wideband dual-band BPFs with controllable in-band ripple factor and TZs has been synthesized and designed. The circuit structures of the proposed dual-wideband BPFs are based on the concept of dividing the passband by inserting TZs between the two passbands. Therefore, two wideband BPFs are parallel connected to generate two pairs of TZs. Three prototype filters have been proposed with their different capability in controlling the TZs and the in-band ripple factor.

For the synthesis procedure, first a dual-band filtering function is studied by directly transforming a bandpass response. The dual-band filtering function is symmetrical with respect to the middle frequency of the two passbands and has one TZ locating at that point. By equating the dual-band circuit response to the filtering function, the circuit parameters are obtained.

4.2 Synthesis Procedure of the Dual-Band BPF

The systematic synthesis procedure follows the four steps, as discussed and documented in [5], [49] and [84], including analyzing the characteristics of the proposed dual-band circuits, choosing a proper filtering function, applying the frequency transformation from a single-band to a dual-band filtering response and

finally, equating the transfer function to the filtering function in order to determine the circuit design parameters.

4.2.1 Circuit Analysis of the Proposed Dual-Band Filters

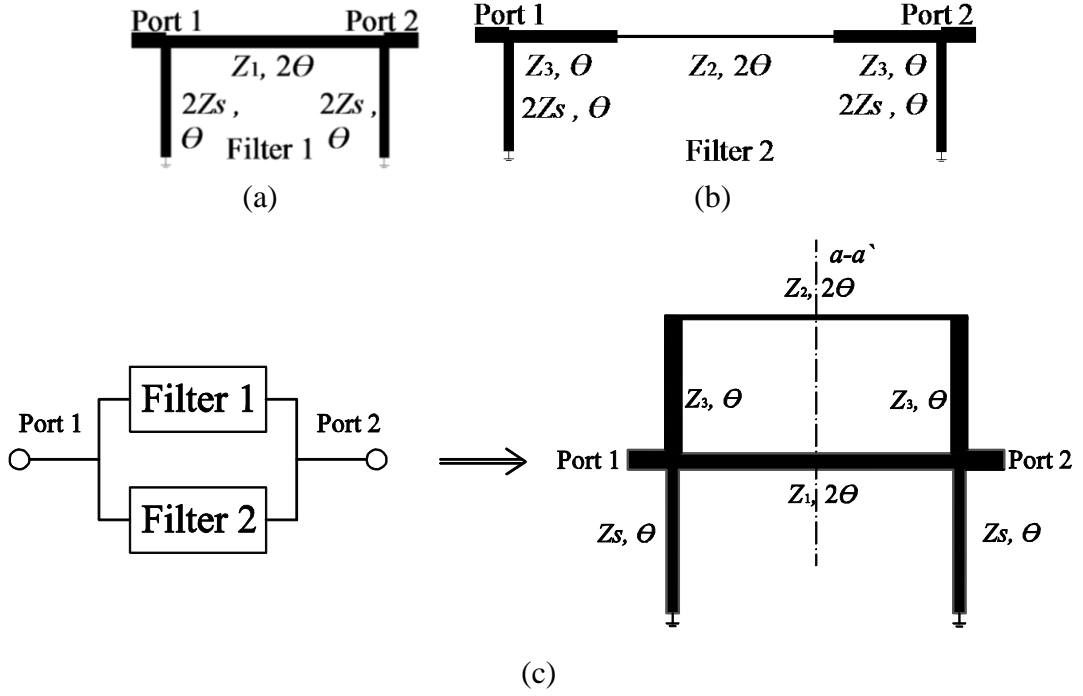


Figure 4-1. (a) Filter 1 formed by uniform MMR with the short-circuited stubs.
(b) Filter 2 formed by the stepped-impedance MMR with the short-circuited stubs.
(c) Dual-band BPF by parallel connecting filter 1 and filter 2.

The basic structure of the proposed dual-band BPFs is formed by parallel connecting two wideband BPFs (referring to the discussion in the previous chapter), as shown in Figure 4-1(a)-(c). The three prototypes of the proposed wideband dual-band BPFs are illustrated in Table 4.1. For every section of the circuits, it is one quarter wavelength long with respect to the middle frequency of the two passbands (ω_o). In the discussion below, the circuit analysis is mainly expressed as a function of $\tan\theta = \tan(\pi\omega/(2\omega_o))$. When $\tan\theta$ is real it indicates a real frequency and when $\tan\theta$ is imaginary it refers to an imaginary frequency in the ω -plane.

According to the signal interference technique [56-60], when the two MMRs are of 180° phase difference, there is one TZ locating in the middle of the two passbands. By adjusting the characteristic impedances of the two MMRs, one pair of TZs could be adjusted either in the real or in the imaginary frequencies, as seen in Table 4.1 Prototype I, where $\tan\theta_{TZ(2,3)}$ represents the pair of TZs in the imaginary frequencies and $\tan\theta_{TZ(4,5)}$ represents the pair of TZs in the real frequencies. To control another pair of TZs, the half wavelength resonator is folded to form coupled lines. This pair of TZs is solely determined by the ratio of the even-/odd-mode characteristic impedances of the coupled lines as seen in Table 4.1, where for Prototype II $\tan\theta_{TZ(2,3)}$ is a function of Z_{1e} and Z_{1o} . Finally, a combination of both short- and open-circuited stubs is used to determine the in-band ripple factor, as summarized in Table 4.1 Prototype III. When compared among the three prototypes, the combined short- and open-circuited stubs provide an adequate controllability of the ripple factor.

Table 4.1 Structures of the Proposed Dual-Band BPF Prototypes

	Prototype I	Prototype II	Prototype III
Filter			
TZs	$\tan\theta_{TZ(0,1)} = 0, \infty$ $\tan\theta_{TZ(2,3)} = \pm\sqrt{t_{z1}} = \pm j$ $\tan\theta_{TZ(4,5)} = \pm\sqrt{t_{z2}} = \pm\sqrt{\frac{Z_2Z_1 + Z_2^2 + Z_3Z_2}{Z_3Z_2 + Z_3^2 - Z_2Z_1}}$	$\tan\theta_{TZ(0,1)} = 0, \infty$ $\tan\theta_{TZ(2,3)} = \pm\sqrt{t_{z1}} = \pm j\sqrt{\frac{Z_{1e}}{Z_{1o}}}$ $\tan\theta_{TZ(4,5)} = \pm\sqrt{t_{z2}} = \pm\sqrt{\frac{Z_2Z_{1o} + Z_2^2 + Z_3Z_2}{Z_3Z_2 + Z_3^2 - Z_2Z_{1e}}}$	$\tan\theta_{TZ(0,1)} = 0, \infty$ $\tan\theta_{TZ(2,3)} = \pm\sqrt{t_{z1}} = \pm j\sqrt{\frac{Z_{1e}}{Z_{1o}}}$ $\tan\theta_{TZ(4,5)} = \pm\sqrt{t_{z2}} = \pm\sqrt{\frac{Z_2Z_{1o} + Z_2^2 + Z_3Z_2}{Z_3Z_2 + Z_3^2 - Z_2Z_{1e}}}$
ϵ	uncontrollable	uncontrollable	controllable

According to the discussion in the work of the previous chapter, filter 1 in Figure 4-1(a) produces the 3 resonances within the passband with the half-wavelength resonator and the short-circuited stubs contributing to 1 and 2 resonance(s); filter 2 in Figure 4-1(b) produces the 5 resonances in the passband with the stepped-impedance MMR and the short-circuited stubs contributing to 3 and 2 resonances, respectively. Therefore, connecting these two BPFs in parallel, as

shown in Figure 4-1(c) produces a total of 6 resonances with the parallel connected MMRs and the short-circuited stubs contributing to 4 and 2 resonances, respectively.

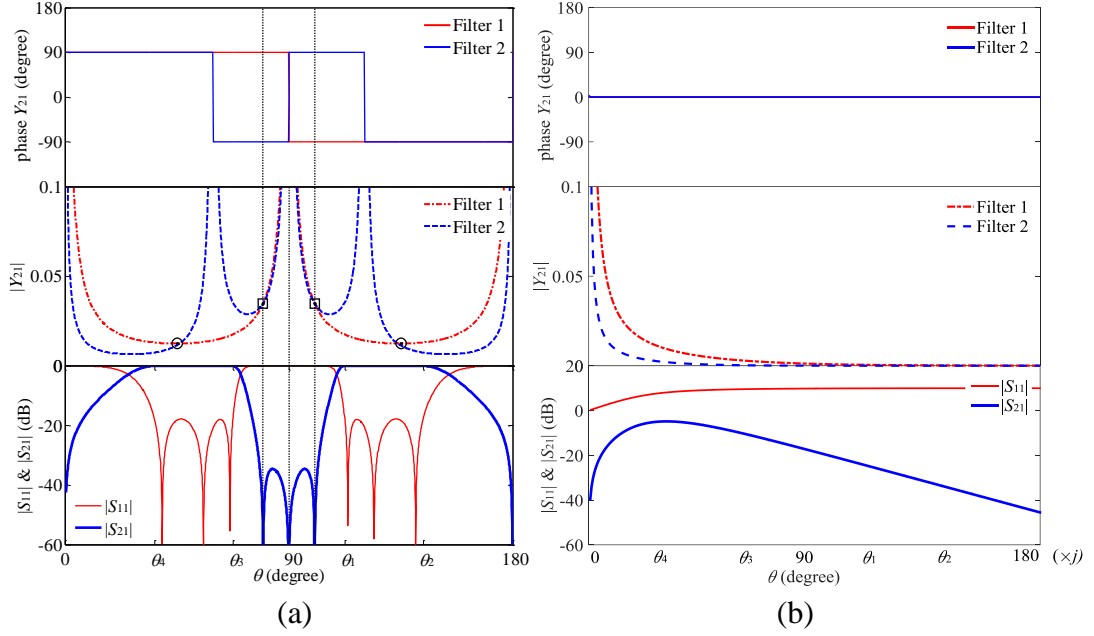


Figure 4-2. The phase and magnitude of Y_{21} of filter 1 and filter 2 and the frequency responses of the dual-band BPF to illustrate the generation of the TZs between the two passbands. (a) Responses under the real frequency sweep. (b) Responses under the imaginary frequency sweep ($Z_1=81.6\ \Omega$, $Z_2=200.8\ \Omega$, $Z_3=69.4\ \Omega$ and $Z_s=83.8\ \Omega$).

In a summary of the analysis mentioned above, the TZs are generated by parallel connecting filter 1 and 2. Through the similar analysis as the signal interference technique in [56], one TZ is produced in the middle of the two passbands by signal cancellation due to 180° phase difference and equal magnitude. Near this TZ, additional pairs of TZs can be generated at the real/imaginary frequencies. Once the TZs are determined, the reflection zeroes are distributed symmetrically in the two bands. Before rigorously analyzing the circuit structure, a filtering response of the proposed filter has been plotted in Figure 4-2, where Y_{21} of equal magnitude and 180° phase difference indicates the generation of TZs. From the responses under the real frequency sweep, as seen in Figure 4-2(a), a pair of TZs is generated at the places where Y_{21} of the two signal transmitting paths is equal magnitude and 180°

phase difference. But, another pair of crossing points of Y_{21} with equal magnitude but 0° phase difference indicates the possibility in creating TZs at the imaginary frequencies. From the responses under the imaginary frequency sweep, as seen in Figure 4-2(b), the TZ is assumed to be at the place of infinity since the Y_{21} magnitude of the two signal transmitting paths is approaching equal to each other as the imaginary frequency increasing to infinity and the phase is maintained at 0° . The exact locations of the TZs as tabulated in Table 4.1 prove the above discussion.

The analysis for the three filter prototypes is conducted by even-/odd-mode analysis method along their symmetrical plane of $a-a'$, seen in Table 4.1. The S -parameters and the transfer function F_{cir} are obtained as [5]

$$S_{11} = \frac{Y_0^2 - Y_{ine}Y_{ino}}{(Y_0 + Y_{ine})(Y_0 + Y_{ino})}, S_{21} = \frac{Y_0(Y_{ino} - Y_{ine})}{(Y_0 + Y_{ine})(Y_0 + Y_{ino})} \quad (4.1)$$

$$F_{cir} = \frac{S_{11}}{S_{21}} = \frac{Y_0^2 - Y_{ine}Y_{ino}}{Y_0(Y_{ino} - Y_{ine})} \quad (4.2)$$

where Y_0 is the input/output port admittance, Y_{ino} and Y_{ine} are the input admittances of the odd- and even-symmetrical circuits, respectively.

Taking the basic structure of the dual-band BPF (prototype I) as an example, Figure 4-2 shows the simulated Y_{21} of filter 1 and 2 and their crossing points. These two pairs of TZs are solely determined by the characteristic impedances of the two MMRs, as tabulated in Table 4.1 and discussed in the later part. Based on the above analysis, the proposed dual-band BPF has 6 resonances with 3 resonances for each passband, and the two passbands are defined by the TZs discussed above.

4.2.2 Generalized Chebyshev Filtering Function

Given the property of the proposed dual-band BPFs, a filtering function is chosen under the following criteria.

(a) The function has a symmetrical response with respect to the two bands, in order to achieve the symmetrical property of the proposed dual-band BPF.

(b) Apart from the two pairs of TZs, there are one TZ locating in the middle of the two passbands and the rest, if any, locating at infinity.

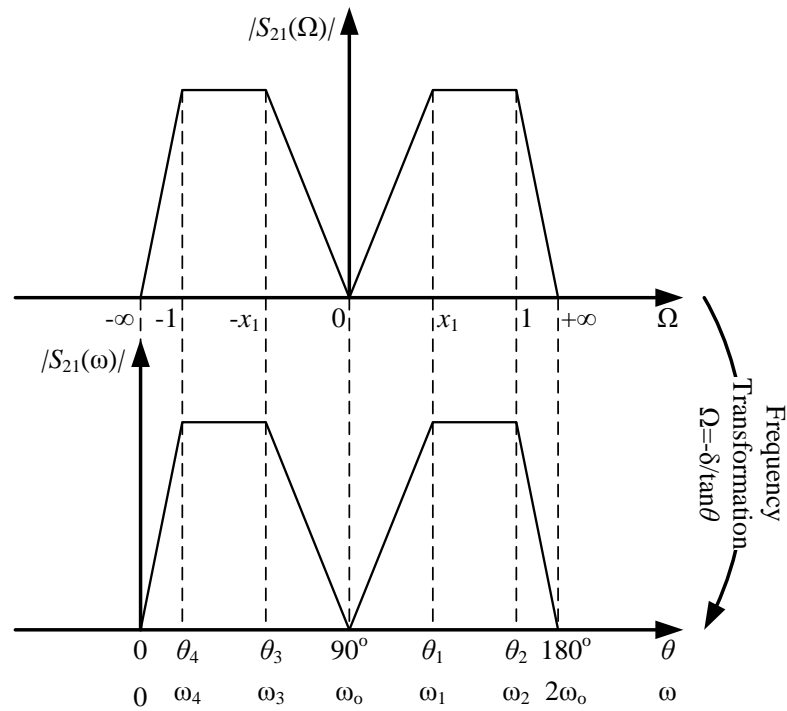


Figure 4-3. Frequency transformation of the filtering function from the Ω -plane to the θ -plane.

Therefore, the commonly used generalized Chebyshev filtering function as well as its transferred dual-band function (as discussed in [26], [71] and [85]) can not be appropriately used in this case. It either fails to have one TZ in the middle of the two

passbands, which is crucial for the wideband design, or lacks the symmetrical property with respect to the dual-bands, which has to correspond to the characteristic of the circuit response.

A generalized Chebyshev filtering function, originally developed for a single-wideband BPF design, is used herein. It directly formulates a filtering function with mirror to the origin. Thus, it has the dual passbands at the positive and negative frequency ranges. To accurately account for the wideband response, a TZ is assigned to locate at the origin. The n th-order filtering function as a function of Ω is given as [23]

$$F_n(\Omega) = \cosh \left(\cosh^{-1} \left(\frac{T_2(\Omega)}{\Omega} \right) + \sum_{k=1}^{n-1} \cosh^{-1} (f_k(\Omega)) \right) \quad (4.3)$$

$$= \sum_{i=1}^{2n} m_i \Omega^i / \sum_{j=1}^{2n-1} n_j \Omega^j$$

A recursion formula is derived in [23] to expand the filtering function to a ratio of two polynomials, namely, $\sum_{i=1}^{2n} m_i \Omega^i$ over $\sum_{j=1}^{2n-1} n_j \Omega^j$, where m_i and n_j are the coefficients of the two polynomials, respectively. The complete definition and the expansion process have been listed in Section 2.2.3 of this dissertation. However, it is noted that the filtering function discussed here is a general case of the one in Section 2.2.3, where the former one is normalized ($\Omega_2=1$) while the latter one is the general case with any assigned upper edge frequency (ω_2). In this sense, their coefficients are labeled in different way as “ m_i and n_j ” used here and “ r_i and h_j ” used in Section 2.2.3.

4.2.3 Frequency Transformation to Dual-Band BPF

The filtering function discussed above has two passbands in the positive and negative Ω ranges, respectively. Therefore, by frequency transformation, a dual-band filtering response is formulated, as shown in Figure 4-3. To get a generic

synthesis procedure, the upper frequency edge of the filtering function is normalized, i.e., $\Omega_2=1$. To achieve two controllable passbands, the lower frequency edge of the filtering function is set according to the filter design specification θ_1 ($\Omega_1=x_1$). The well-known Richard's transformation (mapping from the Ω -plane to the θ -plane) is used here to transfer the single-band response to its dual-band counterpart, as discussed in [25]. The frequency transformation can be derived as [71]

$$\Omega = -\delta / \tan \theta, \quad \theta = \frac{\pi}{2} \frac{\omega}{\omega_0} \quad (4.4)$$

where θ is the electrical length with respect to the middle frequency of the two passbands, ω_0 the middle frequency of the two passbands and δ is a scaling factor to normalize the Ω -plane ($\Omega_2=1$ and $\Omega_4=-1$) which can be derived based on (4.4) and the relation of $\omega_0=(\omega_2+\omega_4)/2$ stated in Figure 4-3 as

$$\Omega_2 = -\delta / \tan \theta_2 \rightarrow 1 = -\delta / \tan \left(\frac{\pi}{2} \frac{\omega_2}{\omega_0} \right) \quad (4.5a)$$

$$-\Omega_4 = -\delta / \tan \theta_4 \rightarrow -1 = -\delta / \tan \left(\frac{\pi}{2} \frac{\omega_4}{\omega_0} \right) \quad (4.5b)$$

$$\begin{aligned} \delta &= -\tan \left(\frac{\pi}{2} \frac{\omega_2}{\omega_0} \right) \\ &= -\tan \left(\frac{\pi}{2} \frac{2\omega_2}{\omega_2 + \omega_4} \right) = -\cot \left(\frac{\pi}{2} - \frac{\pi}{2} \frac{2\omega_2}{\omega_2 + \omega_4} \right) \\ &= -1 / \tan \left(\frac{\pi}{2} \left(1 - \frac{2\omega_2}{\omega_2 + \omega_4} \right) \right) = 1 / \tan \left(\frac{\pi}{2} \frac{\omega_2 - \omega_4}{2\omega_0} \right) \\ &= 1 / \tan \left(\frac{\theta_2 - \theta_4}{2} \right) \end{aligned} \quad (4.5c)$$

where θ_2 and θ_4 is the upper and lower edge of the dual-band BPF, respectively, as seen in Figure 4-3. It is noted that derivation of (4.5c) uses (4.5a) only. The same

results can be obtained by using (4.5b), since ω_2 and ω_4 are symmetrical with respect to ω_0 .

It is noted that the inner edge frequency of the passband x_1 is obtained as

$$x_1 = -\delta / \tan \theta_1 \quad (4.6)$$

where θ_1 is the inner edge in the θ -plane, as seen in Figure 4-3.

After the frequency transformation, $-\infty$, 0 and $+\infty$ in the Ω -plane are transferred to 0, 90° and 180° in the θ -plane. Thus, a dual-band filtering response is obtained in the sequence of specifying the edge frequency in the θ -plane, obtaining the scaling factor by (4.5), calculating the inner edge frequency via (4.6) and finally deriving the filtering function in the Ω -plane.

4.2.4 Circuit Parameter Calculation

Once the transfer function of the dual-band BPF and the theoretical filtering function have been obtained, these two functions are set to be equal as

$$\left| F_{cir}(\tan \theta) \right| = \varepsilon \left| F_n(\Omega) \right|_{\Omega = -\frac{\delta}{\tan \theta}} \quad (4.7)$$

where ε is the in-band ripple factor of the dual-band BPF.

For the transfer function of the dual-band BPF, the denominator and numerator contains the information about the locations of the TZs and the reflection zeroes, respectively. To apply the transfer function of the circuit to the theoretical filtering function, the corresponding coefficients of the numerator and the denominator should be set equal, respectively. The TZs of the proposed dual-band BPFs are only determined by the characteristic impedances of the parallel connected MMRs and have an explicit form, as shown in Table 4.1. These expressions of TZs can be confined under the targeted TZs, thus deriving one set of equations. Another set of

equations is obtained by equating the coefficients of the numerator, to get the same distribution of the reflection zeroes. All the circuit design parameters are obtained by solving two sets of equations.

4.2.5 Synthesis Procedure

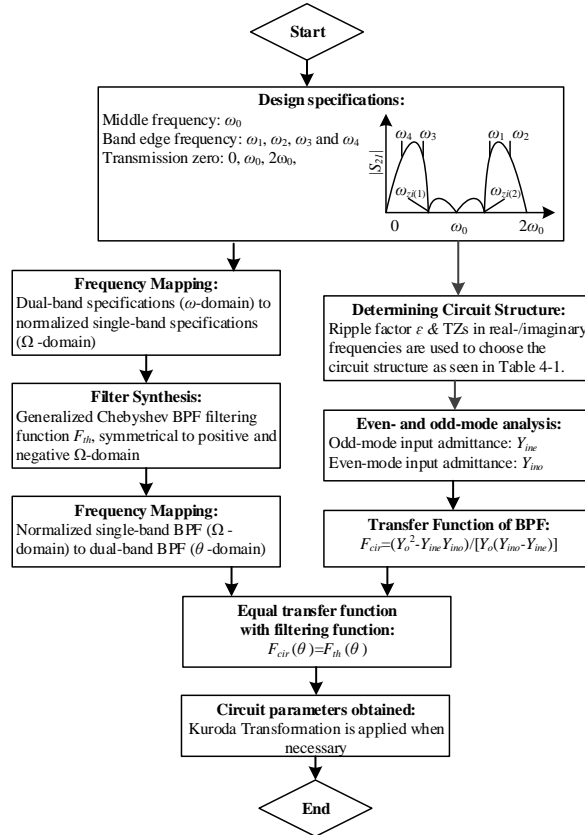


Figure 4-4. Synthesis procedure for the dual-band BPFs discussed in this chapter.

Before the discussion of any circuit schematic, a complete synthesis procedure is summarized in Figure 4-5. First the design specifications are given including the information as the center and the band edge frequencies and the ripple factor. The TZs are considered with their locations in the real and imaginary frequency plane. The filter order for each passband is fixed as three. Next, the filter schematic is chosen based on Table 4.1. The circuit selecting criteria is mainly based on the controllability of the ripple factor and the locations of the TZs. Once the circuit schematic is determined, the even-/odd-mode analysis method is used to derive its

transfer function. In the meanwhile, the design specifications in the ω -plane is transformed to the Ω -plane in order to formulate the filtering function, after which it is transformed back to the θ -plane. Finally, the filtering function and the transfer function are set to be equal by solving a set of non-linear equations. After this process, all the circuit design parameters are obtained. If the characteristic impedances of the parallel connected MMR are too large, the Kuroda transformation can be used.

4.3 Synthesis and Design of Dual-Band BPFs

In this section, the circuit analysis is applied for the three filter prototypes, and with the synthesis method introduced in the previous part, the three types of filters are analyzed to illustrate their distinctive characteristics.

4.3.1 Prototype I with One Pair of Controllable TZs

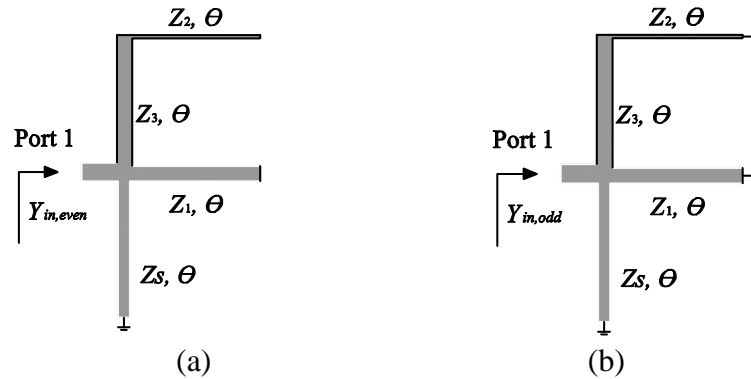


Figure 4-5. (a) Even-mode network of the prototype I. (b) Odd-mode network of the prototype I.

The even- and odd-mode networks of the prototype I are illustrated in Figure 4-5(a) and (b), respectively. Their input admittances are obtained as

$$Y_{ine} = \frac{k_1 + k_2 \tan^2 \theta + k_3 \tan^4 \theta}{k_4 \tan \theta + k_5 \tan^3 \theta}, \quad Y_{ino} = \frac{k_6 + k_7 \tan^2 \theta}{k_8 \tan \theta} \quad (4.8)$$

where

$$\begin{cases} k_1 = Z_3 Z_2 Z_1 \\ k_2 = -(Z_3^2 Z_1 + Z_s Z_1 (Z_3 + Z_2) + Z_3 Z_2 Z_s) \\ k_3 = Z_3^2 Z_s \\ k_4 = j Z_3 Z_2 Z_s Z_1 \\ k_5 = -j Z_3^2 Z_s Z_1 \\ k_6 = (Z_3 Z_2 Z_s + Z_3^2 Z_1 + Z_3 Z_s Z_1 + Z_3 Z_2 Z_s + Z_3^2 Z_s) \\ k_7 = -Z_2 Z_s Z_1 \\ k_8 = j Z_3 Z_s Z_1 (Z_2 + Z_3) \end{cases} \quad (4.9)$$

The transfer function of the prototype I is calculated as

$$F_{cir} = \frac{\left\{ -k_1 k_6 + (Y_0^2 k_4 k_8 - k_1 k_7 - k_6 k_2) \tan^2 \theta \right.}{\left. + (Y_0^2 k_8 k_5 - k_2 k_7 - k_3 k_6) \tan^4 \theta - k_3 k_7 \tan^6 \theta \right\}}{Y_0 \left\{ (k_4 k_6 - k_1 k_8) \tan \theta + (k_4 k_7 + k_6 k_5 - k_8 k_2) \tan^3 \theta \right\}} \quad (4.10)$$

A newly defined parameter, $k_0 (= Y_0(k_7 k_5 - k_8 k_3) = j Y_0 Z_3^2 Z_s^2 Z_1 (Z_2 Z_1 - Z_3 Z_2 - Z_3^2))$, is the coefficient which normalizes the highest degree of the denominator of the F_{cir} . The TZs of the prototype I are obtained under the condition of $S_{21} = 0$ as

$$\begin{aligned} \tan \theta_{TZ(0,1)} &= 0, \infty, \\ \tan \theta_{TZ(2,3)} &= \pm \sqrt{t_{z1}} = \pm j, \\ \tan \theta_{TZ(4,5)} &= \pm \sqrt{t_{z2}} = \pm \sqrt{\frac{Z_2 Z_1 + Z_2^2 + Z_3 Z_2}{Z_3 Z_2 + Z_3^2 - Z_2 Z_1}} \end{aligned} \quad (4.11)$$

For the prototype I, $\tan \theta_{TZ(0,1)}$ generates the TZs at $\theta = 0^\circ$ and 90° . $\tan \theta_{TZ(2,3)}$ represents a pair of TZs at a constant imaginary frequency points, and another $\tan \theta_{TZ(4,5)}$ is determined by the characteristic impedances of the combined MMRs (Z_1 , Z_2 and Z_3). When t_{z2} is a negative value, $\tan \theta_{TZ(4,5)}$ becomes imaginary to adjust

the group delay of the dual-band BPF; when t_{z2} is a positive value, $\tan\theta_{TZ(4,5)}$ becomes real so as to improve the out-of-band rejection between the two passbands.

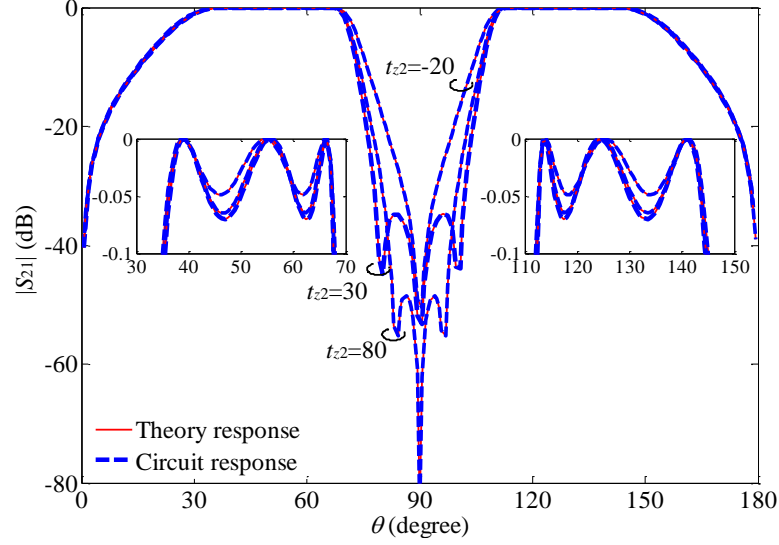


Figure 4-6. Frequency responses of the prototype I under different values of t_{z2} (other design specifications: $\theta_1 = 112.5^\circ$ and $\theta_2 = 144^\circ$).

Table 4.2 Design Parameters of Prototype I under Different t_{z2}

t_{z2}	Characteristic Impedance (Ω)				ε
	Z_1	Z_2	Z_3	Z_s	
-20	106.7	154.7	64.0	89.6	0.107
30	81.6	200.8	69.4	83.8	0.128
80	87.7	184.9	67.4	84.8	0.123

Once the two pairs of TZs (as defined by variable $t_{z1,2}$) and the specifications of the dual-band BPF (θ_1 and θ_2) are set, a theoretical filtering function F_n can be constructed by transferring the θ -plane back to Ω -plane. Then, equating F_n with F_{cir} in the θ -plane gets the following equation

$$\begin{aligned}
& \varepsilon \sum_{i=1}^{2n} m_i \Omega^i \bigg/ \sum_{j=1}^{2n-1} n_j \Omega^j \bigg|_{\Omega = -\frac{\delta}{\tan \theta}, n=3} \\
&= \frac{\varepsilon (m_6 \delta^6 + m_4 \delta^4 \tan^2 \theta + m_2 \delta^2 \tan^4 \theta + m_0 \tan^6 \theta)}{-n_1 \delta \tan \theta (\tan^2 \theta + t_{z1}) (\tan^2 \theta + t_{z2})} \\
&= \frac{j \left\{ -k_1 k_6 + (Y_0^2 k_4 k_8 - k_1 k_7 - k_6 k_2) \tan^2 \theta \right.}{k_0 \tan \theta (\tan^2 \theta + t_{z1}) (\tan^2 \theta + t_{z2})} \\
&\quad \left. + (Y_0^2 k_8 k_5 - k_2 k_7 - k_3 k_6) \tan^4 \theta - k_3 k_7 \tan^6 \theta \right\}}
\end{aligned} \tag{4.12}$$

One set of equations is obtained by equating the corresponding coefficients of the numerator as

$$\begin{cases}
-\varepsilon m_0 / n_1 \delta = -j k_3 k_7 / k_0 \\
-\varepsilon m_2 \delta^2 / n_1 \delta = j (Y_0^2 k_8 k_5 - k_2 k_7 - k_3 k_6) / k_0 \\
-\varepsilon m_4 \delta^4 / n_1 \delta = j (Y_0^2 k_4 k_8 - k_1 k_7 - k_6 k_2) / k_0 \\
-\varepsilon m_6 \delta^6 / n_1 \delta = -j k_1 k_6 / k_0
\end{cases} \tag{4.13}$$

Another set of equation is got as the characteristic impedances are restricted by the position of the TZ (t_{z2}) as shown in Table 4.1.

Therefore, from (4.10)-(4.13), 4 circuit parameters (Z_1 , Z_2 , Z_3 and Z_s) are solved but over-determined by the 5 equations. To avoid this problem, the in-band ripple factor (ε) is treated as an unknown design specification. Another explanation is simply put that the MMR (Z_1 , Z_2 and Z_3) is responsible for defining inner edge frequency as well as to generate the TZs. Z_s is for defining the outer edge frequency as well as to provide an appropriate loading to the MMR (Z_1 , Z_2 and Z_3). Thus, Z_s alone is ill-adequate to achieve a controllable ripple factor. An iterative/optimization method by the commercial toolbox [86] has been used to solve the non-linear equation. The choice of the initial value would be multiple. One example would be the two parallel connected UWB BPFs (seen in Figure 4-1) of the same bandwidth as $(\theta_2 - \theta_4)/90$. Figure 4-5 shows the frequency responses of one pair of controllable TZs. As t_{z2} varies from a negative to positive value, the second pair of TZs is moved from imaginary to real frequencies. The calculated response is indistinguishable from the desired theoretical one, which has verified the synthesis procedure.

4.3.2 Prototype II with Two Pair of Controllable TZs

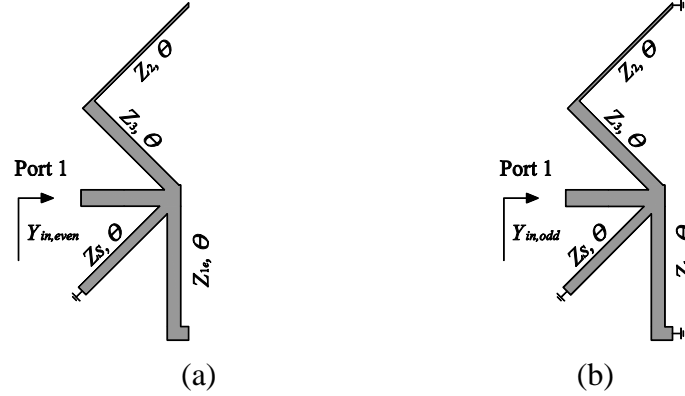


Figure 4-7. (a) Even-mode network of the prototype II. (b) Odd-mode network of the prototype II.

For the prototype II, coupled lines are used to control the pair of TZs in the imaginary frequencies (also it has the influence toward the other pair of TZs as tabulated in Table 4.1). Its even- and odd-mode networks are shown in Figure 4-7(a) and (b), respectively. Since the structure of the even- and odd-mode networks remain unchanged, the S -parameters of the prototype II are in the format as that of the prototype I (as seen in (4.8)), with the only difference in the coefficients of the polynomials as

$$\begin{cases} k_0 = jY_0 Z_3^2 Z_s^2 Z_{1o} (Z_2 Z_{1e} - Z_3 Z_2 - Z_3^2) \\ k_1 = Z_3 Z_2 Z_{1e} \\ k_2 = -(Z_3^2 Z_{1e} + Z_s Z_{1e} (Z_3 + Z_2) + Z_3 Z_2 Z_s) \\ k_3 = Z_3^2 Z_s \\ k_4 = jZ_3 Z_2 Z_s Z_{1e} \\ k_5 = -jZ_3^2 Z_s Z_{1e} \\ k_6 = (Z_3 Z_2 Z_{1o} + Z_3^2 Z_{1o} + Z_3 Z_s Z_{1o} + Z_3 Z_2 Z_s + Z_3^2 Z_s) \\ k_7 = -Z_2 Z_s Z_{1o} \\ k_8 = jZ_3 Z_s Z_{1o} (Z_2 + Z_3) \end{cases} \quad (4.14)$$

The TZs of the prototype II are derived as

$$\begin{aligned}
\tan \theta_{TZ(0,1)} &= 0, \infty \\
\tan \theta_{TZ(2,3)} &= \pm \sqrt{t_{z1}} = \pm \sqrt{-\frac{Z_{1e}}{Z_{1o}}}, \\
\tan \theta_{TZ(4,5)} &= \pm \sqrt{t_{z2}} = \pm \sqrt{\frac{Z_2 Z_{1o} + Z_2^2 + Z_3 Z_2}{Z_3 Z_2 + Z_3^2 - Z_2 Z_{1e}}}
\end{aligned} \tag{4.15}$$

By using the coupled lines, $\tan \theta_{TZ(2,3)}$ is changed from a fixed constant to the even-/odd-mode characteristic impedance ratio of the coupled lines. Thus, the two pairs of TZs are controllable by the characteristic impedances of the parallel connected MMRs.

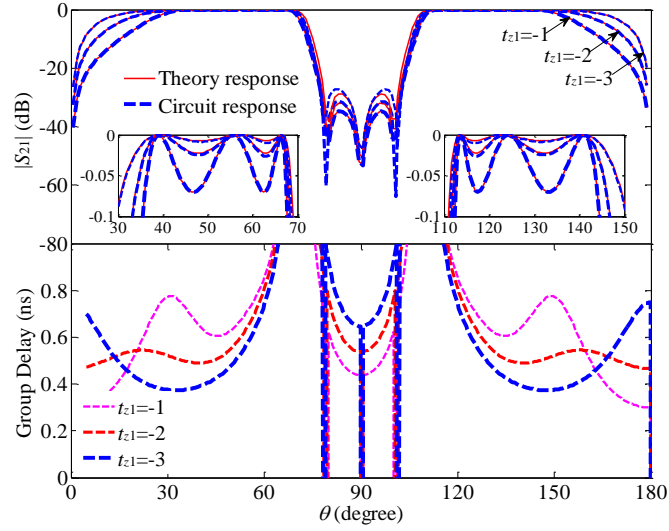


Figure 4-8. Frequency responses of the prototype II under different values of t_{z1} (other design specifications: $t_{z2}=30$, $\theta_1=112.5^\circ$ and $\theta_2=144^\circ$).

Table 4.3 Design Parameters of Prototype I under Different t_{z1}

t_{z1}	Characteristic Impedance (Ω)					ε
	Z_{1e}	Z_{1o}	Z_2	Z_3	Z_s	
-1	81.6	81.6	200.8	69.4	83.8	0.128
-2	99.9	50.0	337.4	91.2	151.8	0.072
-3	118.1	39.4	525.8	115.4	267.7	0.042

To determine the circuit design parameters, the equation in (4.10) is used by the updated coefficients of k_i ($i=0-8$), and another set of equations is by the derived expression of t_{z1} and t_{z2} as shown in Table 4.1.

Thus, there are now 6 equations in total, thus being capable to solve 5 unknown circuit parameters (Z_{1e} , Z_{1o} , Z_2 , Z_3 and Z_s) plus the in-band ripple factor (ϵ). Figure 4-7 shows the variations of one pair of TZs on imaginary frequencies and another pair under the fixed real frequencies. As the value of t_{z1} varies, the group delay is adjustable within the two passbands and the out-of-band rejection is thus affected.

4.3.3 Prototype III with Controllable In-Band Ripple

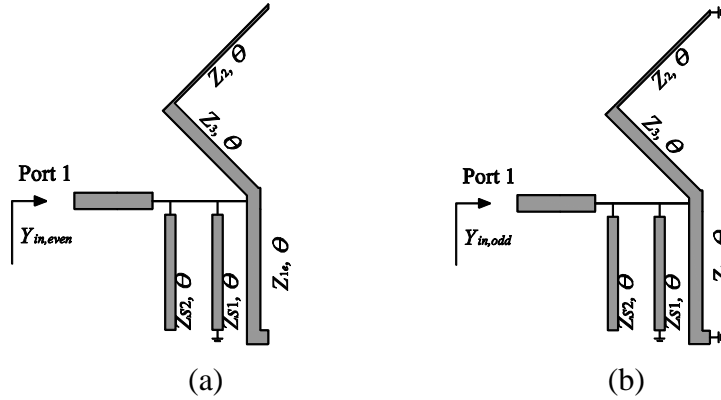


Figure 4-9. (a) Even-mode network of the prototype III. (b) Odd-mode network of the prototype III.

Based on the analysis above, ϵ is always treated as a design parameter since it lacks a degree of the design freedom when solving the equations to get the circuit parameters. Resorting to the physical structure of the dual-band BPFs, the short-circuited stubs alone are not adequate to provide the desired loading to achieve a certain value of ϵ . Thus, an additional design parameter needs to be included to replace ϵ as an unknown design variable. A combination of the short- and open-circuited stubs is used with the two design parameters (Z_{s1} and Z_{s2}) to feed the resonator. The filtering function of the prototype III is still in the same format as that of the prototype I (as seen in equation (4.8)) except the coefficients of the polynomials,

$$\begin{cases}
k_0 = jY_0 Z_3^2 Z_{s1}^2 Z_{s2}^2 Z_{1o} (Z_2 Z_{1e} - Z_3 Z_2 - Z_3^2) \\
k_1 = Z_3 Z_2 Z_{1e} Z_{s2} \\
k_2 = - \left[\begin{aligned} &Z_3^2 Z_{1e} Z_{s2} + Z_{s1} Z_{s2} Z_{1e} (Z_3 + Z_2) \\ &+ Z_3 Z_2 Z_{s1} Z_{s2} + Z_3 Z_2 Z_{s1} Z_{1e} \end{aligned} \right] \\
k_3 = Z_3^2 Z_{s1} Z_{s2} + Z_3^2 Z_{s1} Z_{1e} \\
k_4 = jZ_3 Z_2 Z_{s1} Z_{s2} Z_{1e} \\
k_5 = -jZ_3^2 Z_{s1} Z_{s2} Z_{1e} \\
k_6 = Z_{s2} (Z_3 Z_2 Z_{1o} + Z_3^2 Z_{1o} + Z_3 Z_{s1} Z_{1o} + Z_3 Z_2 Z_{s1} + Z_3^2 Z_{s1}) \\
k_7 = - \left[Z_2 Z_{s1} Z_{s2} Z_{1o} + Z_3 Z_{s1} Z_{1o} (Z_2 + Z_3) \right] \\
k_8 = jZ_3 Z_{s1} Z_{s2} Z_{1o} (Z_2 + Z_3)
\end{cases} \quad (4.16)$$

Since the structure of the parallel connected MMRs has not been changed, the TZs of the prototype III are the same as the ones of the prototype II. With the updated coefficients from k_0 to k_8 , the equations (4.10) and (4.16) can be used to determine all the circuit parameters.

To demonstrate the discussion above, two sets of figures are plotted. Figure 4-10 shows the variation of the in-band ripple factor with fixing the other design specifications (t_{z1} , t_{z2} , θ_1 and θ_2). As the ripple factor changes from 0.1 to 0.3, the rejection for the lower/upper side of the 1st/2nd passband improves slightly, while the rejection between the two passbands drops. Figure 4-11 shows the variation of the TZs in the imaginary frequency plane (as the variation of t_{z1}) with fixing the other design specifications. As t_{z1} changes from -1 to -5, there is little change of the filtering responses as seen in Figure 4-11(a), while there is an obvious change for the group delay as seen in Figure 4-11(b).

In a summary of the three circuit prototypes as tabulated in Table 4.1, according to Figure 4-5, Figure 4-7 and Figure 4-9, these circuit schematics share the similar circuit structure and the design principle, while prototype II has an additional degree of freedom in controlling the group delay and prototype III having the capability in further adjusting the in-band ripple factor. Therefore, it can be concluded that the proposed structure and the synthesis procedure has the capability in effectively controlling the in-band ripple factor (ε) and the dual-band isolation.

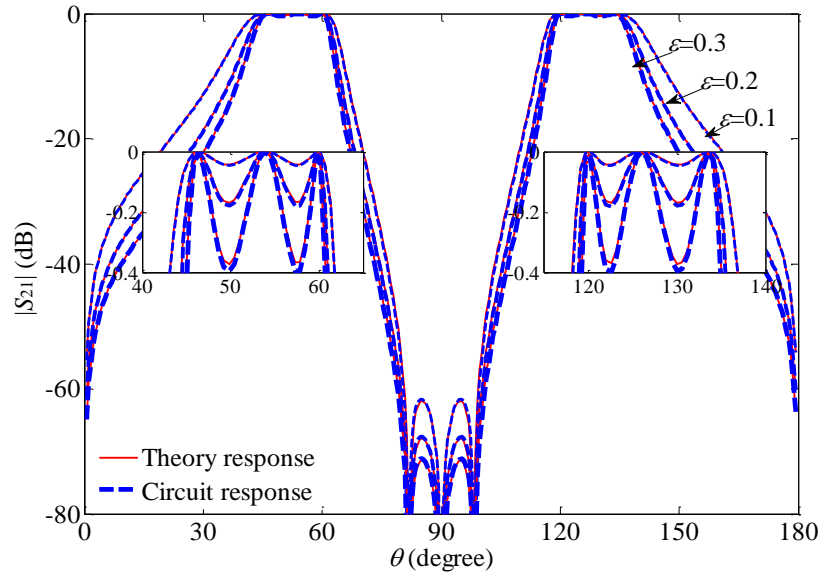


Figure 4-10. Frequency responses of the prototype III under different values of ε (other design specifications: $t_{z1} = -1.5$, $t_{z2} = 50$, $\theta_1 = 119.25^\circ$ and $\theta_2 = 135^\circ$).

Table 4.4 Design Parameters of Prototype III under Different ε

Characteristic Impedance (Ω)						ε
Z_{1e}	Z_{1o}	Z_2	Z_3	Z_{s1}	Z_{s2}	
160.6	107.1	242.1	115.1	31.0	62.5	0.1
163.5	109.0	236.2	115.9	21.0	40.7	0.2
157.0	104.7	223.0	110.8	16.5	31.4	0.3

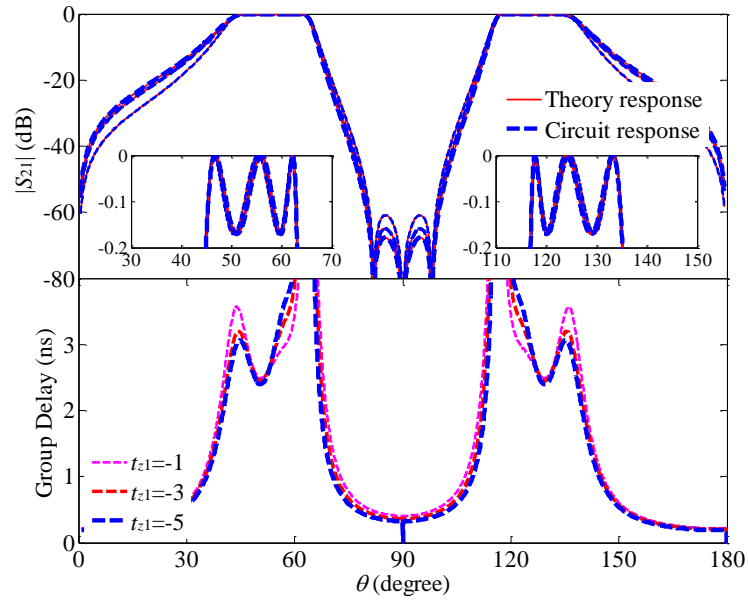


Figure 4-11. Frequency responses of the prototype III under different values of t_{z1} (other design specifications: $\varepsilon = 0.2$, $t_{z2} = 50$, $\theta_1 = 117^\circ$ and $\theta_2 = 135^\circ$).

Table 4.5 Design Parameters of Prototype III under Different t_{z1}

Characteristic Impedance (Ω)					
Z_{1e}	Z_{1o}	Z_2	Z_3	Z_{s1}	Z_{s2}
134.7	134.7	223.9	99.6	23.8	57.7
155.4	51.8	296.0	117.8	24.1	47.2
176.7	35.3	368.9	136.9	23.5	39.9

4.3.4 Circuit Transformation for Appropriate Characteristic Impedances

From the Table 4.2, Table 4.3 and Table 4.4, the calculated characteristic impedances, especially the ones of the parallel connected MMRs, tend to be too high to be achievable in practical fabrication. Therefore, a Kuroda transformation is introduced, as shown in Figure 4-12(a). The short-circuited stubs are moved into the MMR, lowering the characteristic impedances of Z_3 and Z_s . The two inverters left after the Kuroda transformation are absorbed by Z_2 , as shown in Figure 4-11(b). Thus, the characteristic impedance of Z_2 is lowered as well. By using this technique, the characteristic impedances of the short-circuited stubs and the MMR are simultaneously lowered to reach the realizable values.

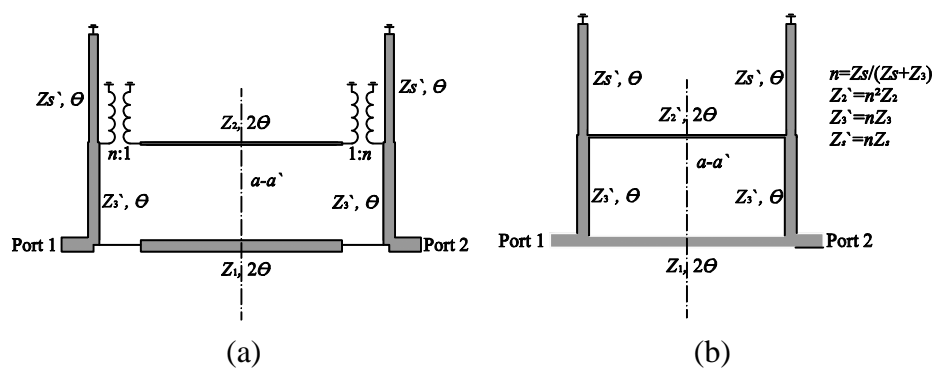


Figure 4-12. (a) Applying Kuroda transformation to the prototype I. (b) Z_2 absorbing the two inverters into Z_2' .

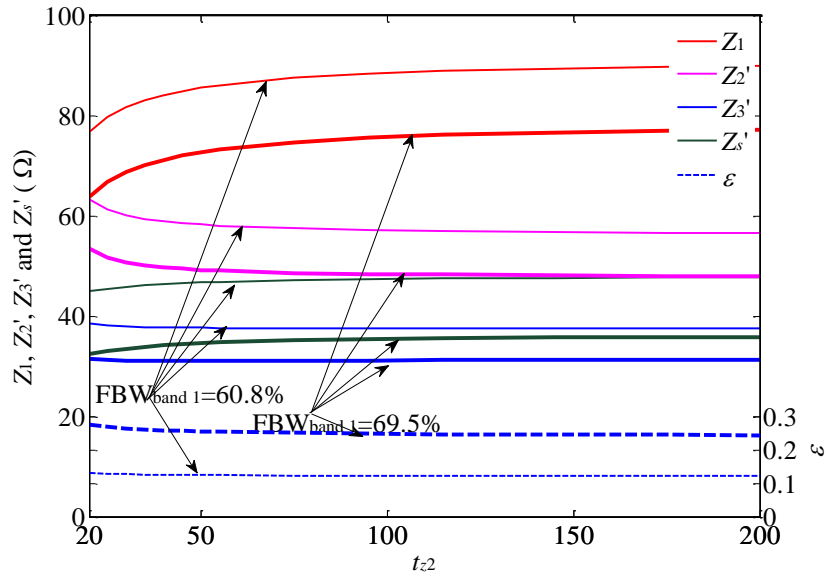


Figure 4-13. Characteristic impedances of the prototype I under varied locations of TZs (θ_{z2}) and 1st-passband FBW ($FBW_{\text{band 1}}$) with a fixed dual-band frequency ratio of 0.4 (the frequency ratio is defined as the ratio of the center frequency of the first over second passband).

Using the discussed Kuroda transformation, a set of design parameters for prototype I can be obtained. Figure 4-13 shows the characteristic impedance variations of the prototype I under different θ_{z2} s and FBW s. For the plotted curves in Figure 4-13, as the FBW increases, all the characteristic impedances drop to the lower ones, while the locations of the TZs have minor influence on the values of the characteristic impedances compared with the FBW . Once the FBW is determined, the in-band ripple factor almost stays at a fixed value.

4.4 Experimental Results and Discussions

Based on the above design process, the three prototypes shown in Table 4.1 are fabricated and measured. Prototype I and II share the same FBW , frequency ratio of the two center frequencies and one pair of TZs in the real frequency, except another pair of TZs in the imaginary frequency, thus it illustrates the capability of prototype II in controlling the TZs in imaginary frequencies. Prototype III is designed with a

different set of design specifications to prove its capability in adjusting the whole set of design specifications mentioned above. The substrate used has a dielectric constant of 10.8, loss tangent of 0.0023, thickness of 50 mils and copper thickness of 0.017 mm. A commercial EM simulator based on Method of Moments is used [89].

4.4.1 Filter Prototype I

The circuit specifications of the prototype I are set as, middle frequency of the two passbands $f_0 = 2.0$ GHz, $f_1 = 2.5$ GHz, $f_2 = 3.2$ GHz, $f_{TZ(2,3)} = \pm \infty j$ GHz and $f_{TZ(4,5)} = \pm 1.8$ GHz, which correspond to $\theta_1 = 112.5^\circ$, $\theta_2 = 144^\circ$, $t_{z1} = -1$ and $t_{z2} = 30$ (as listed in Table 4.1), respectively. The calculation of θ_1 and θ_2 is based on the middle frequency of $f_0 = 2$ GHz and through the relation of $f_{(1,2)} = f_0 \theta_{(1,2)} / 90^\circ$. The definition of both t_{z1} and t_{z2} is listed in Table 4.1. $\delta = 0.7265$ is calculated by (4.4) and the calculated filtering function after the transferring from the Ω -plane to θ -plane, as reference to (4.12), is

$$F_3 = \frac{j(4.26t^6 - 34.13t^4 + 68.18t^2 - 31.28)}{1.00t^5 - 29.00t^3 - 30.00t} \quad (4.17)$$

where $t = \tan(\theta)$. To solve this non-linear equation, the initial values are provided as $Z_1 = 100 \Omega$, $Z_2 = 100 \Omega$, $Z_3 = 100 \Omega$, $Z_s = 100 \Omega$ and $\varepsilon = 0.1$, a gradient based method (such as the “fsolve” or “lsqnonlin”) as integrated in the commercial software MATLAB is used herein. According to the synthesis procedure discussed above, the circuit design parameters are obtained as, $Z_1 = 81.6 \Omega$, $Z_2 = 200.8 \Omega$, $Z_3 = 69.4 \Omega$, $Z_s = 83.8 \Omega$ and $\varepsilon = 0.127$. The evaluated error $((|\varepsilon m_0 / n_1 \delta| - |k_3 k_7 / k_0|) + (|\varepsilon m_2 \delta / n_1| - |(Y_0^2 k_8 k_5 - k_2 k_7 - k_3 k_6) / k_0|) + (|\varepsilon m_4 \delta^3 / n_1| + |(Y_0^2 k_4 k_8 - k_1 k_7 - k_6 k_2) / k_0|) + (|\varepsilon m_6 \delta^5 / n_1| - |k_1 k_6 / k_0|))$ using the above results, $Z_1 = 81.6 \Omega$, $Z_2 = 200.8 \Omega$, $Z_3 = 69.4 \Omega$, $Z_s = 83.8 \Omega$ and $\varepsilon = 0.127$, is around 0.16. Through the Kuroda transformation, seen in Figure 4-11, all the characteristic impedances are updated as $Z_1 = 81.6 \Omega$, $Z_2' = 60.1 \Omega$, $Z_3' = 38.0 \Omega$ and $Z_s' = 45.9 \Omega$. From Figure 4-14, all the three sets of results from the theory, EM simulation and measurement are in good agreement with each other. The measured results show that for the first/second passband, the center frequency (f_{01}/f_{02}) is

1.03/2.85 GHz, the 3-dB fractional bandwidth (*FBW*) is 94.8/35.8%, and the insertion loss (*IL*) is 0.65/0.45 dB, respectively.

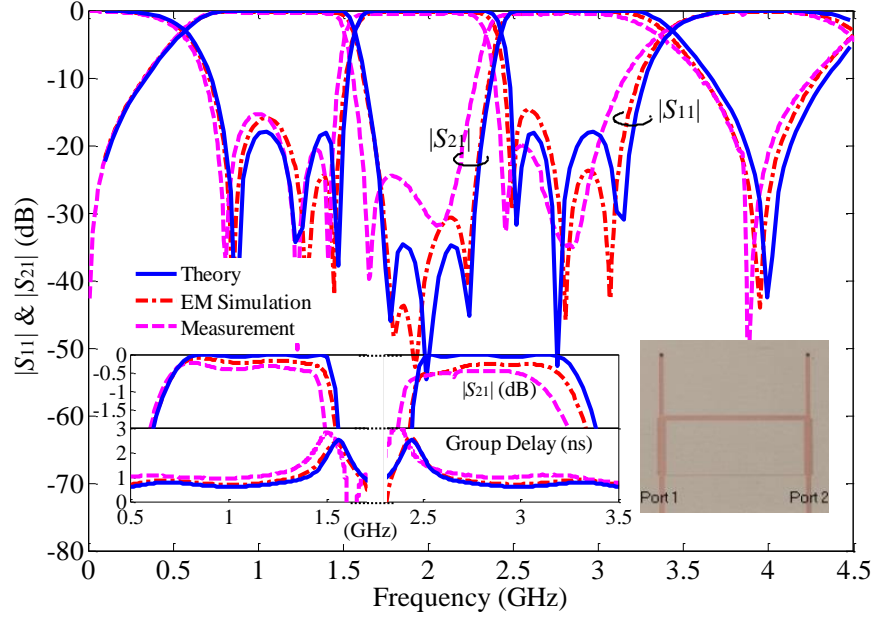


Figure 4-14. Frequency responses and group delays of the theoretical, EM simulated and the measured results of the prototype I.

4.4.2 Filter Prototype II

The circuit specifications of the prototype II are set as, $f_0 = 2.0$ GHz, $f_1 = 2.5$ GHz, $f_2 = 3.2$ GHz, $f_{TZ(2,3)} = -2.0 + 1.5j$, $2.0 - 1.5j$ GHz and $f_{TZ(4,5)} = \pm 1.8$ GHz, which correspond to $\theta_1 = 112.5^\circ$, $\theta_2 = 144^\circ$, $t_{z1} = -1.5$ and $t_{z2} = 30$, respectively. The calculation of θ_1 and θ_2 is based on the middle frequency of $f_0 = 2$ GHz and through the relation of $f_{(1,2)} = f_0 \theta_{(1,2)} / 90^\circ$. The definition of both t_{z1} and t_{z2} is listed in Table 4.1. $\delta = 0.7265$ is calculated by (4.4) and the calculated filtering function after the transferring from the Ω -plane to θ -plane is

$$F_3 = \frac{j(3.72t^6 - 30.28t^4 + 62.06t^2 - 29.06)}{1.00t^5 - 27.37t^3 - 45.00t} \quad (4.18)$$

where $t = \tan(\theta)$. To solve this non-linear equation, the initial values are provided as $Z_{1e} = 100 \Omega$, $Z_{1o} = 50 \Omega$, $Z_2 = 100 \Omega$, $Z_3 = 100 \Omega$ and $Z_s = 100 \Omega$. A gradient based method (such as the “fsolve” or “lsqnonlin”) as integrated in the commercial software MALAB is used herein. The circuit design parameters are obtained as $Z_{1e} = 90.7 \Omega$, $Z_{1o} = 60.5 \Omega$, $Z_2 = 262.4 \Omega$, $Z_3 = 79.9 \Omega$, $Z_s = 112.7 \Omega$ and $\varepsilon = 0.097$. The evaluated error $((|\varepsilon m_0/n_1 \delta| - |k_3 k_7/k_0|) + (|\varepsilon m_2 \delta/n_1| - |(Y_0^2 k_8 k_5 - k_2 k_7 - k_3 k_6)/k_0|) + (|\varepsilon m_4 \delta^3/n_1| + |(Y_0^2 k_4 k_8 - k_1 k_7 - k_6 k_2)/k_0|) + (|\varepsilon m_6 \delta^5/n_1| - |k_1 k_6/k_0|))$ using the above results, $Z_{1e} = 90.7 \Omega$, $Z_{1o} = 60.5 \Omega$, $Z_2 = 262.4 \Omega$, $Z_3 = 79.9 \Omega$, $Z_s = 112.7 \Omega$ and $\varepsilon = 0.097$, is around 0.16. After the Kuroda transformation, $Z_{1e} = 90.7 \Omega$, $Z_{1o} = 60.5 \Omega$, $Z_2' = 89.9 \Omega$, $Z_3' = 46.7 \Omega$ and $Z_s' = 66.0 \Omega$. Figure 4-15 shows the theoretical, EM simulated and the measured results. The measured results show that f_{01}/f_{02} is 1.00/2.86 GHz, 3-dB *FBW* is 102.0/34.6% and IL 0.63/0.99 dB, for the first/second passband, respectively. The measured results match well with the calculated and the simulated ones.

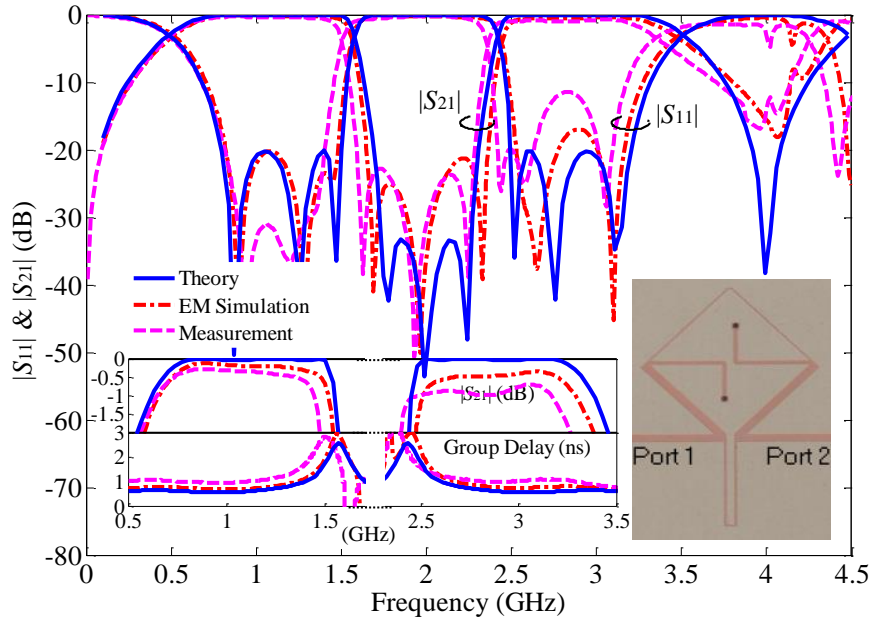


Figure 4-15. Frequency responses and group delays of the theoretical, EM simulated and the measured results of the prototype II.

4.4.3 Filter Prototype III

The circuit specifications of the prototype III are set as, $f_0= 2.0$ GHz, $f_1=2.65$ GHz, $f_2=3.2$ GHz, $f_{TZ(2,3)}=-2.0+1.5j$, $2.0-1.5j$ GHz, $f_{TZ(4,5)}=\pm 1.6$ GHz and $\varepsilon= 0.1$, which correspond to $\theta_1= 119.25^\circ$, $\theta_2= 144^\circ$, $t_{z1}= -1.5$ and $t_{z2}= 8$ (as listed in Table 4.1), respectively. The calculation of θ_1 and θ_2 is based on the middle frequency of $f_0=2$ GHz and through the relation of $f_{(1,2)}=f_0\theta_{(1,2)}/90^\circ$. The definition of both t_{z1} and t_{z2} is listed in Table 4.1. $\delta= 1.00$ is calculated by (4.4) and the calculated filtering function after the transferring from the Ω -plane to θ -plane is

$$F_3 = \frac{j(4.17t^6 - 21.55t^4 + 31.41t^2 - 12.29)}{1.00t^5 - 6.16t^3 - 12.00t} \quad (4.19)$$

where $t= \tan(\theta)$. To solve this non-linear equation, the initial values are provided as $Z_{1e}= 100$, $Z_{1o}= 50 \Omega$, $Z_2= 100 \Omega$, $Z_3= 100 \Omega$, $Z_{s1}= 100 \Omega$ and $Z_{s2}= 100 \Omega$. A gradient based method (such as the “fsolve” or “lsqnonlin”) as integrated in the commercial software MATLAB is used herein. The circuit design parameters are obtained as, $Z_{1e}= 98.7 \Omega$, $Z_{1o}= 65.8 \Omega$, $Z_2= 224.8 \Omega$, $Z_3= 101.7 \Omega$, $Z_{s1}= 81.6 \Omega$ and $Z_{s2}= 119.3 \Omega$. The evaluated error $((|\varepsilon m_0/n_1\delta|/k_3k_7/k_0|)+(|\varepsilon m_2\delta/n_1|-(Y_0^2k_8k_5-k_2k_7-k_3k_6)/k_0|)+(|\varepsilon m_4\delta^3/n_1|+(Y_0^2k_4k_8-k_1k_7-k_6k_2)/k_0|)+(|\varepsilon m_6\delta^5/n_1|/k_1k_6/k_0|))$ using the results, $Z_{1e}= 98.7 \Omega$, $Z_{1o}= 65.8 \Omega$, $Z_2= 224.8 \Omega$, $Z_3= 101.7 \Omega$, $Z_{s1}= 81.6 \Omega$ and $Z_{s2}= 119.3 \Omega$, is around 0.005. After the Kuroda transformation, $Z_{1e}= 98.7 \Omega$, $Z_{1o}= 65.8 \Omega$, $Z_2'= 44.5 \Omega$, $Z_3'= 45.3 \Omega$, $Z_{s1}'= 36.3 \Omega$ and $Z_{s2}= 119.3 \Omega$. Figure 4-16 shows the theoretical, EM simulated and the measured results. All the three sets of results are reasonably matched with each other. The measured results show that f_{01}/f_{02} is 1.04/2.96 GHz, 3-dB *FBW* is 100.0/34.6 %, and IL is 0.73/0.70 dB, for the first/second passband, respectively. The difference between the measured results and the theoretical ones is basically caused by some parasitic effects, such as the junction discontinuities, dispersion of the microstrip line, and the approximate assumption of equal even- and odd-mode phase velocity. The resonance spike appearing in the upper band may be caused by the variation of the phases and magnitudes of signal transmission in the two parallel-connected UWB filters. When

there is a small electrical length variation in either the upper or the lower signal transmitting path, the phase or magnitude does not apply to the condition of generating the TZ, a resonant spike can occur either in the middle of the two passbands (spike I) or the upper sides of the two passbands (spike II). Similarly, when there is a length difference between the open- and short-stubs, they form a resonance around the middle frequency of the two passbands, which again creates a resonant spike (spike I), as seen in Figure 4-17.

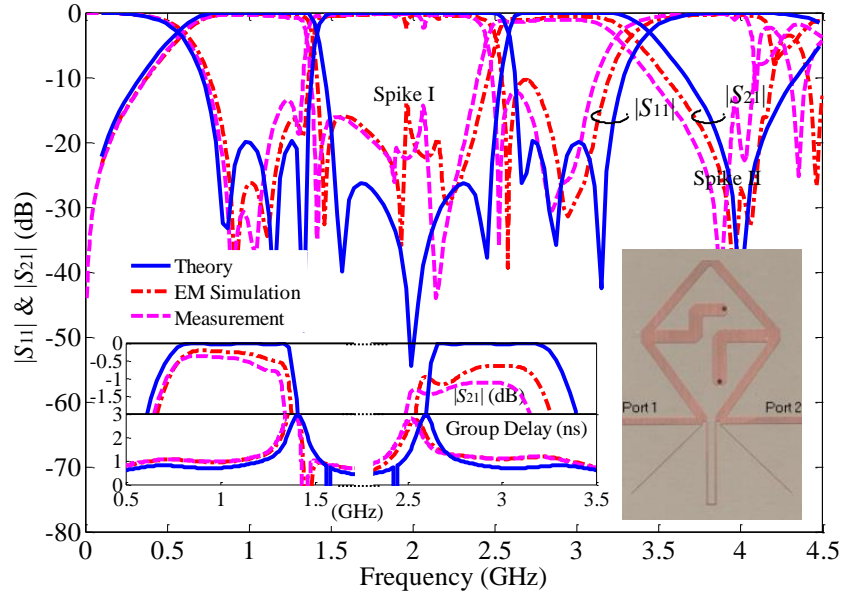


Figure 4-16. Frequency responses and group delays of the theoretical, EM simulated and the measured results of the prototype III.

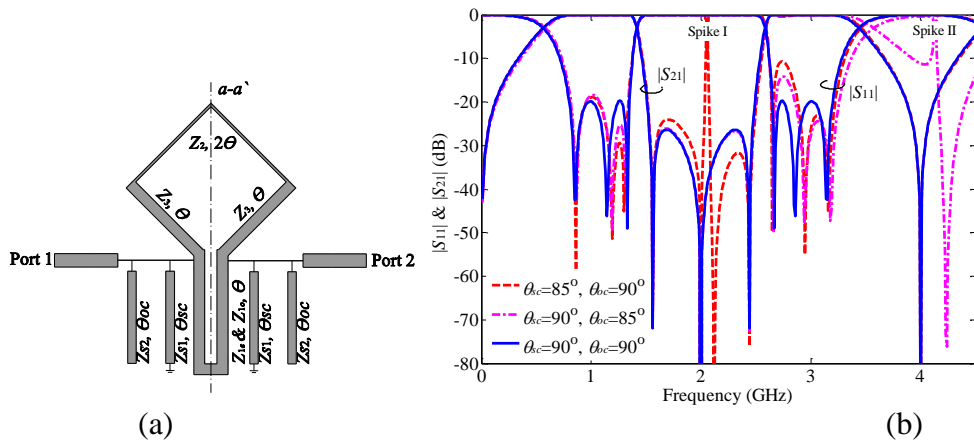


Figure 4-17. (a) Circuit schematic of prototype III with the electrical length of the open- and short-stub labelled as θ_{oc} and θ_{sc} . (b) Simulated results of prototype III under different set of θ_{oc} and θ_{sc} .

4.5 Summary

A class of wideband dual-band BPFs with controllable in-band ripple factor and TZs has been proposed, synthesized and designed. The basic structure of the dual-band BPF is formed by parallel connecting two dissimilar short-circuited MMRs. Two pairs of TZs are generated with one pair either in the imaginary or in the real frequencies. To make effective use of another pair of TZs, coupled lines are used in the second prototype. In addition, to provide a controllable in-band ripple factor, a combined set of short- and open-circuited stubs is constructed. A synthesis method by equating the transfer function of the filter circuits with the chosen filtering function has been developed to explicitly determine the design parameters of the dual-band BPFs. In the final part, the three filter prototypes have been designed, fabricated and measured to verify the proposed design principle.

CHAPTER 5

SYNTHESIS AND DESIGN OF A CLASS OF DUAL-WIDEBAND BANDPASS FILTERS WITH INTERNALLY-COUPLED MICROSTRIP LINES

5.1 Introduction

In this chapter, a class of dual-wideband BPFs with the internally-coupled microstrip lines has been proposed, synthesized and designed. The proposed dual-wideband BPFs have the following characteristics:

- 1, the order of the proposed BPFs can be chosen freely by extending or adding more sections of the coupled microstrip lines;
- 2, the design parameters of the filters can be determined more freely since the presence of the internally coupled lines to allow the designer to specify a preferred value;
- 3, the circuit size can be more compact than the filters proposed in the previous chapter.

The generic circuit structure of the filter is in the form that a multi-mode resonator (MMR) is symmetrically folded to form up the internally-coupled microstrip lines. By adding more sections of the coupled MMR, the order of the proposed filter is increased. Then, a pair of short-circuited stubs is introduced to inductively loading the MMR. By further introducing a mutual coupling between the two short-circuited stubs, another signal transmitting path is formed to generate additional pairs of TZs at either the real or imaginary frequencies.

The synthesis procedure for the proposed BPFs follows a similar procedure as discussed in the previous section, which can be seen as firstly deriving the theoretical filtering function, then analyzing the chosen circuit response based on its transfer function, and finally obtaining the circuit design parameters by equating the two aforementioned functions.

Experimental results for 2nd-3rd order as well as a cascaded dual-band filter are demonstrated in the final part.

5.2 Design and Synthesis Procedure

5.2.1 Circuit Analysis of the Proposed Dual-Band Filters

The generic structure of the proposed dual-band BPF is depicted in Figure 5-1, in which Z_{ie} and Z_{io} ($i= 1, 2, \dots$) denote the even- and odd-mode characteristic impedances of the i -th coupled-line section in the folded MMR, while (Z_{s1e}, Z_{s2e}) and (Z_{s1o}, Z_{s2o}) represent the even- and odd-mode characteristic impedances of the two coupled short-circuited stubs, respectively. To simplify the synthesis procedure, it is assumed that for all the coupled-line sections involved, their electrical lengths are set as the same, $\theta_e = \theta_o = \theta$, regardless of even- or odd-mode cases, where θ is defined at the middle frequency of the two passbands.

For the MMR with the $2i$ line sections in Figure 5-1, it is to introduce $(2i-1)$ reflection zeroes within the interested passbands. By applying this property in a filter design, increasing the section number of the MMR leads to more reflection zeroes within the passband, as discussed in [12]. When the MMR is folded along its symmetrical plane as shown in Figure 5-1, the design parameter is split from the characteristic impedance, Z_i , of an uncoupled line to the even- and odd-mode characteristic impedances, Z_{ie} and Z_{io} , of the coupled lines, releasing twice design parameters compared with the un-coupled MMR. Therefore, it permits an extra degree of freedom in determining these characteristic impedances during the filter

design process. According to the study in [87], the folded MMR modifies or reshapes the phase distribution of current density flowing along its two sides, providing a great potential in creating more pairs of TZs at the specified frequencies.

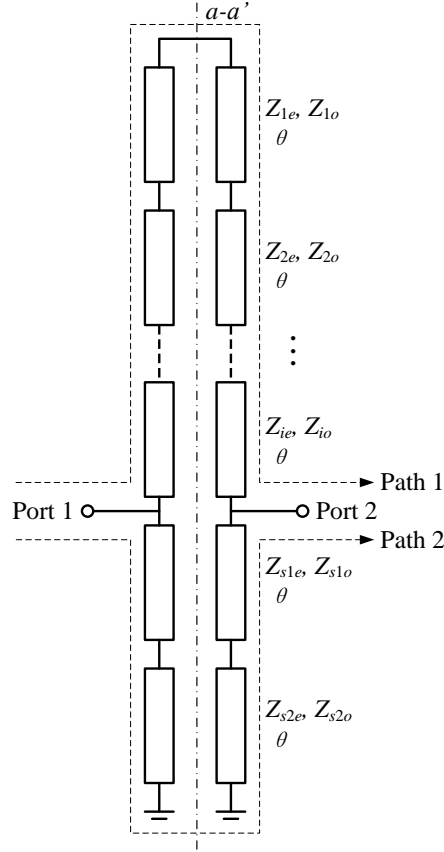


Figure 5-1. General schematic of the proposed dual-wideband BPF with the internally-coupled microstrip lines.

As studied in [12], the two short-circuited stubs are used herein to inductively feed or excite the folded MMR at its two sides, and they also introduce more reflection zeroes in the passbands. In the meantime, these two coupled stubs provide another signal transmitting path beside the coupled MMR. With the help of these two paths, additional reflection zeroes are generated.

First, the theoretical analysis of the proposed dual-band BPF in Figure 5-1 is carried out by applying the even-/odd-mode analysis method with respect to the symmetrical plane of $a-a'$. The transfer function F_{cir} is obtained as [5]

$$F_{cir} = \frac{S_{11}}{S_{21}} = \frac{Y_0^2 - Y_{ine}Y_{ino}}{Y_0(Y_{ino} - Y_{ine})} \quad (5.1)$$

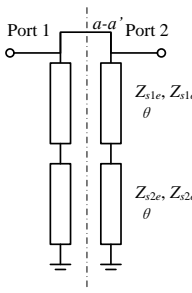
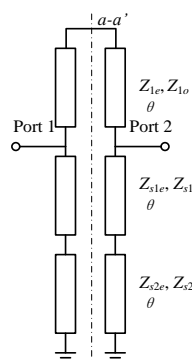
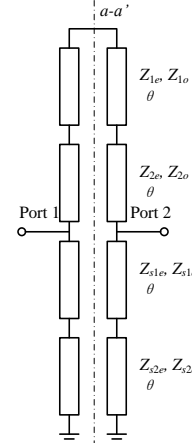
where Y_0 stands for the port admittance, Y_{ine} and Y_{ino} are the input admittances of the one-port even- and odd-symmetrical bisection circuits, respectively.

Table 5.1 depicts the structures of the first three filter prototypes with the 1st-, 2nd- and 3rd-order, and it provides the derived mathematical expressions for the input admittances of the three one-port even- and odd-mode bisections as well as the transfer functions of the three two-port filter circuits to be synthesized.

In (5.1), the numerator of F_{cir} contains the information about the number and positions of the reflection zeroes, and it is in the form of an even order polynomial as a function of t ($t = \tan(\theta)$). Therefore, the reflection zeroes are distributed in pairs with mirror to $\theta = \pi/2$. Meanwhile, the denominator of F_{cir} implies the number and positions of the TZs, and it is in the form of an even order polynomial multiplied by t . Thus, there always exists a TZ at $\theta = 0$ and π , and the rest ones are paired with mirror to $\theta = \pi/2$. It is found that the polynomial of the numerator is one degree higher than that of the denominator. As t approaches infinity, F_{cir} becomes infinite, indicating that a TZ is located at $\theta = \pi/2$. Based on the above discussions, the TZs at $\theta = 0$, $\pi/2$ and π shaping the basic filtering response of the dual-band BPF, and the reflection zeroes locate symmetrically with respect to $\theta = \pi/2$ forming the dual-passband.

5.2.2 Dual-Band Filtering Function

Table 5.1 Structures of the Proposed Dual-Band BPF Prototypes

Filter Structure			
n	1	2	3
$\begin{Bmatrix} Y_{ine} \\ Y_{ino} \end{Bmatrix}$	$\begin{Bmatrix} \frac{k_1 + k_2 t^2}{k_3 t} \\ \infty \end{Bmatrix}$	$\begin{Bmatrix} \frac{k_1 + k_2 t^2}{k_3 t} \\ \frac{k_4 + k_5 t^2}{k_6 t} \end{Bmatrix}$	$\begin{Bmatrix} \frac{k_1 + k_2 t^2 + k_3 t^4}{k_4 t + k_5 t^3} \\ \frac{k_6 + k_7 t^2}{k_8 t} \end{Bmatrix}$
F_{cir}	$\begin{bmatrix} -k_1 \\ -k_2 t^2 \end{bmatrix} \frac{1}{Y_0 t k_3}$	$\begin{bmatrix} -k_1 k_4 \\ (Y_0^2 k_3 k_6 - k_2 k_4 - k_1 k_5) t^2 \\ -k_2 k_5 t^4 \end{bmatrix} \frac{1}{Y_0 t \begin{bmatrix} (k_4 k_3 - k_1 k_6) \\ (k_5 k_3 - k_2 k_6) t^2 \end{bmatrix}}$	$\begin{bmatrix} -k_1 k_6 \\ (Y_0^2 k_8 k_4 - k_1 k_7 - k_6 k_2) t^2 \\ (Y_0^2 k_8 k_5 - k_2 k_7 - k_3 k_6) t^4 \\ -k_3 k_7 t^6 \end{bmatrix} \frac{1}{Y_0 t \begin{bmatrix} (k_6 k_4 - k_8 k_1) \\ (k_7 k_4 + k_6 k_5 - k_8 k_2) t^2 \\ (k_7 k_5 - k_8 k_3) t^4 \end{bmatrix}}$

where $t = \tan(\theta)$, n is the order of each individual band of the dual-band bandpass filter, Y_{ine} and Y_{ino} the input admittance of the even- and odd-mode circuit, respectively, and F_{cir} the transfer function of the filter.

As for the filtering function, a generalized Chebyshev filtering function is established based on a transversal coupling scheme, taking into account the TZ at

origin, instead of the commonly used ones in [71] for the narrow dual-band BPFs. The n^{th} -order filtering function as a function of Ω is given as [23]

$$F_n(\Omega) = \cosh \left(\cosh^{-1} \left(\frac{T_2(\Omega)}{|\Omega|} \right) + \sum_{k=1}^{n-1} \cosh^{-1} (f_k(\Omega)) \right) \quad (5.2)$$

Next, a recursion formula [23] is derived to expand the filtering function to a ratio of two polynomials, as seen in Section 2.2.3 for a detailed discussion of this filtering function.

5.2.3 Synthesis of the Proposed Dual-Band BPFs

The synthesis procedure for the proposed wideband dual-band BPF is illustrated in Figure 5-2, i.e., (a) formulating the filtering function, (b) analyzing the frequency response of the filter circuit, and (c) enforcing the equalization of these two functions so as to determine all the circuit design parameters, as documented in [84]. Since the generalized Chebyshev transfer function to be chosen is only valid for a single band modeling with mirror to the origin, a frequency mapping, namely, Richard's transformation [25], is used to transfer the single-band function to its dual-band counterpart. Accordingly, the transformation from the ω -plane to the Ω -plane [71] can be derived in the form of

$$\Omega = -\delta / \tan \theta, \quad \theta = \frac{\pi}{2} \frac{\omega}{\omega_0} \quad (5.3)$$

$$\delta = 1 / \tan \left[\frac{\pi}{4} \frac{(\omega_2 - \omega_4)}{\omega_0} \right] \quad (5.4)$$

where ω_2 and ω_4 are the upper and lower edge frequencies of the dual-band BPF, respectively, with reference to Figure 5-2.

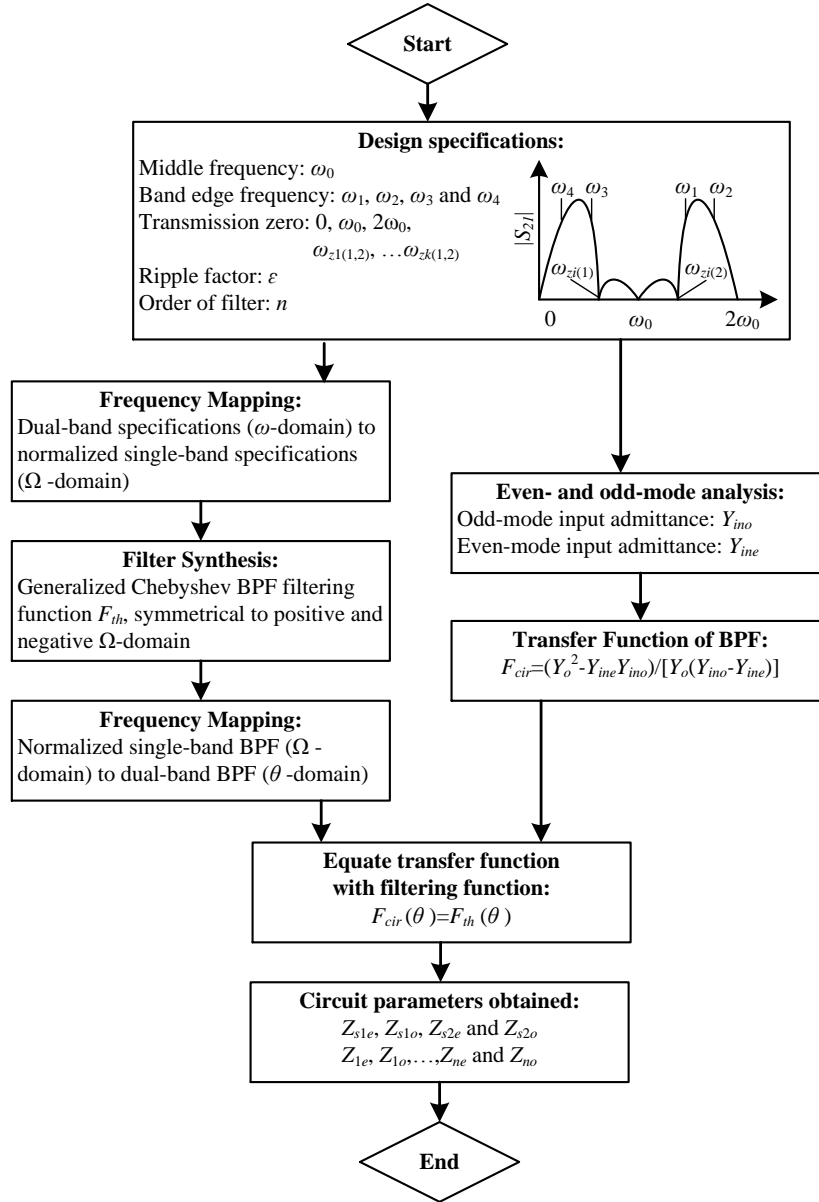


Figure 5-2. Synthesis procedure for the proposed dual-band BPFs.

Once the specifications of the filter are prescribed, these ω -plane frequencies are transformed to the Ω -plane for formulating the filtering function. Afterwards, the filtering function is transformed back to the θ -plane in order to exactly match the transfer function of the circuit in the form of

$$\varepsilon F_n(\Omega) \Big|_{\Omega = \frac{\delta}{\tan \theta}} = jF_{cir}(\tan \theta) \quad (5.5)$$

where ε is the in-band ripple factor for the dual passbands.

A set of non-linear equations is obtained by setting the coefficients of the numerator and the denominator between the two functions to be equal, respectively. An iterative/optimization method [86] is applied herein to solve these non-linear equations. The initial values of the proposed dual-wideband BPFs are determined in close relation to the wideband BPF as seen in Figure 3-1, which are formed by folded single-wideband BPFs with extended short-circuited stubs. But it is noted that there is still some cut-and-try effort used to determine the even- and odd-mode characteristic impedances for the coupled lines, thus it needs adjusting the filtering response approaching the target one.

5.3 Synthesis and Design of Dual-Band BPFs

In this section, the three types of filters as listed in Table 5.1 have been discussed in a more detailed manner. By using the even-/odd-mode analysis method, their transfer functions have been derived to aid the design and explanation of their working mechanisms.

5.3.1 1st-Order Dual-Band BPF Design

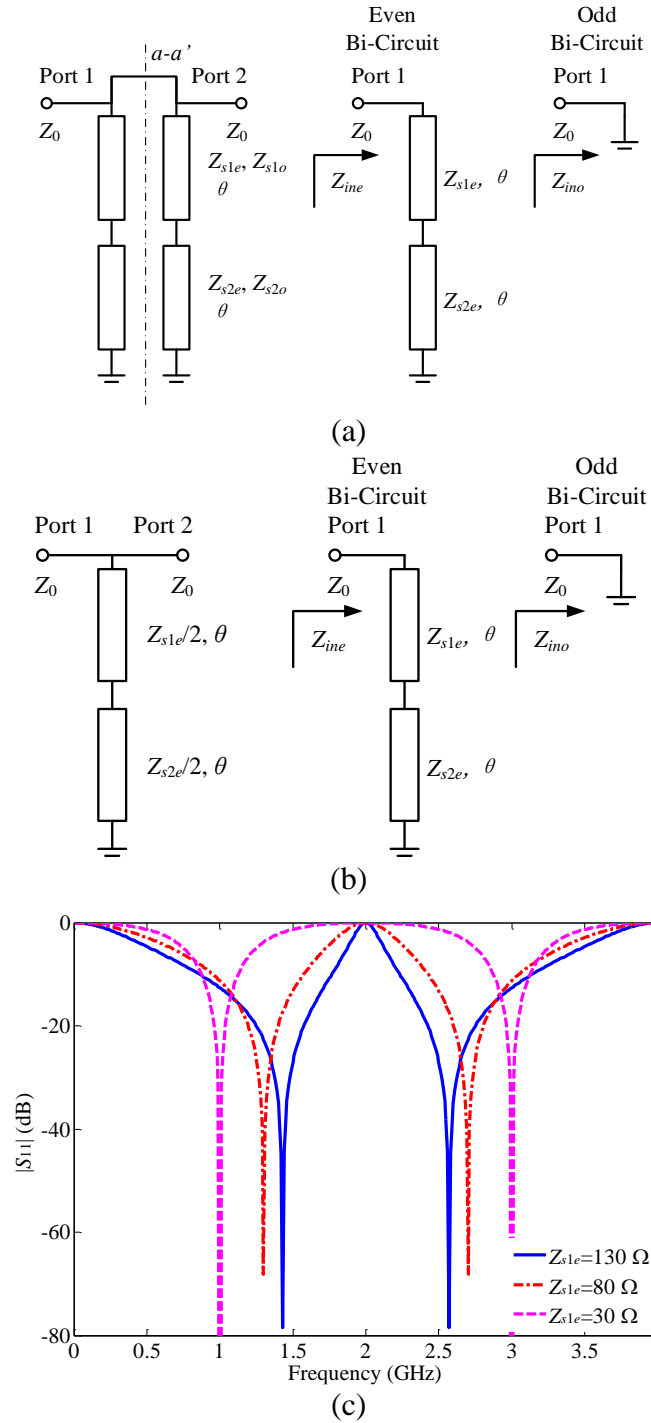


Figure 5-3. (a) Transmission-line characterization of the parallel-coupled short-circuited stubs and its even-/odd-bisection circuits. (b) The stepped-impedance stub and its even-/odd-bisection circuits. (c) Locations of the reflection zeroes under different Z_{s1e} ($Z_{s2e} = 30 \Omega$).

First, a special case formed by two coupled short-circuited stubs is discussed. Under odd-mode excitation, the circuit is virtually shorted to ground. While under even-mode excitation, its bisection circuit contributes to the frequency response in the desired passband. Therefore, the coefficient of the transfer function F_{cir} is only related to its even-mode characteristic impedances as

$$\begin{cases} k_1 = Z_{1se} \\ k_2 = -Z_{2se} \\ k_3 = jZ_{1se}(Z_{2se} + Z_{1se}) \end{cases} \quad (5.6)$$

Actually, the parallel-coupled short-circuited stubs could be further simplified as a two-section stepped-impedance stub, as shown in Figure 5-3(a) and (b). This is because by applying the even-/odd-mode analysis method to both circuits, the even-bisection circuits are the same and the odd-bisection circuits are shorted to ground ($Z_{ine_1} = Z_{ine_2}$ and $Z_{ino_1} = Z_{ino_2}$). Therefore, according to the discussion in (4.1) and (4.2), these two circuits share the same filtering response. Besides the TZs (θ_{tz1}) at multiple integer of $\pi/2$, there is also one pair of reflection zeroes with mirror to the middle frequency of the two passbands. As the characteristic impedance ratio of the stepped-impedance stubs changes, the frequency ratio of the two reflection zeroes varies accordingly [88], as illustrated in Figure 5-3(c). Based on the above discussion, the short-circuited stubs have two main roles for the proposed filter design, first, introducing TZs to shape dual-band frequency-response, second, introducing one pair of tunable reflection zeroes at the desired positions within each band.

5.3.2 2nd-Order Dual-Band BPF Design

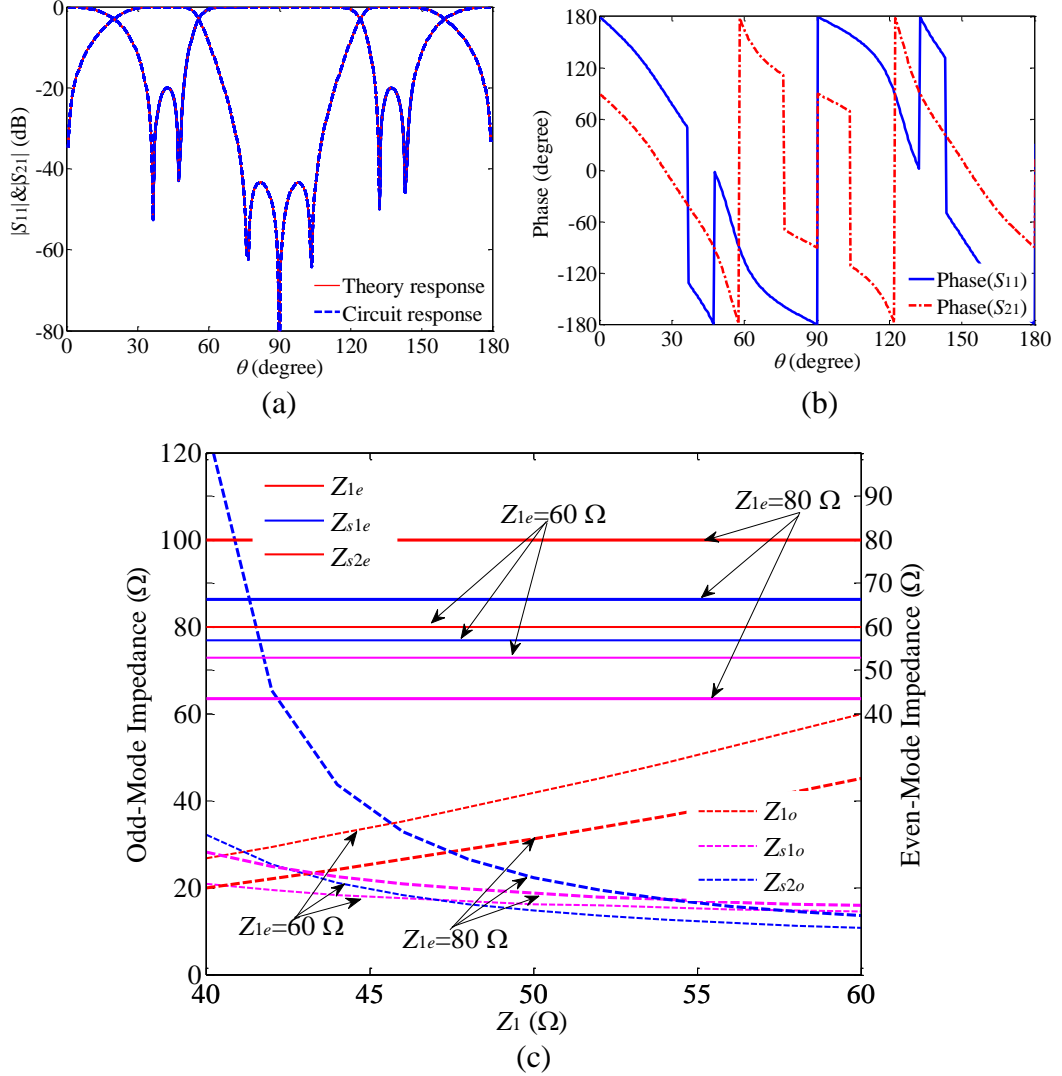


Figure 5-4. (a) Comparison between the theoretical and the circuit responses of a 2nd-order filter with $\varepsilon = 0.1$, $\theta_{tz2} = 76.5^\circ$, $\theta_1 = 123.75^\circ$ and $\theta_2 = 139.5^\circ$. (b) Phase responses. (c) Characteristic impedances versus Z_{1e} and Z_1 for achieving the responses in Figure 5-4(a)-(b).

To increase the filter order for the required sharp rejection slope, one more section is introduced in the coupled MMR, as tabulated in Table 5.1. According to the even-/odd-mode analysis, the transfer function of this 2nd-order dual-band filter is derived, with its definition of the coefficients (k_1 - k_6) as

$$\begin{cases} k_1 = Z_{1e}Z_{s1e} \\ k_2 = -(Z_{s1e}Z_{s2e} + Z_{s1e}Z_{s1e} + Z_{1e}Z_{s2e}) \\ k_3 = jZ_{1e}Z_{s1e}(Z_{s2e} + Z_{s1e}) \\ k_4 = j(Z_{s1o}Z_{s2o} + Z_{s1o}Z_{s1o} + Z_{1o}Z_{s1o}) \\ k_5 = -jZ_{1o}Z_{s2o} \\ k_6 = -Z_{1o}Z_{s1o}(Z_{s2o} + Z_{s1o}) \end{cases} \quad (5.7)$$

Besides the TZs located at $\theta_{tz1} = 0, \pi/2$ and π , there is one pair of TZs at θ_{tz2} , and they could be explicitly expressed as

$$\begin{cases} \tan \theta_{tz1} = 0, \infty \\ \tan \theta_{tz2} = \pm \sqrt{\frac{(k_1k_6 - k_4k_3)}{(k_5k_3 - k_2k_6)}} \end{cases} \quad (5.8)$$

From the derived transfer function in Table 5.1, there are 3 and 2 coefficients for its numerator and denominator, respectively. These unknown coefficients are expressed in the form of characteristic impedances of the circuit. First, the highest order of either the numerator or denominator is normalized, so that the number of the unknown coefficients can be reduced to only 4. Next, for the internally-coupled dual-band BPF, there are 6 characteristic impedances (Z_{1e} , Z_{1o} , Z_{s1e} , Z_{s1o} , Z_{s2e} , and Z_{s2o}) to be solved. So, the 4 unknown coefficients are overly determined by the 6 circuit parameters. In other words, it is possible to have different sets of characteristic impedance to get the same sets of polynomial coefficients in the transfer function, and to obtain the same filtering responses in the end. Therefore, there exists an extra degree of freedom when determining the characteristic impedances. Following this design strategy, 2 of 6 parameters are predefined as certain values as a design example to illustrate the flexibility in controlling the characteristic impedances. These two design variables are the characteristic impedances of the MMR (Z_{1e} and Z_{1o}) and they are selected under the criteria of $Z_1 = \sqrt{Z_{1e}Z_{1o}}$. Under the different choices of Z_{1e} and Z_{1o} , different solutions of Z_{s1e} , Z_{s1o} , Z_{s2e} , and Z_{s2o} are obtained while maintaining the same frequency response.

Figure 5-4(a) plots the typical simulated frequency response of a 2nd-order dual-band BPF using the theoretical filtering function and synthesized circuit transfer function, respectively. Both sets of frequency responses are indistinguishable to each other, so it well verifies the proposed synthesis method. Figure 5-4(b) depicts the phase variations in relevance to the circuit responses, and Figure 5-4(c) presents different sets of characteristic impedance solutions to give the same magnitude and phase responses as those in Figure 5-4(a)-(b). Thus, it proves the proposed technique on an extra degree of freedom in choosing different sets of characteristic impedances as well. It is noted that for Figure 5-4, it shows a set of solutions from the non-linear equations. When the obtained even-mode characteristic impedances are smaller than the odd-mode characteristic impedances, it implies that the chosen design specifications are not suitable for practical implementation by the proposed circuit structure.

Further looking into Figure 5-4(c), once Z_{1e} is chosen as either 60 or 80 Ω , the even-mode characteristic impedances, Z_{s1e} and Z_{s2e} , can be fixed as certain values. A set of straight lines is used to characterize the variation of the even-mode characteristic impedance. As Z_1 is swept, Z_{1o} is changed, as $Z_{1o} = Z_1^2/Z_{1e}$, and it causes the variation of the odd-mode characteristic impedances. Therefore, a set of curves is used for their variation. This regulation can be simply verified by the characteristics of the even-/odd-mode analysis, namely, the design parameters of the even-mode bisection circuit being chosen unrelated to that of its odd-mode counterpart once the even-mode characteristic impedance is larger than the odd-mode characteristic impedance. Therefore, it is possible to get a set of even- and odd-mode characteristic impedances respectively to maintain the frequency response of the corresponding even- and odd-mode bisection circuit, and then the frequency response of the whole circuit keeps the same. This provides a foundation for the proposed BPFs in achieving the extra design freedom of the design parameters while maintaining the exactly same frequency response. With this technique, it is advantageous in choosing a set of preferred characteristic impedances suitable for the design procedure and/or fabrication.

5.3.3 3rd-Order Dual-Band BPF Design

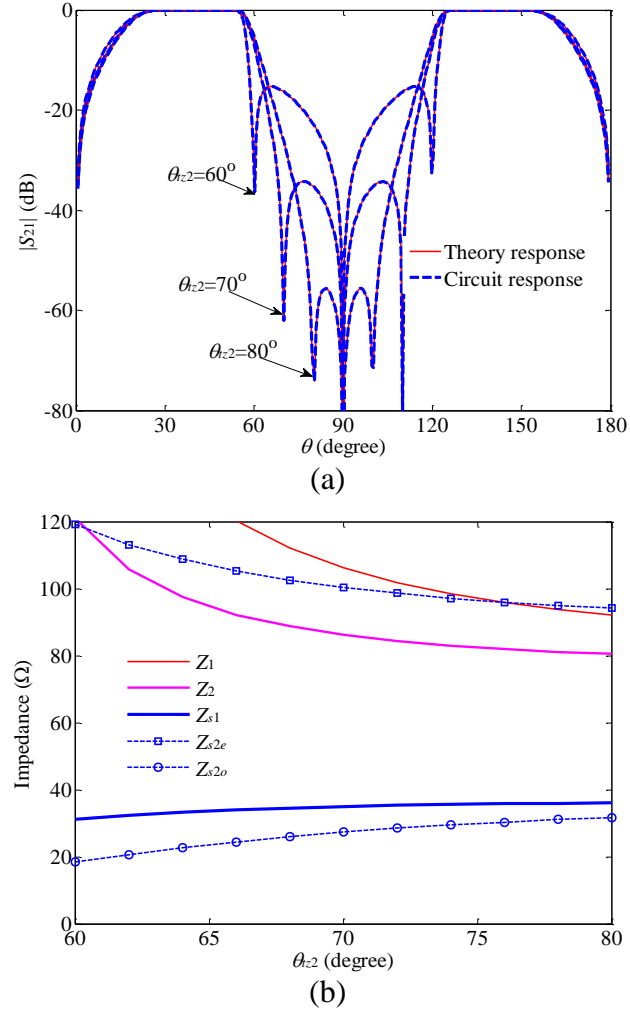


Figure 5-5. (a) Theoretical and circuit responses of a 3rd-order filter with $\varepsilon = 0.1$, $\theta_1 = 117^\circ$ and $\theta_2 = 144^\circ$. (b) Characteristic impedances versus different locations of TZs (θ_{tz2}).

To further increase the order of the filter, the number of the coupled section of the MMR is set as 2, as shown in the schematic in Table 5.1. As the order increases, more design parameters are involved, implying complicated and time-consuming analysis for the solution of these non-linear equations. To simplify our analysis herein, a special case is studied with only one section of the internally-coupled line involved ($Z_{s2e} > Z_{s2o}$). Meanwhile, all the remaining ones are set to be uncoupled

ones ($Z_{1e} = Z_{1o} = Z_1$, $Z_{2e} = Z_{2o} = Z_2$ and $Z_{s1e} = Z_{s1o} = Z_{s1}$). The coefficients of the polynomials (k_1 - k_6) can be accordingly expressed as below,

$$\begin{cases} k_1 = Z_2 Z_{s1} Z_1 \\ k_2 = - \left(\begin{aligned} &Z_{s1} Z_2 Z_{s2e} + Z_{s1} Z_1 Z_{s2e} + Z_{s1} Z_2 Z_{s1} \\ &+ Z_{s1} Z_1 Z_{s1} + Z_2 Z_{s1} Z_2 + Z_2 Z_1 Z_{s2e} \end{aligned} \right) \\ k_3 = Z_2 Z_2 Z_{s2e} \\ k_4 = j Z_{s1} Z_2 Z_1 (Z_{s2e} + Z_{s1}) \\ k_5 = -j Z_{s1} Z_2 Z_2 (Z_{s2e} + Z_{s1}) \\ k_6 = j Z_2 Z_{s1} (Z_{s2o} + Z_{s1} + Z_1 + Z_2) \\ k_7 = - \left[j Z_2 (Z_1 + Z_2) Z_{s2o} + j Z_{s1} (Z_{s2o} + Z_{s1}) Z_1 \right] \\ k_8 = -Z_2 Z_{s1} (Z_1 + Z_2) (Z_{s2o} + Z_{s1}) \end{cases} \quad (5.9)$$

In this way, the 5 characteristic impedances, namely, Z_1 , Z_2 , Z_{s1} , Z_{s2e} and Z_{s2o} , are exactly matched to the 5 unknown coefficients in the numerator and normalized denominator of a filtering function. Though this arrangement lacks the freedom in choosing the preferred characteristic impedances, it leads to an explicit expression of the TZs in the form of

$$\begin{cases} \tan \theta_{tz1} = 0, \infty \\ \tan \theta_{tz2} = \pm \sqrt{\frac{(k_7 k_5 - k_8 k_3)}{(k_8 k_1 - k_6 k_4)}} \\ \tan \theta_{tz3} = \pm j \end{cases} \quad (5.10)$$

Similar to the design of the 2nd-order filter in the previous section, θ_{tz1} introduces TZs at multiple integer of $\pi/2$ for a periodic property of the $\tan(\theta)$ function. The paired TZs (θ_{tz2}) can be properly allocated between the two passbands so as to improve the out-of-band rejection performance in the middle stopband. Besides them, there is one more pair of TZs with the phase of θ_{tz3} fixed at two constant imaginary frequencies.

Figure 5-5(a) depicts the frequency responses under the different locations of the predefined TZs. As the paired TZs move to the middle of the two passbands, the rejection in this stopband gets the enhancement, whereas the roll-off skirt near the edge of the dual passbands deteriorates gradually, and vice versa. Figure 5-5(b)

shows the variation of the three characteristic impedances with respect to the location of the TZs.

5.4 Experimental Results and Discussions

In this section, the 2nd- and 3rd-order dual-band BPFs as well as a higher order dual-band BPF with two kinds of filter blocks cascaded are implemented, fabricated and discussed. The non-linear equation as required in the synthesis procedure is completed by a gradient based optimization method such as “fsolve” integrated in the optimization toolbox of MATLAB. The substrate used has a dielectric constant of 10.8, loss tangent of 0.0023, thickness of 50 mils and copper thickness of 0.017 mm. A commercial EM simulator [89] is applied to get the EM simulation for the microstrip layout.

5.4.1 2nd-Order Dual-Band BPF Design

The circuit specifications of the 2nd-order filter are set as, middle frequency of the two passbands at $f_0 = 2$ GHz, $f_1 = 2.9$ GHz, $f_2 = 3.25$ GHz, $f_{tz2} = 1.7$ GHz and the ripple factor $\varepsilon = 0.1$, which correspond to $\theta_1 = 130.5^\circ$, $\theta_2 = 146.25^\circ$ and $\theta_{tz2} = 76.5^\circ$, respectively. The calculation of θ_1 and θ_2 is based on the middle frequency of $f_0 = 2$ GHz and through the relation of $f_{(1,2)} = f_0 \theta_{(1,2)} / 90^\circ$. The definition of t_{z2} is in (5.8). According to the synthesis procedure discussed above, the filtering function is obtained as

$$F_2(t) = \frac{141.50t^4 - 249.13t^2 + 94.32}{t^3 - 17.35t} \quad (5.11)$$

A gradient based method (such as the “fsolve” or “lsqnonlin”) as integrated in the commercial software MALAB is used herein. The initial value of the circuit design parameters are set as $Z_{1e} = 60.0 \Omega$, $Z_{1o} = 24.0 \Omega$, $Z_{s1e} = 70.0 \Omega$, $Z_{s1o} = 20.0 \Omega$, $Z_{s2e} = 70.0 \Omega$ and $Z_{s2o} = 20.0 \Omega$, and after solving the non-linear equations they are obtained as, $Z_{1e} = 60.00 \Omega$, $Z_{1o} = 24.00 \Omega$, $Z_{s1e} = 52.90 \Omega$, $Z_{s1o} = 22.75 \Omega$, $Z_{s2e} = 56.79$

Ω and $Z_{s2o} = 44.93 \Omega$. The error term using the above results is around 0.0051. Due to the approximate assumption of equal even- and odd-mode phase velocity in the circuit design, a compensation method [76] and [90] is utilized herein by adding a capacitor or capacitive element at the two ends of the coupled lines, and an inter-digital capacitor structure is used to realize the required admittance as studied in [90]. The photograph of the fabricated filter is shown in Figure 5-6(a). In Figure 5-6(b), all the three sets of results from the theory, EM simulation and measurement are in good agreement with each other. The measured results show that the center frequency (f_{01}/f_{02}) is 1.03/2.85 GHz, the 3-dB fractional bandwidth (FBW) is 94.8/35.8%, and the insertion loss (IL) is 0.65/0.45 dB, respectively, for the first/second passband.

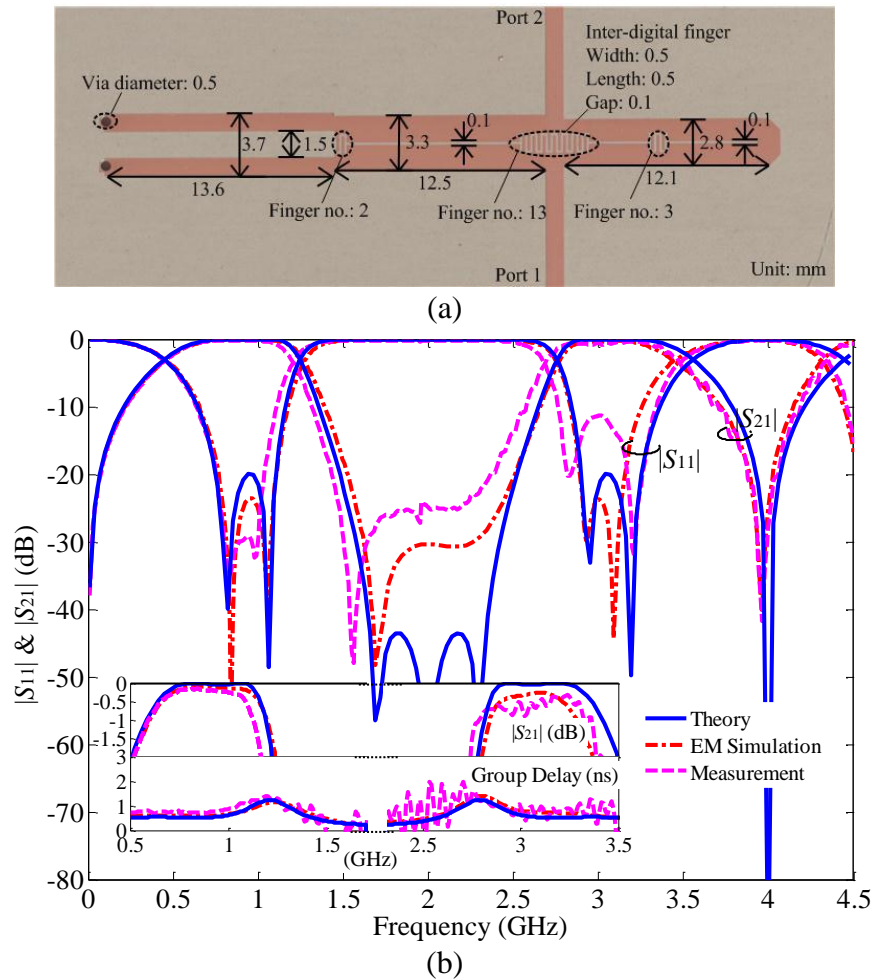


Figure 5-6. (a) Photograph of the fabricated 2nd-order dual-band filter with dimensions labelled. (b) Comparison between the theoretical, EM simulated and measured results of the dual-band filter.

5.4.2 3rd-Order Dual-Band BPF Design

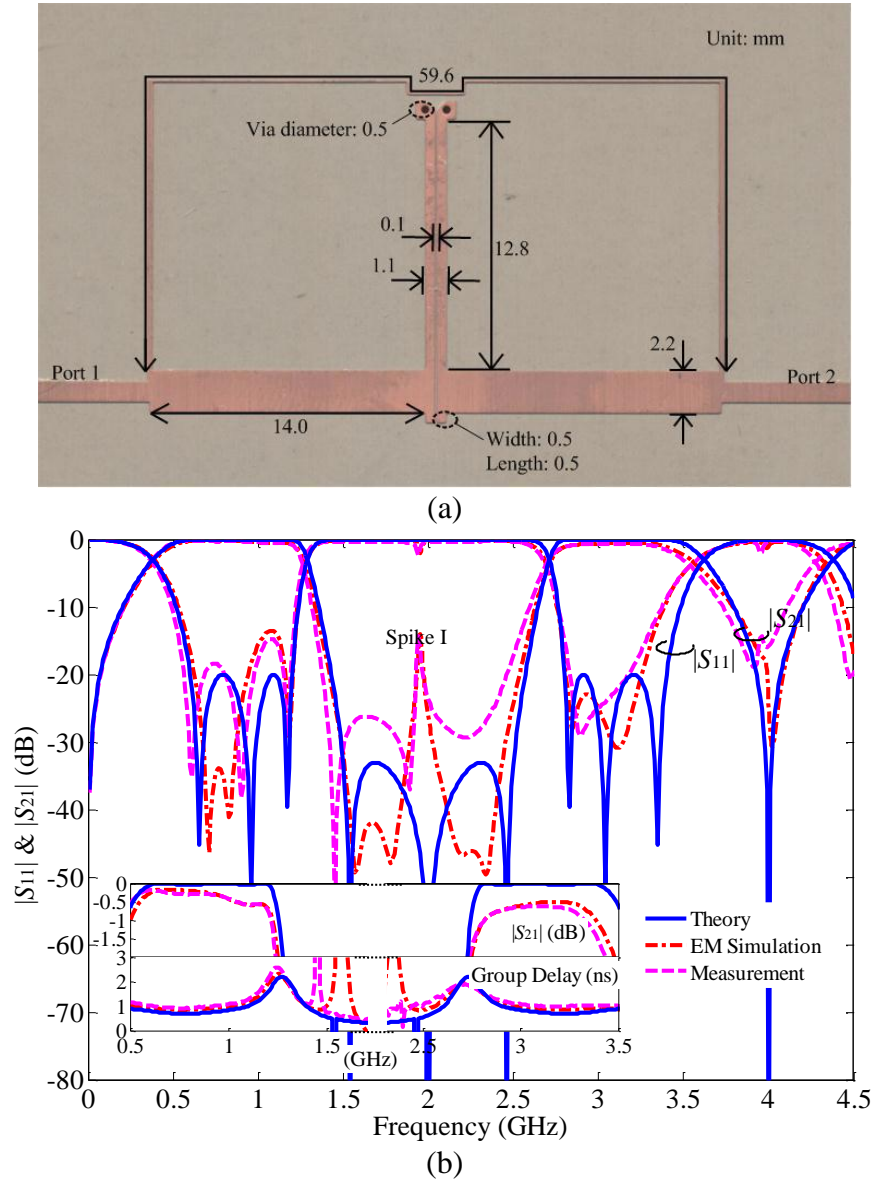


Figure 5-7. (a) Photograph of the fabricated 3rd-order dual-band filter with dimensions labelled. (b) Comparison between the theoretical, EM simulated and measured results of the dual-band filter.

The circuit specifications of the 3rd-order filter are set as, $f_0=2$ GHz, $f_1=2.8$ GHz, $f_2=3.4$ GHz, $f_{t2}=1.54$ GHz and $\varepsilon=0.1$, which correspond to $\theta_1=126^\circ$, $\theta_2=153^\circ$ and $\theta_{t2}=69.3^\circ$, respectively. The calculation of θ_1 and θ_2 is based on the middle frequency of $f_0=2$ GHz and through the relation of $f_{(1,2)}=f_0\theta_{(1,2)}/90^\circ$. The

definition of t_{z2} is from defining $(k_7k_5-k_8k_3)/(k_8k_1-k_6k_4)=7$ as seen in (5.10). The filtering function is obtained as

$$F_3(t) = \frac{-81.14t^6 + 237.93t^4 - 191.01t^2 + 39.30}{t^5 - 6.00t^3 - 7.00t} \quad (5.12)$$

A gradient based method (such as the “fsolve” or “lsqnonlin”) as integrated in the commercial software MALAB is used herein. The initial value of the design parameters are set as $Z_1=30\ \Omega$, $Z_2=100\ \Omega$, $Z_{s1}=100\ \Omega$, $Z_{s2e}=150\ \Omega$ and $Z_{s2o}=50\ \Omega$, after that the circuit design parameters are obtained as $Z_1=108.14\ \Omega$, $Z_2=87.02\ \Omega$, $Z_{s1}=34.84\ \Omega$, $Z_{s2e}=101.10\ \Omega$ and $Z_{s2o}=26.87\ \Omega$. The error term using the above results, $Z_1=108.14\ \Omega$, $Z_2=87.02\ \Omega$, $Z_{s1}=34.84\ \Omega$, $Z_{s2e}=101.10\ \Omega$ and $Z_{s2o}=26.87\ \Omega$, is around 0.0003. To compensate for unequal even- and odd-mode phase velocities, a section of extended coupled-stubs is used to realize the weak mutual capacitive coupling, as can be seen in Figure 5-7(a).

Figure 5-7(b) shows the theoretical, EM simulated and the measured results. The measured results show that f_{01}/f_{02} is 0.83/3.13 GHz, 3-dB *FBW* 105.9/27.3% and IL 0.60/0.85 dB, for the first/second passband, respectively. The measured results match well with the calculated and simulated ones. The difference between the measured results and theoretical ones is basically caused by some parasitic effects, such as junction discontinuities, frequency dispersion of a microstrip line, and the approximate assumption of equal even- and odd-mode phase velocities. The resonant spike appearing in the upper and middle of the two bands may be caused by of two signal transmitting paths, as seen in Figure 5-1 as path 1 and path 2.

5.4.3 4th-Order Dual-Band BPF Design

A 4th-order BPF is formed by cascading two 1st and one 2nd-order BPFs, and it is designed to prove the possibility by the method of cascading to have a higher order BPF with improved out-of-band rejection. Different from the commonly used design

strategy in [58] and [59], the two filter blocks used here are in different orders, serving as an alternative approach. It is noted that although an individual filter block can be obtained by synthesis method discussed herein, the cascading case requires different design strategy. The design for this filter starts with the filter block in the middle, which the synthesis method can be applied. After that some tuning/adjusting work has to apply to the rest shunt stubs and the transmission line in between the two filter blocks. The circuit design parameters are, for the 1st-order filter block, $Z_{s1e,1}=60\ \Omega$, $Z_{s1o,1}=24\ \Omega$ and $Z_{s2}=33.5\ \Omega$, for the 2nd-order filter block, $Z_{1e,2}=60.0\ \Omega$, $Z_{1o,2}=24.0\ \Omega$, $Z_{s1e,2}=52.9\ \Omega$, $Z_{s1o,2}=22.7\ \Omega$, $Z_{s2e,2}=56.8\ \Omega$ and $Z_{s2o,2}=44.5\ \Omega$, and for the line connecting these two blocks, $Z_l=65.7\ \Omega$.

Figure 5-8(a) shows the photograph of the fabricated filter. Figure 5-8(b) plots the three sets of results from the theory, EM simulation and measurement, and they are found in good agreement with each other. The measured results show that for the first/second passband, f_{01}/f_{02} is 1.03/2.85 GHz, the 3-dB *FBW* is 94.8/35.8%, and the IL is 0.65/0.45 dB, respectively. The differences between the measured results and theoretical ones, especially the resonant spike (spike I and II) occurred in the middle of the two passbands, are basically caused by some parasitic effects, which are not considered during the theoretical analysis. There are mainly three kinds of effects, namely junction discontinuities, dispersion of the microstrip line and the approximate assumption of equal even- and odd-mode phase velocity. The junction effect introduces the phase variation for the two signal transmitting paths, thus the phase difference is not 180 degree to generate TZs and a resonant spike is occurred, which is similar to the plot as seen in Figure 4-15, where the generation of the spike I and II is discussed. The dispersion of the microstrip line causes some slight changes of the passband. The even- and odd-mode phase velocity is compensated by the inter-digital fingers.

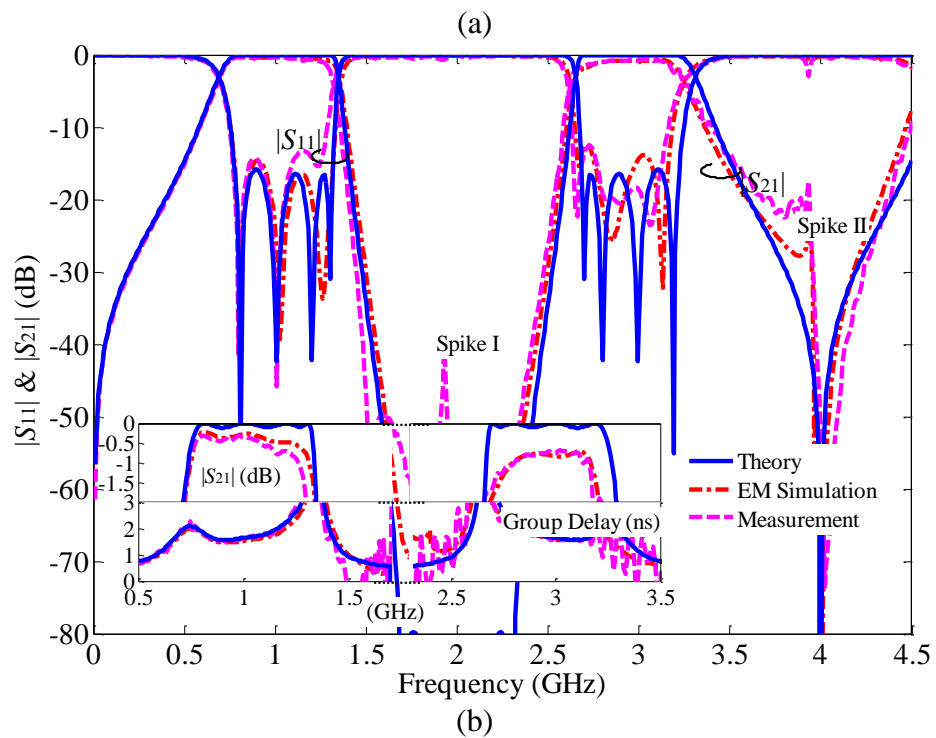
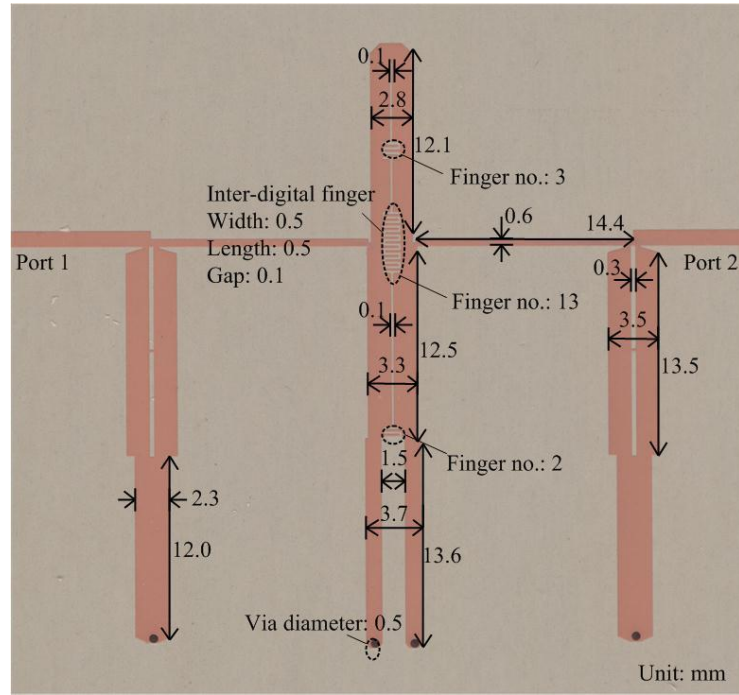


Figure 5-8. (a) Photograph of the fabricated dual-band filter of cascaded structure with dimensions labelled. (b) Comparison between the theoretical, EM simulated and measured results of the dual-band filter.

5.5 Summary

In this section, a class of wideband dual-band BPFs with internally-coupled microstrip lines have been proposed, synthesized and designed. The general structure of the dual-band BPF is formed by a folded MMR and parallel-coupled short-circuited stubs. Due to existence of two dissimilar signal transmitting paths, additional pairs of TZs can be generated in between the two passbands. The synthesis procedure follows by theoretically deriving the filtering function, analyzing the circuit response and determining the circuit design parameters under the two equalized functions. As design examples, 1st-, 2nd- and 3rd-order wideband dual-band BPFs have been analyzed, discussed and synthesized. In the end, three filter prototypes have been designed, fabricated and measured to verify the proposed design principle in experiment.

CHAPTER 6

CONCLUSIONS

AND RECOMMENDATIONS

6.1 Conclusions

In this dissertation, a class of single-/dual-wideband BPFs has been proposed and designed. As the foundation of this research work, a single-wideband filter with stepped-impedance MMR has been introduced in the first place. By varying the characteristic impedances of the MMR, the resonances are quasi-equally distributed within the passband. To feed this resonator, short-circuited stubs are placed in shunt on the two sides, which also block the DC-component. To introduce a pair of TZs at the edges of the passband, the composite short-/open-circuited stubs have been used instead of using short-circuited stubs only. Following this design, a dual-wideband filter has been reported by parallel connecting two wideband BPFs as mentioned above. Similar to the design concept of the signal interference, a TZ is introduced in the middle of the two passbands when the two transmitting paths are in 180° phase difference and equal magnitude. Additional pairs of TZs are introduced at either real or imaginary frequencies by adjusting the characteristic impedances of the two signal transmitting paths. To prove this design principle, three filter prototypes of different functions have been designed. After that, an improved design based on the internally coupled MMRs has been proposed. By simultaneously folding the MMR and the short-circuited stubs, the filter design is realized with compact size, good flexibility in choosing characteristic impedances and the capability in achieving different filter orders.

For the above proposed circuit structures, a generic synthesis method has been further explored to exactly determine the design parameters. It includes the following three main steps.

(a) According to the even-/odd-mode analysis, their corresponding input admittances have been derived. After that, the transfer function is calculated to represent the locations of TZs and reflection zeroes as a $\tan\theta$ function.

(b) An appropriate filtering function is selected based on the format of the derived transfer function. This filtering function is formulated according to the desired design specifications.

(c) Once both the transfer function and the filtering function have been obtained, these two functions are set to be equal. Solving this set of non-linear equations by a method of optimization, the design parameters of the circuit are determined.

For the above mentioned synthesis procedure, formulation of the two functions, namely, the transfer function from the filter circuit and filtering function from the design specifications, is critical. Commensurate lines with quarter wavelength at the center frequency of the passband are used to permit the derivation in the form of $\tan\theta$ function. Through the Richard's transformation, the $\tan\theta$ function is transformed to a function of polynomial. Next, the characterization of the locations of TZs and reflection zeroes allows us to know whether it is applicable to any existing filtering functions. That is, for these two functions, the polynomials in the denominator and numerator are in the same highest order, and they are possibly set to be equal. With this design principle, other single-/dual-wideband BPFs could be synthesized in the future.

6.2 Recommendations for Future Work

There are several limitations of the proposed research methodology, but the outcome of this dissertation can serve as the starting point for many future works as listed below.

(a) Because both the normalized filtering function and the frequency transformation are symmetrical, the finalized frequency response also shares this property. For realizing some practical filters with the specified asymmetrical property, one of the direct ways is to use an asymmetrical filtering function or frequency transformation. So far, some preliminary circuit design examples with non-commensurate lines have been reported to verify this design technique. For the proposed circuit in this dissertation, the most direct way for the asymmetrical design is to resort to varied length of transmission lines. Instead of using a single $\tan\theta$ function with uniform length, a combined ($\tan\theta_1$ and $\tan\theta_2$) function with different length promises to design asymmetrical responses.

(b) To simplify the design process and to verify the circuit response, most of the filter designs are in the form of a filtering unit block. To further improve the out-of-band rejection, a solution could be simply got by cascading multiple unit blocks, as shown in Figure 6-1.

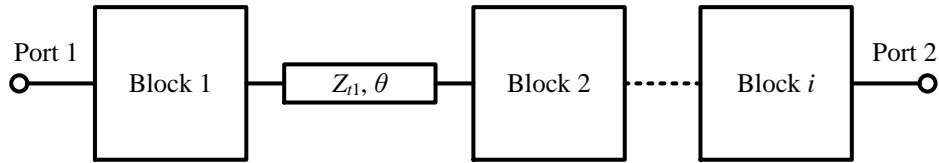


Figure 6-1. Circuit schematic of cascading i filter blocks.

The next point of recommendation focuses on the design of a cascaded structure. As seen in Figure 6-1, the whole filter schematic is by cascading single unit filtering blocks separated by a section of transmission line. With this technique, the design task of a higher order filter could be divided into a few pieces, thus

reducing the design complexity and shortening the tuning or optimization period for the whole filter design. However, due to its cascading characters, the circuit analysis method and the filtering function could be different from the ones in this dissertation.

(c) As a well-known property for commensurate lines, they have a periodic property, which directly contribute to the multiple harmonic. To properly overcome this drawback, many techniques have been reported so far to extend the bandwidth of the rejection band, such as integrating slow wave structures and lowpass filters into the transmission lines in [35], [40] and [79]. However, they still require a cut-and-try effort which is not in the category of a systematic design process. Very recently, a design strategy by assigning resonances in the complex frequency has been proposed to suppress the harmonic passband [91], probably providing another research direction for future works.

(d) Although the proposed circuit structures and the synthesis method are theoretically applicable for any bandwidth and frequency ratio of the two passbands, they are practically limited by the realizable characteristic impedances. One solution proposed by this dissertation is to provide extra design parameters to obtain a degree of freedom in choosing these variables. However, it is still not enough for a practical engineering problem with large range of design specifications. Thus, new circuit topologies are to be explored with its corresponding applicable range. Once a design target is given, an appropriate circuit scheme is chosen readily.

REFERENCES

- [1] R. J. Cameron, R. Mansour, and C. M. Kudsia, *Microwave Filters for Communication Systems: Fundamentals, Design and Applications*. Wiley-Interscience, 2007.
- [2] J.-S. Hong and M. J. Lancaster, *Microstrip Filters for RF/Microwave Applications*. New York, USA: John Wiley & Sons, Inc., 2001.
- [3] L. Zhu, S. Sun, and R. Li, *Microwave Bandpass Filters for Wideband Communications*. Hoboken, New Jersey: John Wiley & Sons, 2012.
- [4] George Matthaei, L. Young, and E. M. T. Jones, *Microwave Filters, Impedance-Matching Networks, and Coupling Structures*. Norwood, MA: Artech House, 1980.
- [5] I. Hunter, *Theory and Design of Microwave Filters*. Stevenage, UK: The Institution of Engineering and Technology, 2001.
- [6] L. Zhu, S. Sun, and W. Menzel, "Ultra-wideband (UWB) bandpass filters using multiple-mode resonator," *IEEE Microwave and Wireless Components Letters*, vol. 15, no. 11, pp. 796–798, Nov. 2005.
- [7] H. Wang, L. Zhu, and W. Menzel, "Ultra-wideband bandpass filter with hybrid microstrip/CPW structure," *IEEE Microwave and Wireless Components Letters*, vol. 15, no. 12, pp. 844–846, Dec. 2005.
- [8] H. Ishida and K. Araki, "Design and analysis of UWB band pass filter with ring filter," *IEEE MTT-S International Microwave Symposium Digest*, vol. 3, pp. 1307–1310, Jun. 2004.
- [9] L. Szydlowski, N. Leszczynska, A. Lamecki, and M. Mrozowski, "A substrate integrated waveguide (SIW) bandpass filter in a box configuration with frequency-dependent coupling," *IEEE Microwave and Wireless Components Letters*, vol. 22, no. 11, pp. 556–558, Nov. 2012.
- [10] L. Szydlowski, A. Lamecki, and M. Mrozowski, "Coupled-resonator waveguide filter in quadruplet topology with frequency-dependent coupling—a design based on coupling matrix," *IEEE Microwave and Wireless Components Letters*, vol. 22, no. 11, pp. 553–555, Nov. 2012.
- [11] M. Makimoto and S. Yamashita, "Bandpass filters using parallel coupled stripline stepped impedance resonators," *IEEE Transactions on Microwave Theory and Techniques*, vol. 28, no. 12, pp. 1413–1417, Dec. 1980.

- [12] R. Li, S. Sun, and L. Zhu, "Direct synthesis of transmission line low-/high-pass filters with series stubs," *IET Microwaves, Antennas & Propagation*, vol. 3, no. 4, pp. 654–662, Jun. 2009.
- [13] R. Li, S. Sun, and L. Zhu, "Synthesis design of ultra-wideband bandpass filters with composite series and shunt stubs," *IEEE Transactions on Microwave Theory and Techniques*, vol. 57, no. 3, pp. 684–692, Mar. 2009.
- [14] R. J. Wenzel, "Synthesis of combline and capacitively loaded interdigital bandpass filters of arbitrary bandwidth," *IEEE Transactions on Microwave Theory and Techniques*, vol. 19, no. 8, pp. 678–686, Aug. 1971.
- [15] R. Levy and S. B. Cohn, "A history of microwave filter research, design, and development," *IEEE Transactions on Microwave Theory and Techniques*, vol. 32, no. 9, pp. 1055–1067, Sep. 1984.
- [16] S. Amari, "Synthesis of cross-coupled resonator filters using an analytical gradient-based optimization technique," *IEEE Transactions on Microwave Theory and Techniques*, vol. 48, no. 9, pp. 1559–1564, 2000.
- [17] I. C. Hunter, L. Billonet, B. Jarry, and P. Guillon, "Microwave filters-applications and technology," *IEEE Transactions on Microwave Theory and Techniques*, vol. 50, no. 3, pp. 794–805, Mar. 2002.
- [18] R. Levy, R. V. Snyder, and G. Matthaei, "Design of microwave filters," *IEEE Transactions on Microwave Theory and Techniques*, vol. 50, no. 3, pp. 783–793, Mar. 2002.
- [19] F. Seyfert and S. Bila, "General synthesis techniques for coupled resonator networks," *IEEE Microwave Magazine*, vol. 8, no. 5, pp. 98–104, Oct. 2007.
- [20] Z. Hao and J.-S. Hong, "Ultrawideband filter technologies," *IEEE Microwave Magazine*, vol. 11, no. 4, pp. 56–68, Jun. 2010.
- [21] R. J. Cameron, "General coupling matrix synthesis methods for Chebyshev filtering functions," *IEEE Transactions on Microwave Theory and Techniques*, vol. 47, no. 4, pp. 433–442, Apr. 1999.
- [22] R. J. Cameron, "Advanced coupling matrix synthesis techniques for microwave filters," *IEEE Transactions on Microwave Theory and Techniques*, vol. 51, no. 1, pp. 1–10, Jan. 2003.
- [23] S. Amari, F. Seyfert, and M. Bekheit, "Theory of coupled resonator microwave bandpass filters of arbitrary bandwidth," *IEEE Transactions on Microwave Theory and Techniques*, vol. 58, no. 8, pp. 2188–2203, Aug. 2010.

- [24] S. Amari, U. Rosenberg, and J. Bornemann, "Adaptive synthesis and design of resonator filters with source/load-multiresonator coupling, " *IEEE Transactions on Microwave Theory and Techniques*, vol. 50, no. 8, pp. 1969-1978, Aug 2002.
- [25] P. I. Richards, "Resistor-transmission-line circuits," *Proceedings of the IRE*, vol. 36, no. 2, pp. 217-220, Feb. 1948.
- [26] A. Garcia-Lamperez and M. Salazar-Palma, "Single-band to multiband frequency transformation for multiband filters," *IEEE Transactions on Microwave Theory and Techniques*, vol. 59, no. 12, pp. 3048-3058, Dec. 2011.
- [27] J. Lee, M. S. Uhm, and I. Yom, "A dual-passband filter of canonical structure for satellite applications," *IEEE Microwave and Wireless Components Letters*, vol. 14, no. 6, pp. 271-273, Jun. 2004.
- [28] J. Lee and K. Sarabandi, "Design of triple-passband microwave filters using frequency transformations," *IEEE Transactions on Microwave Theory and Techniques*, vol. 56, no. 1, pp. 187-193, Jan. 2008.
- [29] A. M. Abu-Hudrouss, A. B. Jayyousi, and M. J. Lancaster, "Triple-band HTS filter using dual spiral resonators with capacitive-loading," *IEEE Transactions on Applied Superconductivity*, vol. 18, no. 3, pp. 1728-1732, Sep. 2008.
- [30] R. J. Cameron, M. Yu, and YingWang, "Direct-coupled microwave filters with single and dual stopbands," *IEEE Transactions on Microwave Theory and Techniques*, vol. 53, no. 11, pp. 3288-3297, Nov. 2005.
- [31] F. C. Commission, "Revision of part 15 of the commission's rules regarding ultra-wideband transmission systems," *Tech.Rep.*, vol. ET-Docket .
- [32] H. Shaman and J.-S. Hong, "A novel ultra-wideband (UWB) bandpass filter (BPF) with pairs of transmission zeroes," *IEEE Microwave and Wireless Components Letters*, vol. 17, no. 2, pp. 121-123, Feb. 2007.
- [33] H. Wang, G. Yang, W. Kang, C. Miao, and W. Wu, "Application of cross-shaped resonator to the ultra-wideband bandpass filter design," *IEEE Microwave and Wireless Components Letters*, vol. 21, no. 12, pp. 667-669, Dec. 2011.
- [34] J. Xu, W. Wu, W. Kang, and C. Miao, "Compact UWB bandpass filter with a notched band using radial stub loaded resonator," *IEEE Microwave and Wireless Components Letters*, vol. 22, no. 7, pp. 351-353, Jul. 2012.

- [35] A. M. Abbosh, "Design method for ultra-wideband bandpass filter with wide stopband using parallel-coupled microstrip lines," *IEEE Transactions on Microwave Theory and Techniques*, vol. 60, no. 1, pp. 31–38, Jan. 2012.
- [36] C. H. Kim, S. Member, and K. Chang, "Ultra-wideband (UWB) ring resonator bandpass filter with a notched band," *IEEE Microwave and Wireless Components Letters*, vol. 21, no. 4, pp. 206–208, Apr. 2011.
- [37] L. Zhu and H. Wang, "Ultra-wideband bandpass filter on aperture-backed microstrip line," *Electronics Letters*, vol. 41, no. 18, p. 1015, 2005.
- [38] W. Han, Z. Lei, and W. Menzel, "Ultra-wideband bandpass filter with hybrid microstrip/CPW structure," *IEEE Microwave and Wireless Components Letters*, vol. 15, no. 12, pp. 844–846, Dec. 2005.
- [39] J. Gao, L. Zhu, W. Menzel, F. Bogelsack, G. Jing, and Z. Lei, "Short-circuited CPW multiple-mode resonator for ultra-wideband (UWB) bandpass filter," *IEEE Microwave and Wireless Components Letters*, vol. 16, no. 3, pp. 104–106, Mar. 2006.
- [40] S. Sun and L. Zhu, "Capacitive-ended interdigital coupled lines for UWB bandpass filters with improved out-of-band performances," *IEEE Microwave and Wireless Components Letters*, vol. 16, no. 8, pp. 440–442, Aug. 2006.
- [41] R. Li and L. Zhu, "Compact UWB bandpass filter using stub-loaded multiple-mode resonator," *IEEE Microwave and Wireless Components Letters*, vol. 17, no. 1, pp. 40–42, Jan. 2007.
- [42] S. W. Wong and L. Zhu, "Implementation of compact UWB bandpass filter with a notch-band," *IEEE Microwave and Wireless Components Letters*, vol. 18, no. 1, pp. 10–12, Jan. 2008.
- [43] T. B. Lim, S. Sun, and L. Zhu, "Compact ultra-wideband bandpass filter using harmonic-suppressed multiple-mode resonator," *Electronics Letters*, vol. 43, no. 22, p. 1205, 2007.
- [44] H. Shaman and J.-S. Hong, "Ultra-wideband (UWB) bandpass filter with embedded band notch structures," *IEEE Microwave and Wireless Components Letters*, vol. 17, no. 3, pp. 193–195, Mar. 2007.
- [45] H. Miyake, S. Kitazawa, T. Ishizaki, T. Yamada, and Y. Nagatomi, "A miniaturized monolithic dual band filter using ceramic lamination technique for dual mode portable telephones," in *IEEE MTT-S International Microwave Symposium Digest*, 1997, vol. 2, pp. 789–792.
- [46] S. Oshima, K. Wada, R. Murata, and Y. Shimakata, "Multilayer dual-band bandpass filter in low-temperature co-fired ceramic substrate for ultra-

- wideband applications,” *IEEE Transactions on Microwave Theory and Techniques*, vol. 58, no. 3, pp. 614–623, Mar. 2010.
- [47] L.-C. Tsai and C.-W. Hsue, “Dual-band bandpass filters using equal-length coupled-serial-shunted lines and Z-transform technique,” *IEEE Transactions on Microwave Theory and Techniques*, vol. 52, no. 4, pp. 1111–1117, Apr. 2004.
 - [48] A. Liu, T. Huang, and R. Wu, “A dual wideband filter design using frequency mapping and stepped-impedance resonators,” *IEEE Transactions on Microwave Theory and Techniques*, vol. 56, no. 12, pp. 2921–2929, Dec. 2008.
 - [49] X. Guan, Z. Ma, P. Cai, Y. Kobayashi, T. Anada, and G. Hagiwara, “Synthesis of dual-band bandpass filters using successive frequency transformations and circuit conversions,” *IEEE Microwave and Wireless Components Letters*, vol. 16, no. 3, pp. 110–112, Mar. 2006.
 - [50] S. Sun and L. Zhu, “Compact dual-band microstrip bandpass filter without external feeds,” *IEEE Microwave and Wireless Components Letters*, vol. 15, no. 10, pp. 644–646, Oct. 2005.
 - [51] W.-S. Chang and C.-Y. Chang, “Analytical design of microstrip short-circuit terminated stepped-impedance resonator dual-band filters,” *IEEE Transactions on Microwave Theory and Techniques*, vol. 59, no. 7, pp. 1730–1739, Jul. 2011.
 - [52] S. Luo, L. Zhu, and S. Sun, “Compact dual-mode triple-band bandpass filters using three pairs of degenerate modes in a ring resonator,” *IEEE Transactions on Microwave Theory and Techniques*, vol. 59, no. 5, pp. 1222–1229, May 2011.
 - [53] Y. C. Chiou, C. Y. Wu, and J. T. Kuo, “New miniaturized dual-mode dual-band ring resonator bandpass filter with microwave C-sections,” *IEEE Transactions on Microwave Theory and Techniques*, vol. 20, no. 2, pp. 67–69, Feb. 2010.
 - [54] Y.-T. Kuo and C.-Y. Chang, “Analytical design of two-mode dual-band filters using E-shaped resonators,” *IEEE Transactions on Microwave Theory and Techniques*, vol. 60, no. 2, pp. 250–260, Feb. 2012.
 - [55] S. Fu, B. Wu, J. Chen, S.-J. Sun and C.-H. Liang, “Novel second-order dual-mode dual-band filters using capacitance loaded square loop resonator,” *IEEE Transactions on Microwave Theory and Techniques*, vol. 60, no. 3, pp. 477–483, Mar. 2012.
 - [56] M. Mandal and S. Sanyal, “Compact bandstop filter using signal interference technique,” *Electronics Letters*, vol. 43, no. 2, pp. 3–4, 2007.

- [57] M. K. Mandal, K. Divyabramham, and V. K. Velidi, "Compact wideband bandstop filter with five transmission zeroes," *IEEE Microwave and Wireless Components Letters*, vol. 22, no. 1, pp. 4–6, Jan. 2012.
- [58] R. Gomez-Garcia, M. Sanchez-Renedo, B. Jarry, J. Lintignat, and B. Barelaud, "A class of microwave transversal signal-interference dual-passband planar filters," *IEEE Microwave and Wireless Components Letters*, vol. 19, no. 3, pp. 158–160, Mar. 2009.
- [59] R. Gomez-Garcia and M. Sanchez-Renedo, "Microwave dual-band bandpass planar filters based on generalized branch-line hybrids," *IEEE Transactions on Microwave Theory and Techniques*, vol. 58, no. 12, pp. 3760–3769, Dec. 2010.
- [60] R. Gomez-Garcia and M. Sanchez-Renedo, "Application of generalized Bagley-polygon four-port power dividers to designing microwave dual-band bandpass planar filters," in *IEEE MTT-S International Microwave Symposium*, 2010, pp. 580–583.
- [61] M. A. Sanchez-Soriano, E. Bronchalo, and G. Torregrosa-Penalva, "Dual band bandpass filters based on strong coupling directional couplers," in *European Microwave Conference*, 2009, pp. 1401–1404.
- [62] J. Lee and K. Sarabandi, "A synthesis method for dual-passband microwave filters," *IEEE Transactions on Microwave Theory and Techniques*, vol. 55, no. 6, pp. 1163–1170, Jun. 2007.
- [63] R. Gomez-Garcia, J.-M. Munoz-Ferreras, and M. Sanchez-Renedo, "Signal-interference stepped-impedance-line microstrip filters and application to duplexers," *IEEE Microwave and Wireless Components Letters*, vol. 21, no. 8, pp. 421–423, Aug. 2011.
- [64] K. C. Gupta, R. Garg, and R. Chadha, *Computer Aided Design of Microwave Circuits*. New York, USA: Artech House, Inc., 1981.
- [65] S. S. Rao, *Optimiztion Theory and Applications*. New Delhi: Wiley Eastern Limited, 1978.
- [66] C. Charalambous, "A unified review of optimization," *IEEE Transactions on Microwave Theory and Techniques*, vol. 22, no. 3, pp. 289–300, Mar. 1974.
- [67] S. Director, "Survey of circuit-oriented optimization techniques," *IEEE Transactions on Circuit Theory*, vol. 18, no. 1, pp. 3–10, 1971.
- [68] J. W. Bandler, "Optimization methods for computer-aided design," *IEEE Transactions on Microwave Theory and Techniques*, vol. 17, no. 8, pp. 533–552, Aug. 1969.

- [69] D. Swanson and G. Macchiarella, "Microwave filter design by synthesis and optimization," *IEEE Microwave Magazine*, vol. 8, no. 2, pp. 55–69, Apr. 2007.
- [70] W. A. Atia, K. A. Zaki, and A. E. Atia, "Synthesis of general topology multiple coupled resonator filters by optimization," in *IEEE MTT-S International Microwave Symposium Digest*, 1998, vol. 2, pp. 821–824.
- [71] J.-Y. Li, C.-H. Chi, and C.-Y. Chang, "Synthesis and design of generalized chebyshev wideband hybrid ring based bandpass filters with a controllable transmission zero pair," *IEEE Transactions on Microwave Theory and Techniques*, vol. 58, no. 12, pp. 3720–3731, Dec. 2010.
- [72] M. Meng, I. C. Hunter, and J. D. Rhodes, "The design of parallel connected filter networks with nonuniform resonators," *IEEE Transactions on Microwave Theory and Techniques*, vol. 61, no. 1, pp. 372–381, 2013.
- [73] M. Dydyk, "Microstrip directional couplers with ideal performance via single-element Compensation," *IEEE Transactions on Microwave Theory and Techniques*, vol. 47, no. 6, pp. 956–964, 1999.
- [74] S. Lee and Y. Lee, "An inductor-loaded microstrip directional coupler for directivity enhancement," *IEEE Microwave and Wireless Components Letters*, vol. 19, no. 6, pp. 362–364, Jun. 2009.
- [75] J. Muller, M. N. Pham, and A. F. Jacob, "Directional coupler compensation with optimally positioned capacitances," *IEEE Transactions on Microwave Theory and Techniques*, vol. 59, no. 11, pp. 2824–2832, Nov. 2011.
- [76] M. Dydyk, "Accurate design of microstrip directional couplers with capacitive compensation," in *IEEE International Digest on Microwave Symposium*, 1990, pp. 581–584.
- [77] H. J. Carlin and W. Kohler, "Direct synthesis of band-pass transmission line structures," *IEEE Transactions on Microwave Theory and Techniques*, vol. 13, no. 3, pp. 283–297, May 1965.
- [78] H. J. Riblet, "The application of a new class of equal-ripple functions to some familiar transmission-line problems," *IEEE Transactions on Microwave Theory and Techniques*, vol. 12, no. 4, pp. 415–421, 1964.
- [79] J. Garcia-Garcia, J. Bonache, and F. Martin, "Application of Electromagnetic Bandgaps to the Design of Ultra-Wide Bandpass Filters With Good Out-of-Band Performance," *IEEE Transactions on Microwave Theory and Techniques*, vol. 54, no. 12, pp. 4136–4140, Dec. 2006.

- [80] X.-H. Wu, Q.-X. Chu, X.-K. Tian, and O. Xiao, "Quintuple-mode UWB bandpass filter with sharp roll-off and super-wide upper stopband," *IEEE Microwave and Wireless Components Letters*, vol. 21, no. 12, pp. 661–663, 2011.
- [81] T. H. Duong and I. hn S. Kim, "Steeply Sloped UWB Bandpass Filter Based on Stub-Loaded Resonator," *IEEE Microwave and Wireless Components Letters*, vol. 20, no. 8, pp. 441–443, Aug. 2010.
- [82] P. Cai, Z. Ma, X. Guan, X. Yang, Y. Kobayashi, T. Anada, and G. Hagiwara, "A compact UWB bandpass filter using two-section open-circuited stubs to realize transmission zeroes," in 2005 Asia-Pacific Microwave Conference Proceedings, 2005, vol. 5, pp. 1–4.
- [83] P. K. Singh, S. Basu, and Y. Wang, "Planar ultra-wideband bandpass filter using edge coupled microstrip lines and stepped impedance open stub," *IEEE Microwave and Wireless Components Letters*, vol. 17, no. 9, pp. 649–651, Sep. 2007.
- [84] G. C. Temes and J. W. LaPatra, *Introduction to Circuit Synthesis and Design*. McGraw-Hill, 1977.
- [85] G. Macchiarella and S. Tamiazzo, "Design techniques for dual-passband filters," *IEEE Transactions on Microwave Theory and Techniques*, vol. 53, no. 11, pp. 3265–3271, Nov. 2005.
- [86] *MATLAB Ver. R2010b*. Natick, Massachusetts: The MathWorks Inc., 2010.
- [87] B. M. Schiffman, "A new class of broad-band microwave 90-Degree phase shifters," *IEEE Transactions on Microwave Theory and Techniques*, vol. 6, no. 2, pp. 232–237, Apr. 1958.
- [88] H.-M. Lee and C.-M. Tsai, "Dual-band filter design with flexible passband frequency and bandwidth selections," *IEEE Transactions on Microwave Theory and Techniques*, vol. 55, no. 5, pp. 1002–1009, May 2007.
- [89] *Advanced Design System (ADS). Ver. 2005a*. Palo Alto, CA: Agilent Technol., 2005.
- [90] G. D. Alley, "Interdigital capacitors and their application to lumped-element microwave integrated circuits," *IEEE Transactions on Microwave Theory and Techniques*, vol. 18, no. 12, pp. 1028–1033, Dec. 1970.
- [91] C. Tang, C. Tseng, S.-H. Chiu, and P.-H. Wu, "Design of wide passband/stopband microstrip bandpass filters with the stepped coupled line," *IEEE Transactions on Microwave Theory and Techniques*, vol. 61, no. 3, pp. 1095–1103, Mar. 2013.

Author's Publications

Journal Papers

1. **R. Zhang**, S. Luo, and L. Zhu, "Asymmetrical-response dual-band bandpass filters on $\lambda/8$ transmission lines with modified Richard's transformation," *IEEE Microw. Wireless Compon. Lett.*, accepted.
2. **R. Zhang** and L. Zhu, "Synthesis and design of wideband dual-band bandpass filters with controllable in-band ripple factor and dual-band isolation," *IEEE Trans. Microw. Theory Tech.*, vol. 61, no. 5, pp. 1820–1828, May 2013.
3. **R. Zhang** and L. Zhu, "Synthesis of dual-wideband bandpass filters with source-load coupling network," *IEEE Trans. Microw. Theory Tech.* vol. 62, no. 3, pp. 441–449, Mar. 2014.
4. **R. Zhang** and L. Zhu, "Design of a compact dual-band bandpass filter using coupled stepped-impedance resonators" *IEEE Microw. Wireless Compon. Lett.*, vol. 24, no. 1, pp. 155–157, Mar. 2014.
5. **R. Zhang** and L. Zhu, "Design of a wideband bandpass filter with composite short- and open-circuited stubs," accepted by *IEEE Microw. Wireless Compon. Lett.*, vol. 24, no. 2, pp. 96–98, Feb. 2014.
6. **R. Zhang** and L. Zhu, "Synthesis and design of a class of wideband dual-band bandpass filters with internally-coupled microstrip lines," accepted by *IET Microwave Antennas & Propagation*.
7. **R. Zhang**, L. Zhu, and S. Luo, "Dual-mode dual-band bandpass filters with adjustable frequency ratio using an annular ring resonator," *IEEE Microw. Wireless Compon. Lett.*, vol. 23, no. 1, pp. 13–15, Jan. 2013.
8. **R. Zhang** and L. Zhu, "Synthesis design of a wideband bandpass filter with inductively coupled short-circuited multi-mode resonator," *IEEE Microw. Wireless Compon. Lett.*, vol. 22, no. 10, pp. 509–511, Oct. 2012.
9. **R. Zhang**, L. Zhu, and S. Luo, "Dual-mode dual-band bandpass filter using a single slotted circular patch resonator," *IEEE Microw. Wireless Compon. Lett.*, vol. 22, no. 5, pp. 233–235, May 2012.
10. **R. Zhang** and L. Zhu, "Microstrip bandpass filters using triple-mode patch-loaded cross resonator," *Progress In Electromagnetics Research Letters*, vol. 30, pp. 13–20, 2012.

Conference Papers

1. **R. Zhang**, L. Zhu, and S. Luo, "Design methodology of a class of triple-mode bandpass filters using a patch-loaded cross resonator," in *Int. Wireless Symp.*, Apr.2013, pp.14-18.
2. **R. Zhang**, L. Zhu, and S. Luo, "Compact dual-band microstrip bandpass filters using composite cross and open/short-circuited E-shaped resonators," in *Proc. Asia-Pacific Microw. Conf.*, Dec. 2012, pp. 664–666.
3. **R. Zhang** and L. Zhu, "A new triple-mode microstrip bandpass filter using a patch-loaded cross resonator," in *IEEE MTT-S Int. Microw. Symp. Dig.*, Jun. 2012, pp. 1–3.
4. **R. Zhang**, L. Zhu, and S. Luo, "Characterization of a slotted circular patch resonator for adjustable dual-mode dual-band bandpass filters," in *IEEE MTT-S Int. Microw. Symp. Dig.*, Jun. 2012, pp. 1–3.